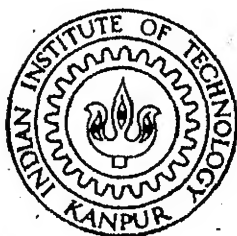


INITIATION AND PROPAGATION TOUGHNESS OF INTERLAMINAR CRACKS IN FRP LAMINATES UNDER IMPACT LOADING

by
RAMAKRISHNA ALLURI



DEPARTMENT OF MECHANICAL ENGINEERING

INDIAN INSTITUTE OF TECHNOLOGY KANPUR

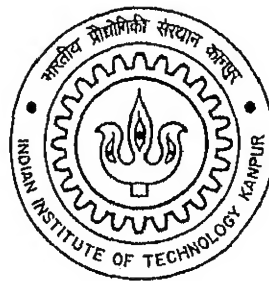
JANUARY 1997

ME
1997
M
ALL
INI

INITIATION AND PROPAGATION TOUGHNESS OF INTERLAMINAR CRACKS IN FRP LAMINATES UNDER IMPACT LOADING

A Thesis Submitted
in Partial Fulfilment of the Requirements
for the Degree of
MASTER OF TECHNOLOGY

by
RAMAKRISHNA ALLURI



to the
Department of Mechanical Engineering
INDIAN INSTITUTE OF TECHNOLOGY KANPUR
JANUARY, 1997

10 MAR 1997

CENTRAL LIBRARY
F.T. 100

10176 A 123190

ME-1997-M-ALL-IN

CERTIFICATE

It is certified that the work contained in the thesis entitled "**INITIATION AND PROPAGATION TOUGHNESS OF INTERLAMINAR CRACKS IN FRP LAMINATES UNDER IMPACT LOADING**", by Ramakrishna Alluri, has been carried out under my supervision and that this work has not been submitted elsewhere for a degree.



(Prof. Prashant Kumar)

Department of Mechanical Engineering
Indian Institute of Technology, Kanpur

January, 1997

Dedicated to
MY PARENTS

CONTENTS

Acknowledgements	vi
Abstract	vii
List of tables	viii
List of figures	ix

1 Introduction

1.1	Introduction	1
1.2	Literature survey	1
1.3	Present work	5

2 Finite element modelling of crack propagation

2.1	Introduction	6
2.2	Finite element formulation	6
2.3	Flow chart	10
2.4	Crack propagation simulation	10
2.5	Closure	11

3 Experimental technique

3.1	Introduction	22
3.2	Overall experimental setup	22
3.2.1	Solid block	23
3.2.2	Striker and the load bar	23
3.2.3	Stress pulses	24
3.2.4	Details of bridge circuit	25
3.2.5	Oscilloscope and its integration with PC	28
3.2.6	Crack velocity	28
3.3	Specimen details	28
3.3.1	Basic raw materials	28
3.3.2	Preparation of FRP laminate	29

3.3.3	Geometry of the specimen	29
3.3.4	Crack sharpening	30
3.3.5	Bonding of the strain gauges to the specimen	30
3.4	Closure	31
4 Results and discussion		
4.1	Introduction	44
4.2	Results of interlaminar initiation toughness	44
4.3	Results of interlaminar propagation toughness	48
4.4	Comparison of dynamic interlaminar toughness with quasistatic interlaminar toughness	50
4.5	Closure	51
5 Conclusions and Scope for future work		
5.1	Conclusions	83
5.2	Suggestions for further work	84
References		85
Appendix - A		87

ACKNOWLEDGEMENTS

I am grateful to Prof. Prashant Kumar for his invaluable guidance throughout this work. Without his constant encouragement and constructive suggestions I could not have surmounted the difficulties during this work.

I am thankful to Prof. N.N Kishore for his expert guidance during computational part.

I am grateful to Dr. S.K.Verma, Mr. K.K.Bajpai, Mr.Nyalapogula, Mr. Ravi and my senior Mr.S.R.M.Reddy for their help in one or the other way.

My sincere thanks is due to Mr. Anurag Goel for his cooperation in timely preparing the laminate. A word of appreciation is due to Mr. R.C.Tewari and Mr. B.D.Pandey for their help in preparing the specimens. I am also thankful to Mr. Pankaj for constant help throughout this work.

It gives me immense pleasure to recall my association with Ravindranatha Reddy, Sunil, Ramarao, Naveen, Govindarajan, Satyanarayan who made my stay here at IIT Kanpur a pleasant memory. It is also great pleasure to recall my association with Hall IV guys especially Jagan, Babu and others.

My thanks are also due to Mr. B.K.Jain of ACMS lab for his cooperative attitude in conducting experiments.

I don't claim that the above list is complete nor do I repudiate any help offered by my other friends who made my stay here a memorable one.

Last, but not least I am grateful to Aeronautical Research Development Board (Structures Panel) for providing financial assistance from the project ME\ARDB\93157.

ABSTRACT

A technique using a combined experiment and finite element method is developed to determine interlaminar initiation toughness and propagation toughness of slender unidirectional fibre reinforced epoxy laminate. In the experimental technique, one cantilever of DCB specimen is bonded to a flat rigid surface and the other cantilever is loaded through a compressive pulse in a load bar. The load bar is impacted by a striker and the incident and reflected pulses are monitored by two strain gauges to obtain deflection history of the cantilever end. The velocity of the fast moving interlaminar crack is measured by monitoring the responses of strain gauges mounted in series ahead of the crack tip on the side face of the cantilever. Thus, the experiment provides crack initiation time, crack velocity and the deflection of the cantilever end with respect to a time.

These experimental data is used as input to the FE code to obtain initiation toughness and propagation toughness by the gradual release of nodal forces to model the crack propagation of the interlaminar crack. The initiation fracture toughness and propagation fracture are evaluated for interlaminar crack propagating between 500 and 1500 m/s. The initiation and propagation toughness were found to vary between 90-230 J/m² and 1-50 J/m² respectively.

LIST OF TABLES

Table 4.1	Length of precrack in the DCB specimen and strain gauge locations for Expt.1 to 5	45
Table 4.2	Crack lengths, time at different gauges, initiation time and initiation toughness for Expt. 1 to 5.	47
Table 4.3	Crack velocity, initiation toughness for Expt. 1 to 5.	50
Table 4.4	Quasistatic interlaminar toughness (G_{IC}) for Expt. Q1 to Q3.	51
Table A1	Values of elastic modulus in longitudinal direction	89
Table A2	Values of elastic modulus in transverse direction	89
Table A3	Values of modulus of rigidity	89

LIST OF FIGURES

2.1	DCB specimen	12
2.2	DCB bonded to a solid block and impacted to develop high crack velocity	13
2.3	Comparison J-integral for different mesh sizes	14
2.4	Mesh for DCB specimen (one half)	15
2.5	Variation of J-integral with time for different time step used in integration scheme	16
2.6	Contour for J-integral	17
2.7	Flow chart	18
2.8	A typical variation of J-integral with time for stationary crack ...	19
2.9	A typical variation of J-integral with time for stationary crack and propagating crack	20
2.10	Crack opening scheme	21
3.1	Schematic diagram of the experimental setup	32
3.2	Photograph of the experimental set up	33
3.3	Photograph of the blown up view of experimental setup	34
3.4	A typical record of stress pulses in the load bar	35
3.5	Time-distance (t-x) diagram	36
3.6	Bridge Circuit	37
3.7	Photograph of the bridge circuit	38
3.8	DCB specimen	39
3.9	Photograph of the DCB specimen	40
3.10	Crack sharpening figure	41
3.11	Photograph of the crack sharpening fixture	42
3.12	Schematic diagram of strain gauge of 0.2 mm gauge length supplied by Tokyosokki Kenkyujo Co., Ltd., Japan	43
4.1	Oscilloscope traces of Expt.1	52
4.2(a)	Velocity input at the cantilever end of the specimen obtained	

	through incident and reflected pulses of the load bar for Expt.1 ..	53
4.2(b)	Cantilever end deflection vs. time obtained by integrating the velocity input curve	53
4.3	Blown up view of the recorded peak responses of strain gauge bonded to the specimen of Expt.1	54
4.4(a)	Variation of crack length with time of Expt.1 shown with interpolation upto the length of precrack	55
4.4(b)	Variation of crack propagation speed with time obtained by differentiating the crack length vs.time curve	55
4.5	Initiation toughness of Expt.1	56
4.6	Oscilloscope traces of Expt.2	57
4.7(a)	Velocity input at the cantilever end of the specimen obtained through incident and reflected pulses of the load bar for Expt.2 ..	58
4.7(b)	Cantilever end deflection vs. time obtained by integrating the velocity input curve	58
4.8(a)	Variation of crack length with time of Expt.2 shown with interpolation upto the length of precrack	59
4.8(b)	Variation of crack propagation speed with time obtained by differentiating the crack length vs.time curve	59
4.9	Initiation toughness of Expt.2	60
4.10	Oscilloscope traces of Expt.3	61
4.11(a)	Velocity input at the cantilever end of the specimen obtained through incident and reflected pulses of the load bar for Expt.3 ..	62
4.11(b)	Cantilever end deflection vs. time obtained by integrating the velocity input curve	62
4.12(a)	Variation of crack length with time of Expt.3 shown with interpolation upto the length of precrack	63
4.12(b)	Variation of crack propagation speed with time obtained by differentiating the crack length vs.time curve	63
4.13	Initiation toughness of Expt.3	64
4.14	Oscilloscope traces of Expt.4	65
4.15(a)	Velocity input at the cantilever end of the specimen obtained	

	through incident and reflected pulses of the load bar for Expt.4 . .	66
4.15(b)	Cantilever end deflection vs. time obtained by integrating the velocity input curve	66
4.16(a)	Variation of crack length with time of Expt.4 shown with interpolation upto the length of precrack	67
4.16(b)	Variation of crack propagation speed with time obtained by differentiating the crack length vs. time curve	67
4.17	Initiation toughness of Expt.4	68
4.18	Oscilloscope traces of Expt.5	69
4.19(a)	Velocity input at the cantilever end of the specimen obtained through incident and reflected pulses of the load bar for Expt.5 . .	70
4.19(b)	Cantilever end deflection vs. time obtained by integrating the velocity input curve	70
4.20(a)	Variation of crack length with time of Expt.5 shown with interpolation upto the length of precrack	71
4.20(b)	Variation of crack propagation speed with time obtained by differentiating the crack length vs. time curve	71
4.21	Initiation toughness of Expt.5	72
4.22	Variation of J-integral with time for stationary crack and propagating crack for Expt.1	73
4.23	Variation of J-integral after the crack starts propagating for Expt.1	74
4.24	Variation of J-integral with time for stationary crack and propagating crack for Expt.2	75
4.25	Variation of J-integral after the crack starts propagating for Expt.2	76
4.26	Variation of J-integral with time for stationary crack and propagating crack for Expt.3	77
4.27	Variation of J-integral after the crack starts propagating for Expt.3	78
4.28	Variation of J-integral with time for stationary crack and propagating crack for Expt.4	79

4.29	Variation of J-integral after the crack starts propagating for Expt.4	80
4.30	Variation of J-integral with time for stationary crack and propagating crack for Expt.5	81
4.31	Variation of J-integral after the crack starts propagating for Expt.5	82

CHAPTER-1

INTRODUCTION

1.1 INTRODUCTION

Recent development of composite materials has made it possible to adapt them for various fields eg. automobiles, aircrafts, boats, sport articles etc. Laminates fabricated by bonding slender sheets together are known to be susceptible to interlaminar crack propagation. In fact the critical energy release rate of interlaminar crack in laminates of fibre reinforced plastics (FRP) is found to be considerably less than that for a through the thickness crack for the same laminate. So far, the stress analysis and fracture of composite structure have been studied by many researchers, which have been mainly studied in the static state. But it is seriously necessary to study the composite fracture mechanics in the dynamic state, for many actual fracture problems of composite are apt to occur in a dynamic load rate.

A laminate shows considerable delamination damage when it is impacted by a stone, projectile or dropped tools. Under dynamic loading the interlaminar cracks can propagate at high velocities exceeding 500 m/s. Because of this reason the dynamic fracture is of special interest in the case of composite materials and laminates of slender sheets. In the case of dynamic fracture role of material becomes significant. The inertia effect may arise due to two reasons (i) rapidly applied loading on a cracked solid and (ii) rapid crack propagation. In the first case the influence of load is transferred to the crack by stress wave through the material. In the second case the material particle on opposite crack faces displace with respect to each other once the crack has advanced. The inertia effect in the first case, is considered significant when the time taken to load the specimen to maximum value is small compared to time required for the stress wave to travel at a characteristic wave speed of the material over a characteristic dimension of the body.

In the second case the inertia effect should be accounted for whenever the crack velocity is a significant factor of the characteristic velocity (eg. Raleigh wave velocity).

Dynamic fracture phenomenon has several important features. The mathematical models are more complex than static models. The boundaries of body change with time. From experimental point of view, many parameters have to be measured accurately within a very short period. Therefore, in the present work, a new hybrid technique which involves both experiment and finite element method, developed by Verma[1996], is adopted to determine the interlaminar initiation toughness and propagation toughness for crack moving at high speeds (100-1400m/s) in a unidirectional fibre reinforced epoxy laminates.

1.2 LITERATURE SURVEY

There is no literature available for the dynamic crack propagation in FRP laminates, to the best of author's knowledge. The survey of literature is presented on related fields.

Sun and Grady[1988] investigated dynamic delamination fracture toughness in a [90/10]_{5s} T900/934 graphite/epoxy laminate using impact loading. Delamination cracks of three different sizes were embedded at the mid-plane of the composite specimen. The threshold impact velocity that causes propagation of the delamination crack was used in the dynamic analysis with the finite element method. From the finite element solution, the time-history of the strain energy release rate was calculated. The critical strain energy release rate was taken equal to that of the maximum value of the response history.

Rosakis, Duffy and Freund[1984] performed dynamic crack propagation experiments using wedge loaded double cantilever beam specimens of an austenized, quenched and tempered 4340 steel. They measured the dynamic stress intensity factor by means of the optical method of caustics. The experimental data was obtained from the shadow spot patterns photographed with a Cranz-Schardin high speed camera. The interpretation of the data was based on an elastodynamic analysis. They obtained the instantaneous value

of the dynamic stress intensity factor K_{Id} as a function of crack tip velocity. It is observed that the fracture toughness increases with increase in crack velocity. The specimen used by them was large in size and therefore the technique cannot be used for DCB specimen with thin cantilevers.

Nishioka and Atluri[1983] studied the use of path independent J-integral for dynamic crack propagation, which has the physical meaning of energy release rate, by the finite element method. Other path independent integrals are also investigated along with the J-integral. Numerical results showed that combined use of the J-integral and the finite element method is a useful tool to obtain the fracture parameters such as the stress intensity factors and the energy release rates. The use of the several other types of path-independent integrals, despite their lack of a direct interpretation as energy release rates, is also demonstrated. This is so, because the alternate path-independent integrals have been explicitly expressed in terms of the time-dependent K-factors.

Nishioka et. al.[1991]studied the specimen size effects on dynamic crack propagation and arrest in DCB specimens using laser caustic method. They worked on polymethyl methacrylate (PMMA) made specimens in mode I. Dynamic condition was obtained using the conventional technique of storing energy through a blunt crack. They worked with maximum crack velocities of the order of 200 m/s. The specimen length was changed inorder to study the specimen size effects on dynamic crack propagation and arrest. They found that dynamic stress intensity factor decreases as the crack moves forward. They also observed that K_{Id} increases with crack velocity. However the studies were conducted on large specimens.

Takahashi and Arakawa[1984] employed the caustic methods in combination with high-speed photography to study velocity effect on the dynamic-stress-intensity factor of fast cracks in polymethyl methacrylite and in Araldite D. The specimen geometry was so determined that both the accelerating and decelerating crack propagation occurred noticeably in one fracture event. Instantaneous crack velocity as well as its acceleration were expressed as a function of the crack length by using polynomials of the ninth order which were given on the basis of the least-square method. The results show that the

dynamic-stress-intensity factor depends not only on the crack velocity but also on crack acceleration, and that the accelerating crack has a small value stress intensity factor than the decelerating crack at the same velocity.

Kolednik[1991] in his theoretical study gave a physical interpretation of the J-R curves for elastic-plastic fracture. He derived the difference between the crack-initiation toughness and crack-growth toughness using energy balance under quasi-static conditions. He considered three point bend specimens each of which consists of two parts glued together along the ligament. Here also large specimens were analyzed.

Ravichandran and Clifton[1989] developed a special technique to study the initiation and propagation of crack in steel specimen under dynamic loading. They presented a plate impact experiment and related finite difference model to study the fracture process that occurs in sub-micron loading. A disc containing a mid-plane prefatigued edge crack that has been propagated half way across the diameter is impacted by a thin flyer plate of same material. A compressive pulse propagates through the specimen and reflects from the rear surface as a step tensile pulse with a duration of $1\ \mu\text{s}$. The plane wave loads the crack and cause the initiation and propagation of the crack. The motion of the rear surface is monitored by using the laser interferometer system. The location of the crack front was mapped before and after the experiment using a focused ultrasonic transducer. Experiments were conducted on 4340 VAR steel at temperature ranging from room temperature to -100°C . A finite difference method was used for numerical simulation of the experiments. Crack velocities were prescribed corresponding to various fracture models.

Potty[1992] investigated SIF in a DCB specimen with thin cantilevers through a combined scheme of experimentally measuring the strain near the crack tip and analyzing this data by using FEM. In the finite element programme he developed a relationship between stress intensity factor and strain near the crack tip. The strain measured near the crack tip with the help of a very small strain gauge (gauge length 0.2 mm) is used in the FEM programme to obtain the SIF of the DCB specimen. Lovi[1993] improved upon Potty's method by using two strain gauges one on each cantilever to neutralize the

possibility of recording the bending strains in the cantilevers which might develop during specimen preparation.

Ray[1994] developed an experimental technique to determine the dynamic interlaminar toughness for slender steel DCB specimens. A load bar technique is used to apply dynamic load pulse to one of the cantilevers of the DCB specimen. Propagation gauges, which are bonded to the side face of DCB specimen, monitors the crack velocity. These experimental data was used as input to FE code, developed by Kishore, Kumar and Verma[1993], to obtain the dynamic interlaminar toughness parameters for slender laminates.

1.3 PRESENT WORK

A technique, which was developed by Verma[1996], has been adopted to determine the interlaminar initiation toughness and propagation toughness of unidirectional fibre reinforced epoxy laminates. This technique employs a combined experimental and numerical work. For numerical work the finite element code developed by Kishore, Kumar and Verma[1993] has been modified to use the material elastic constants of the FRP specimen adopted in this study.

The experimental work determines the crack initiation time, crack velocity and the corresponding cantilever end deflections with time of DCB specimen. These experimental data is used as input by the finite element code to simulate the interlaminar fracture behaviour of slender composite laminates.

Chapter 2 of the thesis gives the brief details of the finite element code, which was developed by Kishore, Kumar and Verma[1993], and adopted in the present work with some modifications. Chapter 3 explains the details of the specimen and the experimental setup. Chapter 4 presents the results and discussion. The conclusions and suggestions for further work is outlined in Chapter 5.

CHAPTER-2

FINITE ELEMENT MODELLING OF CRACK PROPAGATION

2.1. INTRODUCTION

As a part of combined experimental and numerical technique to determine the interlaminar dynamic fracture toughness of DCB specimen (Fig.2.1) in mode I, the experimental measurements consists of obtaining the (i) deflection of cantilever end with time (at point 'A' as shown in Fig.2.2, (ii) crack propagation velocity with the help of three strain gauges bonded ahead of the crack tip on one side face of the cantilever and (iii) crack initiation time. These data are used in finite element code to simulate the dynamic fracture behaviour of the DCB specimen. The finite element simulation determines initiation and propagation fracture toughnesses. A brief outline of the finite element formulation as developed by Kishore, Kumar and Verma[1993] is presented in this chapter.

2.2. FINITE ELEMENT FORMULATION

The following finite element equations in matrix form governs the linear dynamic response an elastic body (neglecting damping forces)

$$[M] \{\ddot{u}\} + [K] \{\dot{u}\} = \{R\} \quad 2.1$$

where $[M]$ and $[K]$ are the mass and stiffness matrices respectively, and R is external load vector; $\{u\}$ and $\{\dot{u}\}$ are

displacements and acceleration vectors of finite element assemblage respectively. It may be noted in the Eq.2.1 that

$$[M] = \sum [M]^e$$

$$[K] = \sum [K]^e$$

$$[R] = \sum [R]^e$$

where mass, stiffness and traction matrices of individual elements are given by

$$[M]^e = \int_v \rho [N]^T [N] dV$$

$$[K]^e = \int_v \rho [B]^T [D] [B] dV$$

$$[R]^e = \int_s [N] \{t\} dS$$

In these expressions $[N]$ is the shape function, $[B]$ is the derivative of shape functions, $[D]$ is the elastic constitutive relation matrix and t is the traction vector. The elastic constitutive relation matrix for the present work is described in Appendix A.

Equation 2.1 can be solved either by time integration or by node superposition of which the former is preferred in the wave propagation problem of present kind. A computer code has been developed for 2-D using finite element discretisation in space analysis and Newmark integration method for the variable as presented in Bathe[1990]. Since the specimen dimension along the third direction (Z-direction of Fig.2.1) is large this is a plain strain problem.

A computer code was developed by Kishore, Kumar, Verma[1993] to generate mesh of four noded elements. Figure 2.3 shows comparison of J-integral for different mesh sizes. Compared with a mesh size of 0.4X0.35 mm, J-integral is not effected much for a mesh size of 0.2X0.175 during prior to the crack initiation as well as during the crack propagation. Also for a dynamic problem, as discussed by Seron et al.(1990), the higher order elements are not required. Therefore four noded isoparametric elements are used in this study. At the same time, to avoid non-uniformity in mass distribution which leads to reflection of waves, uniform mesh throughout the specimen is generated. The mesh of size is 0.4mm X 0.35mm chosen in the study as shown in Fig.2.4.

Also, as discussed by Verma[1996], for both configurations of full DCB specimen and half DCB specimens there is not a much difference in J-integral. Hence to avoid unnecessary computations, only rear cantilever of the DCB specimen is analyzed.

To study the effect of time step on the value, J-integral was evaluated for different time steps under same loading conditions as shown in Fig.2.5. It is observed that upto the initiation point J-integral does not depend much on time step even for a time step of

0.5 μ s. But during propagation phase, there is a wide variation in J-integral for a large time step of 0.5 μ s compared with a time step of 0.1 μ s. However, there is hardly any change in J-integral when the time step was reduced from 0.1 μ s to 0.035 μ s. J-integral is therefore calculated with a time step of 0.5 μ s upto the initiation point and 0.1 μ s after the initiation and during propagation.

Atluri[1982] and Nishioka and Atluri[1983] have under taken the studies of several path independent integrals in the analysis of crack growth initiation and propagation of cracks in elastic or inelastic materials under quasistatic and dynamic conditions. In the present work J is defined as follows.

$$J = \lim_{\epsilon \rightarrow 0} \int_{\Gamma + \Gamma_c} [Wn_1 - t_i u_{i,1}] dS + \int_{V-V_e} \rho \ddot{u} u_{i,1} dV$$

where W is the strain energy density, n_1 is the direction cosine of the unit outward normal, t_i is the surface traction and the definition of the paths $\Gamma_e, \Gamma_c, \Gamma$ and the volume V, V_e are shown in Fig.2.6.

The value of J is independent of the choice of Γ of Fig.2.6 only under stringent ideal conditions (eg. steady state crack growth). In many cases, though these conditions are obviously not met the independence of J integral can still be established within certain allowable error. The path is held stationary as the crack tip extends in a self similar manner.

2.3. FLOW CHART

The flow chart of the finite element code developed by Kishore, kumar, and Verma is shown in Fig.2.7. Input required for the programme are material properties, mesh size, time step, load pulse, crack propagating history and displacement boundary conditions.

2.4. CRACK PROPAGATION SIMULATION

When the velocity of the crack propagation is zero (stationary crack) a typical variation of J-integral with time is shown in Fig.2.8. J-integral increases till initiation time. After the initiation the J-integral drops sharply to a low value as shown in Fig.2.9. Inorder to simulate the propagation of the crack, Gradual nodal Release Method was used. Suppose that the actual crack tip is located at c in between the nodes B & D as shown in Fig.2.10. Usually holding back force F at node B is gradually reduced to zero as the crack tip reaches the node D.

For having gradual and smooth opening of crack Kishore, Kumar and Verma[1993] tried an alternative method. The holding back force at the crack tip B is linearly decreased to zero when the crack reaches the end of the next element.

Thus, when the crack tip goes beyond node B, then

$$\frac{F_B}{F_{HB}} = \left[1 - \frac{b}{2d} \right]$$

where F_{HB} is reaction at node B when the node was closed, b is the crack extension and d , the element length as shown in Fig.2.6. When the crack moves beyond node D to a point D_1 ,

$$\frac{F_B}{F_{HB}} = \left[1 - \frac{d + b_2}{2d} \right]$$

$$\frac{F_B}{F_{HD}} = \left[1 - \frac{b_2}{2d} \right]$$

where F_{HD} is the reaction at node D, when the node was closed.

2.5 CLOSURE

The aim of this chapter was to present the finite element formulation, which was developed by Kishore, Kumar and Verma[1993]. This FE code was used in the present work to simulate the dynamic fracture behaviour of the interlaminar cracks in FRP laminates. The elastic constitutive relation matrix in the FE code has been changed to suit to the present problem. The details of this material property matrix is given in Appendix A.

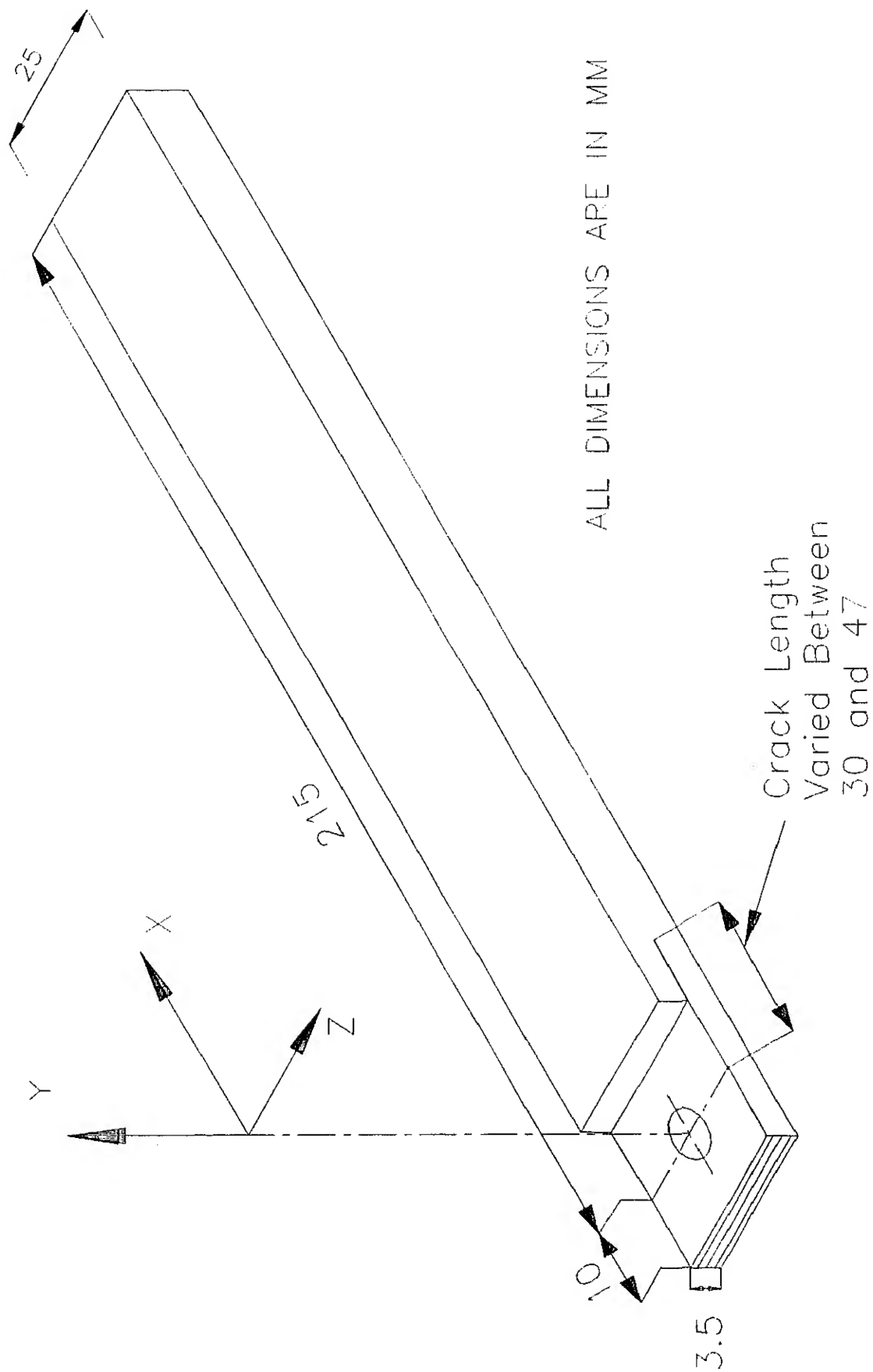


Fig. 2.1 DCB specimen

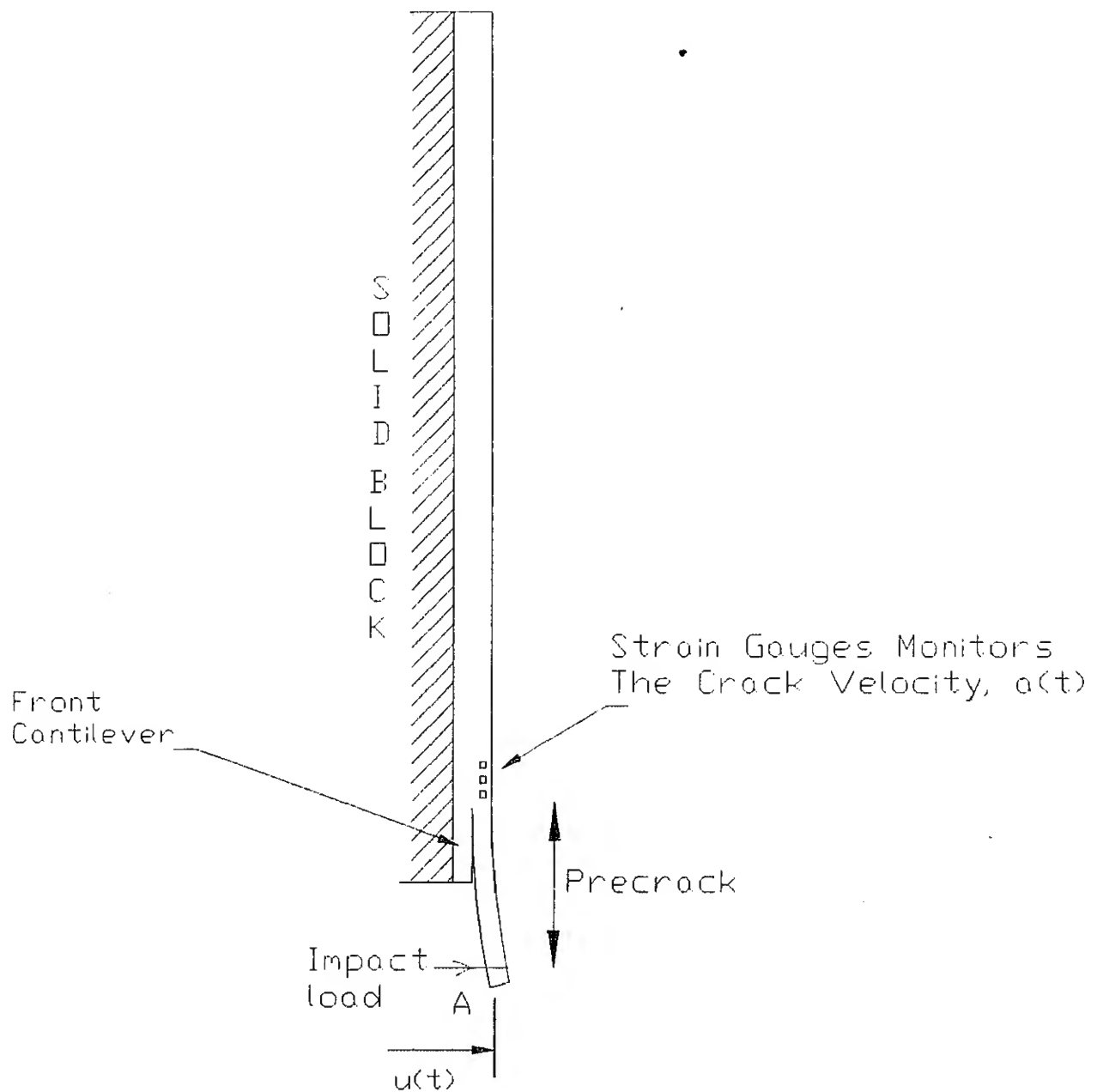


Fig.2.2 DCB specimen bonded to a solid block and impacted to develop high crack velocity

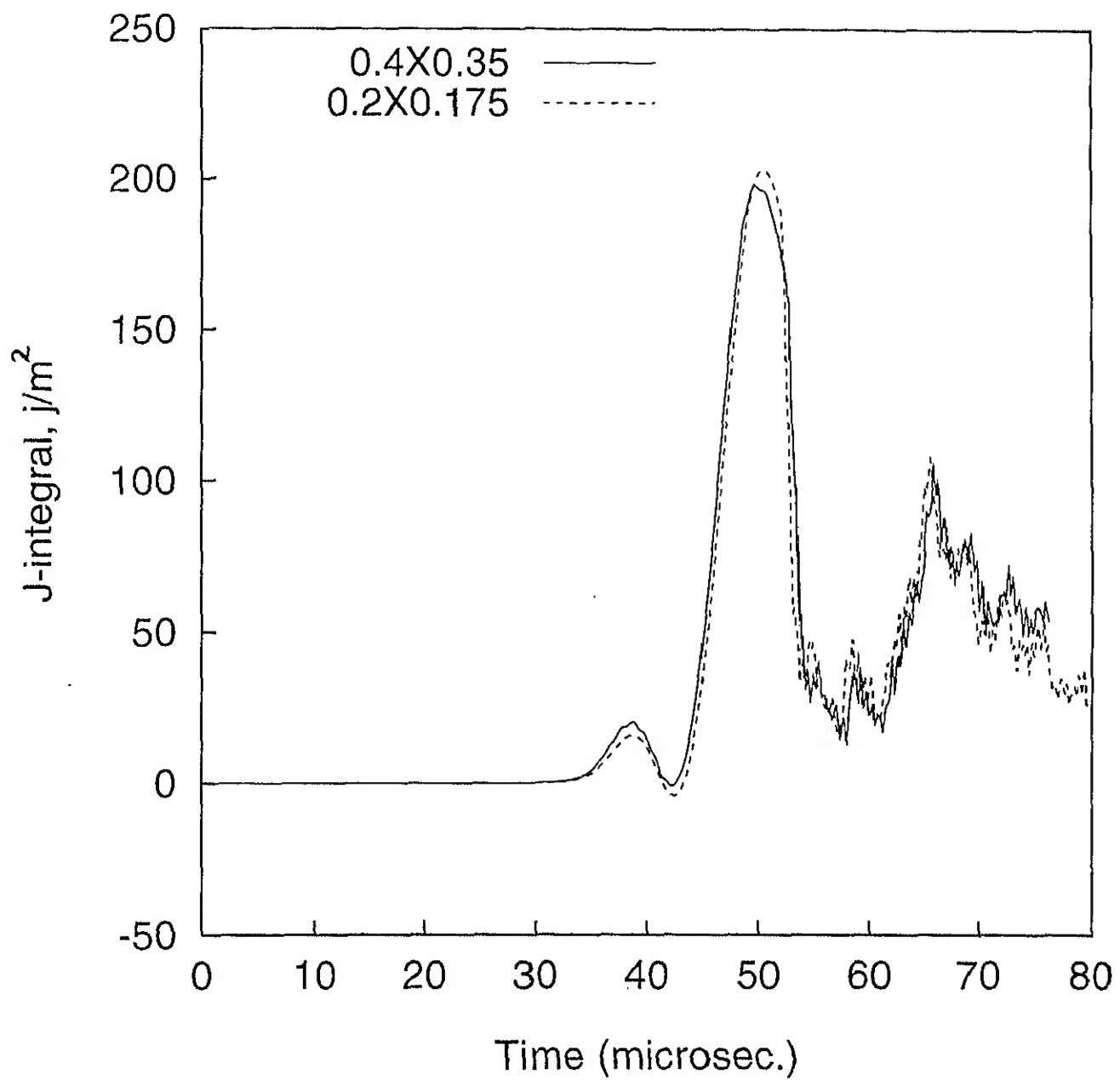


Fig.2.3 Comparison of J-integral for different mesh sizes

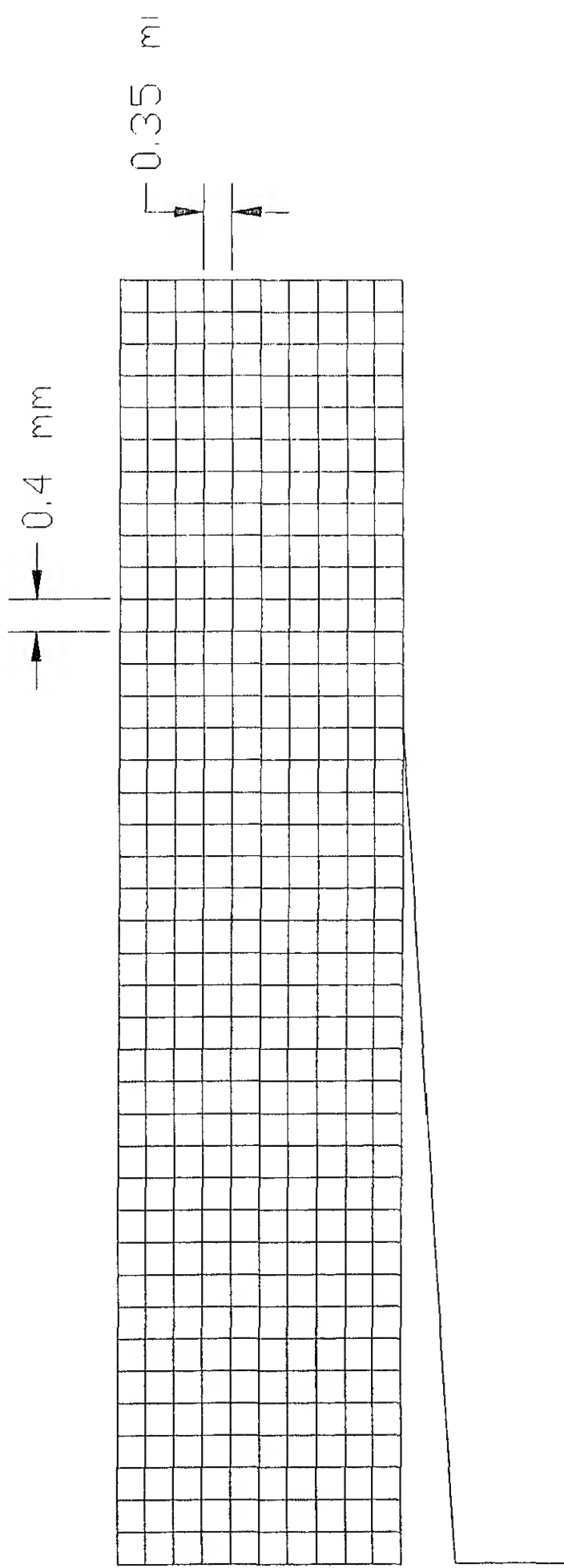


Fig.2.4 Mesh for DCB specimen (one half)

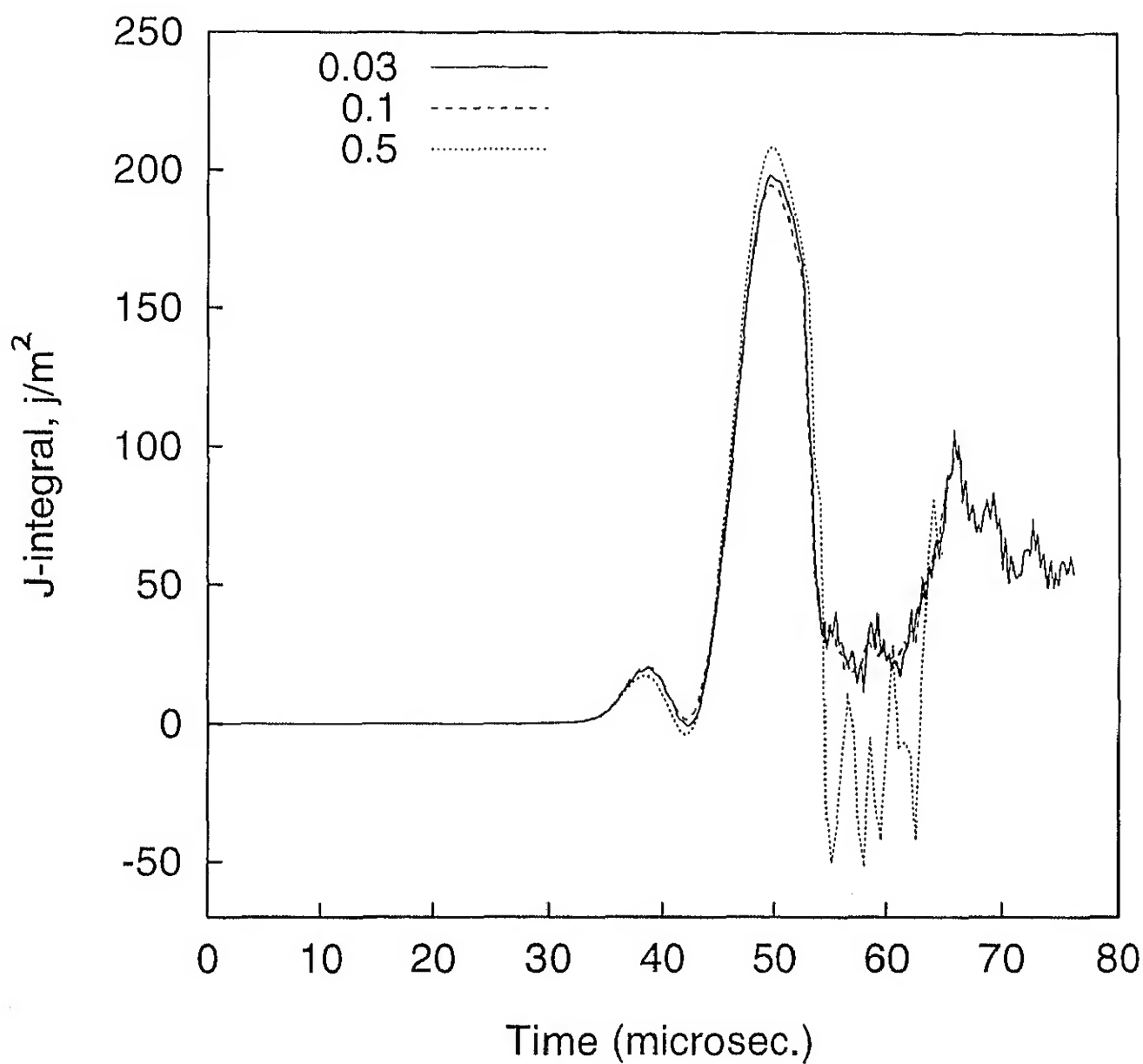
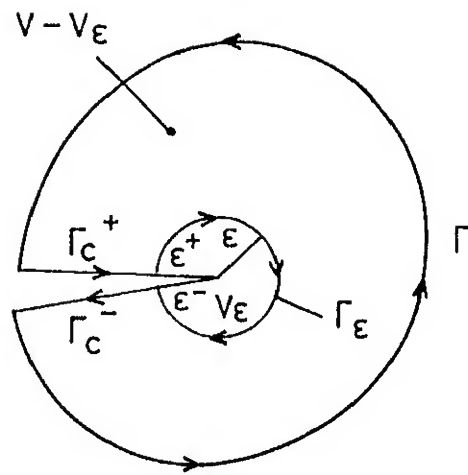


Fig.2.5 Variation of J-integral with time for different time steps used in integration scheme



$$\Gamma_C = \Gamma_C^+ + \Gamma_C^-$$

$$\delta(V - V_\epsilon) = \Gamma + \Gamma_C - \Gamma_\epsilon$$

Fig. 2.6 Contour for \hat{J} -integral.

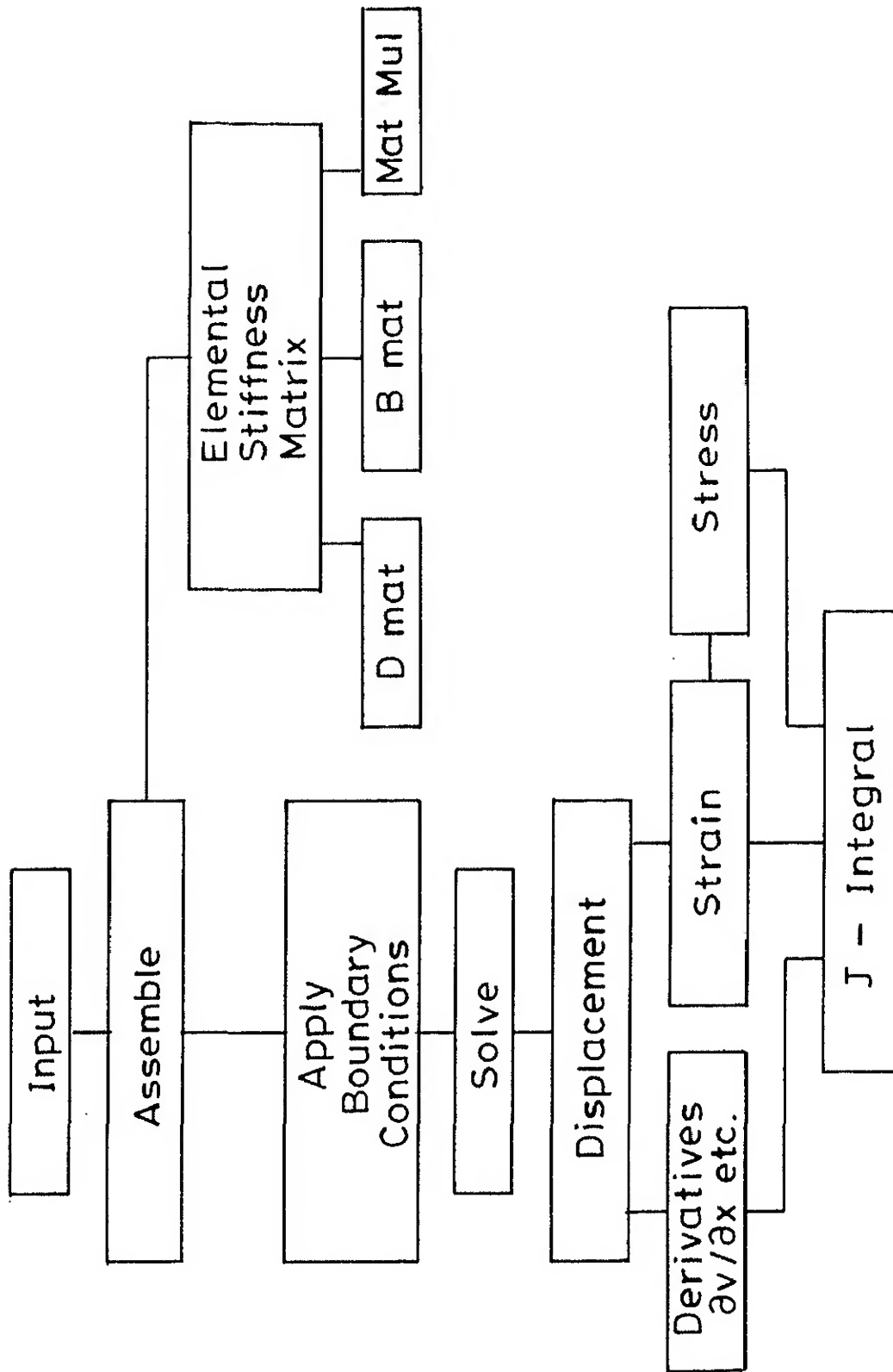


Fig.2.7 Flow chart of the finite element code.

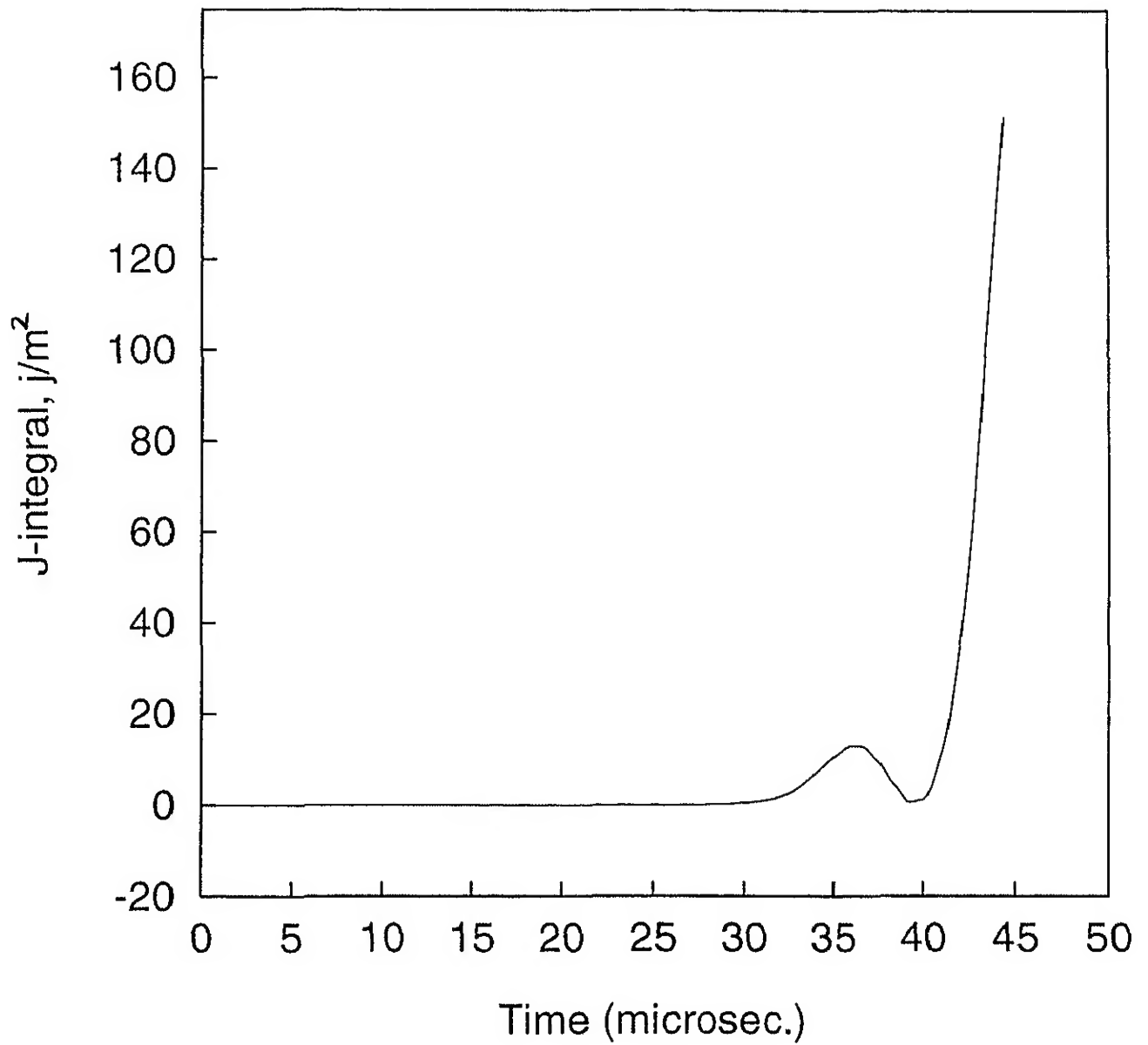


Fig.2.8 A typical variation of J-integral with time for a stationary crack

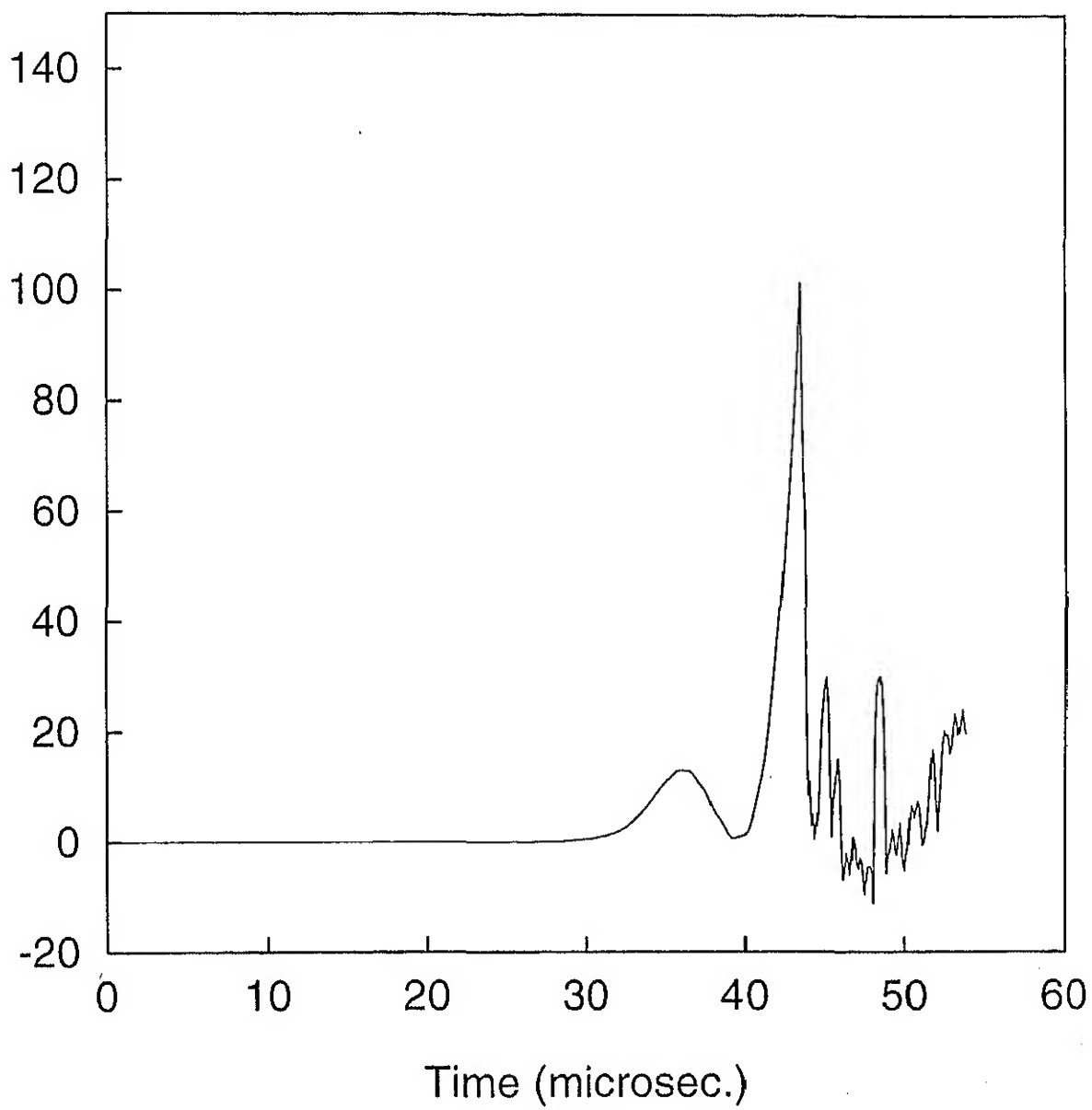


Fig.2.9 A typical variation of J-integral with time for stationary crack and propagating crack

CHAPTER-3

EXPERIMENTAL TECHNIQUE

3.1. INTRODUCTION

Experiments are conducted (i) to obtain the deflection of cantilever end with time, (ii) to measure the initiation time for crack propagation, and (iii) to determine the interlaminar crack velocity of double cantilever beam (DCB) specimen. This data is fed into the finite element (FE) code to simulate displacement field in the specimen and propagation of crack after the initiation time. This leads to initiation toughness (J_{init}) and propagation toughness (J_{prop}).

The work is carried on unidirectional fibre reinforced epoxy (FRP) laminates. The technique of determination of initiation & propagation toughness was developed by Verma[1996]. He applied the technique to a specimen made of two steel plates bonded with epoxy. In this work, the same technique is applied to FRP laminates with a precrack. This chapter describes the principle of the technique, details of specimen preparation, experimental setup, experimental measurements and data processing.

3.2. OVERALL EXPERIMENTAL SETUP

The Fig.3.1 shows the schematic diagram of the experimental setup. In this the front cantilever of the DCB specimen is bonded to the rigid block, which is clamped to a rigid by using a C-clamp. The rear cantilever is screwed to the load bar. The load bar is bonded with two strain gauges at symmetrically opposite locations in the longitudinal direction. These strain gauges are connected to the oscilloscope through a bridge circuit. To measure the crack velocity and crack initiation time, three strain gauges are bonded ahead of the crack tip on one side face of the cantilever. Each one of the three strain

gauges is also connected to the same oscilloscope through a bridge circuit.

When the striker bar, accelerated in the barrel of the airgun, impacts the load bar a compressive stress pulse propagates in the load bar towards the specimen. A part of its energy is transmitted through the specimen and rest is reflected back as tensile pulse. The strain gauges on the load bar monitors both propagated and reflected pulses. The part of the pulse that is transmitted to the specimen causes deflection of the cantilever end and extends the crack. The oscilloscope records the strain pulses in the load bar which are analyzed using one dimensional stress wave analysis to obtain deflection history of the cantilever's end. Responses of strain gauges recorded on the same oscilloscope, provide the initiation time of the crack growth and the crack velocity. The photograph of the setup is shown in Fig.3.2.

3.2.1 Solid Block

As shown in Fig.3.1 the front cantilever of the DCB specimen is bonded to a block of mild steel (50mm X 50mm X 150mm) which acts as a rigid mass. The block is placed on a base plate and after aligning the specimen to the load bar the block is firmly clamped to the base plate with the help of C-clamp (Fig.3.3).

3.2.2 Striker and the Load Bar

The striker and the load bar are made of cold rolled mild steel rod of 19 mm diameter. The striker bar is used to produce a compressive pulse in the load bar, part of which is transmitted to the specimen and the rest is reflected back as a tensile pulse. Both the stress pulses are monitored through two strain gauges of 120 Ω resistance and 6 mm gauge length, are bonded to the load bar along its axis. The strain gauges are bonded diagonally opposite to each other to cancel the effect of bending wave, if there is any.

3.2.3 Stress Pulses

As explained in Sec.2.2 when the striker bar hits the load bar a compressive stress pulse propagates through the load bar, towards the specimen. After reflection at the end of the load bar a tensile reflected pulse is again monitored by the strain gauges. A typical record of the incident pulse and reflected tensile pulse recorded by the strain gauge is shown in Fig.3.4. From this experimental record the load pulse imparted to the specimen can be obtained using one dimensional wave propagation theory. Figure 3.5 shows the time distance (t-x) diagram for propagation of stress pulse in the load bar. When the striker bar impacts the load bar, compressive incident pulse propagates towards the DCB specimen and is recorded at the location 1. The reflected tensile pulse is recorded at the same location but at different time and is depicted by point 3 in the t-x diagram. The aim is to express particle velocity v_2 in terms of experimentally recorded σ_1 and σ_3 . One dimensional wave equation along the characteristic with the acoustic impedance, ρc is expressed as

$$d\sigma - \rho c dv = 0 \quad (\text{Along +ve characteristic})$$

$$d\sigma + \rho c dv = 0 \quad (\text{Along -ve characteristic})$$

Using above equations the relation along characteristic 1-2 simplifies to

$$\sigma_2 - \rho c v_2 = \sigma_1 - \rho c v_1 \quad 3.1$$

Along the characteristic 1-5

$$\sigma_1 + \rho c v_1 = \sigma_5 + \rho c v_5 \quad 3.2$$

But $\sigma_5 = 0$ and $v_5 = 0$ because the load bar is initially at rest and stress waves never reaches at point 5. Then the above equation gives

$$\sigma_1 = -\rho c v_1 \quad 3.3$$

substituting Eq.3.3 in Eq.3.1

$$\sigma_2 - \rho cv_2 = 2\sigma_1 \quad 3.4$$

Relation along characteristics 2-3 and 3-4 are

$$\sigma_2 + \rho cv_2 = \sigma_3 + \rho cv_3 \quad 3.5$$

$$\sigma_3 - \rho cv_3 = \sigma_4 - \rho cv_4 \quad 3.6$$

$\sigma_4 = 0$ and $v_4 = 0$ at point 4, because the striker and the load bar are of the same material and the striker comes to rest. The above two equations yield

$$\sigma_2 + \rho cv_2 = 2\sigma_3 \quad 3.7$$

$$v_2 = (\sigma_3 - \sigma_1)/(\rho c) \quad 3.8$$

Since σ_1 is compressive and σ_3 is tensile in nature, the particle velocity of the cantilever end (v_2) can be found by taking sum of the absolute values of incident and reflected pulses.

3.2.4 Details Of Bridge Circuit

The bridge circuit converts the change in resistance of the strain gauges bonded to the load bar into a potential difference. This potential difference is recorded on the oscilloscope. Figure 3.6 shows the configuration of the bridge circuit used in this study. Figure 3.7 shows the photograph of the same. R_1 , R_2 , R_3 and R_4 are four strain gauges each having a resistance value of $120 \pm 0.3 \Omega$. R_1 and R_3 represent the strain gauges bonded to the load bar. R_2 and R_4 are the dummy gauges. These dummy strain gauges are bonded on a steel bar, diameter and material same as of the load bar which acts as a heat sink to the heat generated in the strain gauge when current flows through it. The bridge circuit is balanced to give zero voltage output by connecting 1.0Ω

resistance for coarse adjustment and $1\text{M}\Omega / 1.0\text{k}\Omega$ for fine adjustment as shown in the circuit. To calibrate the bridge circuit a calibration resistance R_c ($47.0\text{k}\Omega$) connected parallel to one of the active gauges through a switch (K). The equations involving the calibration of the bridge circuit are as follows. For a balanced bridge circuit the output voltage (Δe) is given by

$$\frac{\Delta e}{E} = \frac{R_1 \cdot R_2}{(R_1 + R_2)^2} \left(\frac{\Delta R_1}{R_1} - \frac{\Delta R_2}{R_2} + \frac{\Delta R_3}{R_3} - \frac{\Delta R_4}{R_4} \right) \quad 3.9$$

where E is the input voltage. It can be seen from the equation that similar (both positive or both negative) changes in resistance of opposite arms of the bridge circuit are added up and dissimilar (one positive and other negative) changes are cancelled out. Thus by having the active strain gauges at the opposite arms only compressive pulse is recorded and bending effect is rejected.

The relation between the strain in the strain gauge and corresponding change in its resistance is governed by the following equation

$$G.F. = \frac{\Delta R/R}{\Delta L/L}$$

where G.F. is the gauge factor and $\Delta L/L$ is the strain recorded by the strain gauge. Rearranging the above Eq. one obtains

$$\frac{\Delta L}{L} = \frac{\Delta R/R}{G.F.} \quad 3.10$$

The change in resistance of the arm CD after connecting R_c is given by

$$\Delta R_3 = R_3 - \left(\frac{R_3 R_c}{R_3 + R_c} \right) \quad 3.11$$

leading to

$$\Delta R_3 / R_3 = \frac{R_3}{R_3 + R_c} \quad 3.12$$

Corresponding to this change in resistance a voltage difference (Calibration Voltage, V_c) develops between terminals A and C. Similar resistance change will also occur in R_1 and R_3 when the load bar experiences the load pulses. From Eqs. 3.10 and 3.12 the calibration voltage corresponds to the strain

$$\epsilon_c = \Delta L / L = \frac{R_3}{2(R_3 + R_c) G.F.} \quad 3.13$$

The strain value ϵ_c will thus correspond to the Calibration Voltage, V_c . A factor of 1/2 is introduced to average out the strains recorded by the two strain gauges R_1 and R_3 which are at the opposite arms of the bridge circuit. By the linearity of the relation (Eq.3.9 and Eq.3.10) between voltage drop across AC and strain in the strain gauges bonded to the load bar, the strain in the load bar corresponding to a voltage V recorded on the oscilloscope can be given as

$$\epsilon = \frac{\epsilon_c}{V_c} \cdot V \quad 3.14$$

Generally strain gauges are connected to the Wheatstone bridge through BNC connectors mounted on the wall of the box. However, BNC connectors available locally are of poor quality and not reliable. These BNC connectors were replaced by specially designed cap and stud arrangement (Fig.3.7) to have press contact at the terminals (Verma[1996]).

3.2.5 Oscilloscope and its integration with PC

A 4-channel storage oscilloscope of model 1624 (Gould Inc., U.K) was used to monitor strain gauge responses. The data is be stored in 55 memory blocks and remains in the memory even if the power is switched off. It has 8 bit resolution (i.e., 256 points) in vertical direction and 12 bit resolution (i.e., 4096 points on the screen) in horizontal direction. The maximum sensitivity is 0.025 mV in the vertical direction and 0.25 μ s in the horizontal direction. The oscilloscope is provided with differential input facility to each channel. This oscilloscope is integrated with personnel computer (PC 386), so that the stored data can be transferred to the PC for further processing.

3.2.6 Crack Velocity

Crack velocity of the DCB specimen is measured by bonding three strain gauges ahead of the crack tip. The first strain gauge was mounted close to the crack tip of pre-crack. As the crack advances, after dynamic load on one end of DCB specimen is applied, the strain gauge output starts increasing to a maximum value due to singular stress field around the crack tip and then decreases as the crack passes underneath the strain gauge. In this way the time, at which the strain gauge records the maximum strain, is known. A curve is then plotted for the crack length as a function of time. The slope of this curve gives the crack velocity

3.3 SPECIMEN DETAILS

The specimen used throughout this work is unidirectional fibre reinforced epoxy composite. This section describes the material, geometry and preparation of specimen.

3.3.1 Basic Raw Materials

The basic raw materials are glass fibre, epoxy resin mixture. The epoxy resin mixture has following compositions.

Araldite	LY556	100 parts by weight
Hardener	HT976	35 parts by weight
Accelerator	XY73/HT973	1 parts by weight
Coupling Agent(γ -Amino aropyl triethoxy silane)		0.5 parts by weight

Unidirectional glass fibres are used as reinforcement material. These fibres have been procured from CEAT Tyers of India Ltd.

3.3.2 Preparation of FRP Laminate

The laminate is made from unidirectional prepegs. Prepegs are made from fibres with above mentioned epoxy mixture through a 150mm wide prepeg making machine available in the laboratory. The prepeg is cut to a required length and 32 of these pieces are stacked together with a precrack. Precrack is made by placing a thin teflon film (20 μ m thick) at the middle of the laminate at one end. The stacked laminae is then placed between two plates of a hydraulic press. Initially the laminate in the hydraulic press is heated to 120⁰ by applying the pressure gradually to 0.7 Mpa for an hour. Then the temperature is increased upto 140⁰ c and at that pressure it is maintained for 6 hours. It is then cooled to room temperature.

3.3.3 Geometry Of The Specimen

The specimen for the present work used have a size of 7 mm thick (each cantilever is 3.5 mm), 25 mm wide and the length ranging from 190 - 220 mm. As shown in Fig.3.8 end of front cantilever is cut to an offset of 20 mm so that the rear cantilever can be impacted by the load bar. A small hole of 9 mm is drilled on the rear cantilever so that it can be screwed to load bar by a M5 tap screw and a washer. Figure 3.9 shows the photograph of the DCB specimen.

3.3.4. Crack Sharpening

The pre-crack introduced in the DCB specimen by placing a teflon film needs further preparation before the specimen is impacted. The tip of the as cast pre-crack is not very sharp due to the finite thickness of BOPP sheet. Therefore the precrack should be grown further by a few millimetre. A fixture was designed to sharpen the crack. The Fig.3.10 shows the details of the fixture and the photograph of the same is shown in Fig.3.11. In the fixture the specimen is clamped between two thick pressure plates which are cut to a depth of 2 mm leaving a width of 8 mm at the ends. To have a uniform pressure on the specimen the ends of the plates are grounded flat. Before the pressure plates are tightened between the two jaws of a vice, the specimen and both the plates are placed on their side face over the third base plate of the fixture whose top surface is also grounded flat. This ensures that the edges of the pressure plates are parallel to the crack front. The specimen is placed between pressure plates in such a way that the tip of the pre-crack is out by 2-3 mm beyond the edges of the plates. The specimen between the pressure plates is pressed properly between the jaws of the vice (Fig.3.10). Now, by cautiously pressing a sharp chisel between the two cantilevers of the DCB specimen the crack extends upto the edges of the pressure plates with a sharp tip.

3.3.5 Bonding Of The Strain Gauges to the specimen

The strain gauges used in these experiment have been supplied by Tokyo Sokki Kenkyujo Co.,Ltd., Japan. They have a gauge length of 0.2mm and a gauge width of 1.4 mm. Figure 3.12 shows the details of the strain gauge. The base of the strain gauge is rectangular with dimensions 3.5mmX2.5mm. Its resistance is $120 \pm 0.3 \Omega$ and a gauge factor 2.07.

Extreme care is taken in fixing the strain gauges as it has a very small area. Approximate distance between the strain gauges is marked on the surface of the specimen with the help of scale and angle decker. The strain gauges are bonded on those marks. For bonding fevi-kwick (supplied by Pidilite Industries Ltd., Mumbai) is used. The exact distance between the strain gauges are measured thereafter under

travelling microscope.

3.4 CLOSURE

The aim of this chapter is to describe the complete experimental setup, specimen preparation, experimental measurements and the associated data processing. In the experimental setup the rear end of the DCB specimen is screwed to load bar, which is impacted by a striker bar accelerated in the airgun. The stress pulses, which is recorded by two strain gauges bonded on the load bar, is analyzed using one dimensional wave propagation theory to obtain the displacement boundary condition of the cantilever's end. The crack velocity is monitored by bonding three strain gauges on the side face of the DCB specimen ahead of precrack. Finally the preparation of unidirectional glass fibre reinforce epoxy laminate and the specimen are described.

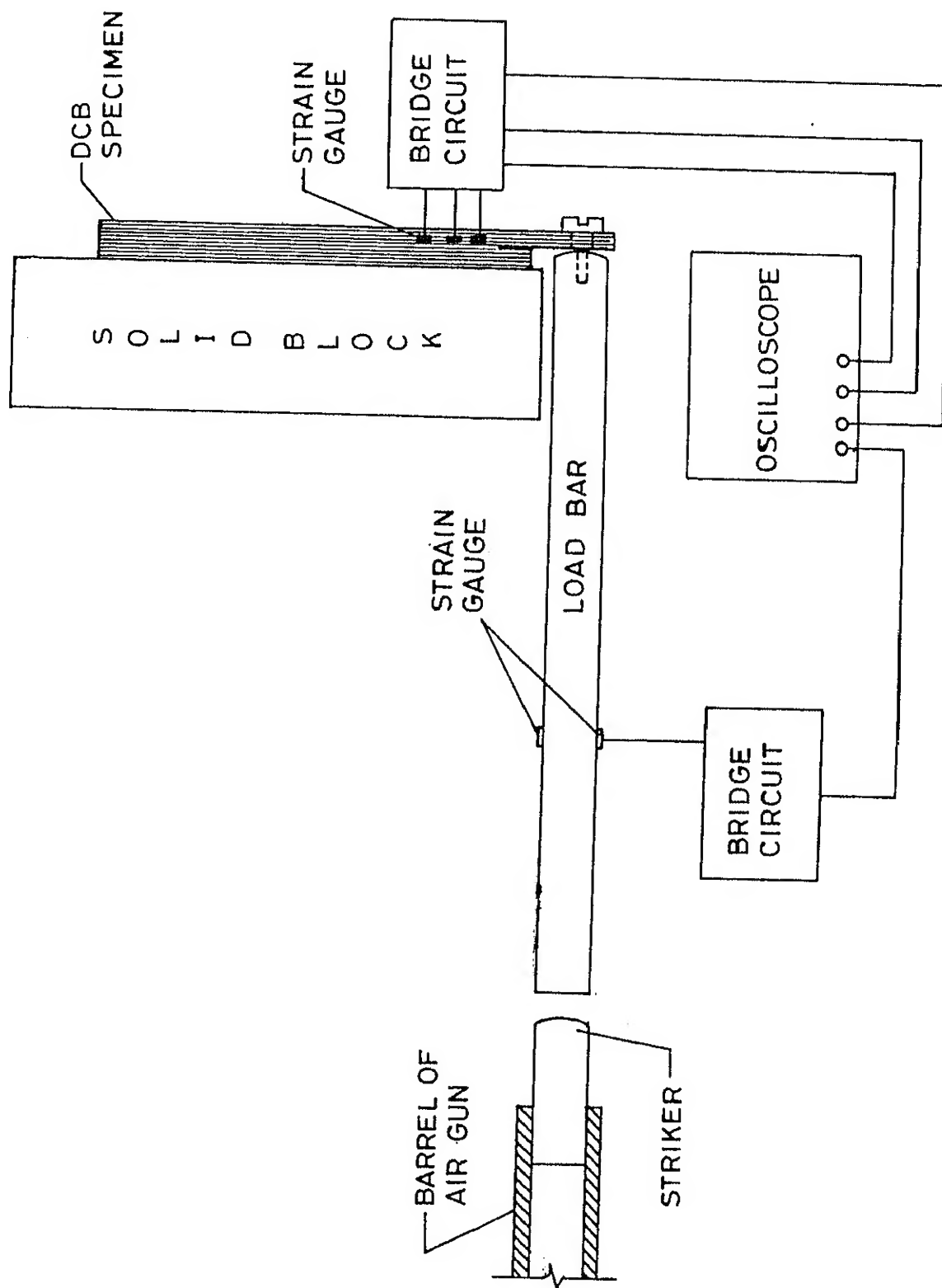


Fig. 3.1 Schematic diagram of the experimental setup.

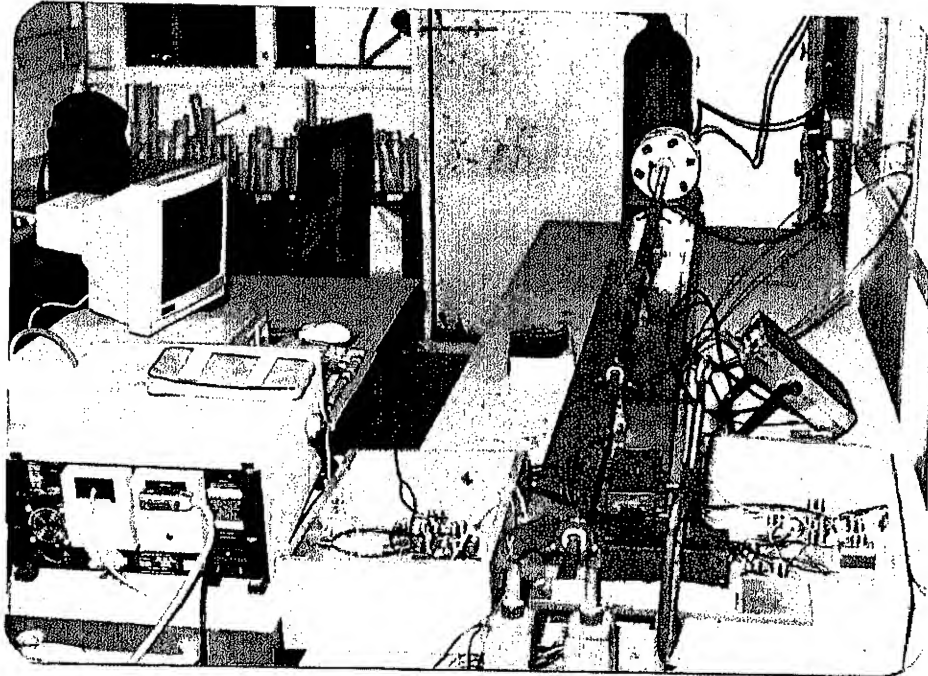


Fig.3.2 Photograph of the experimental setup

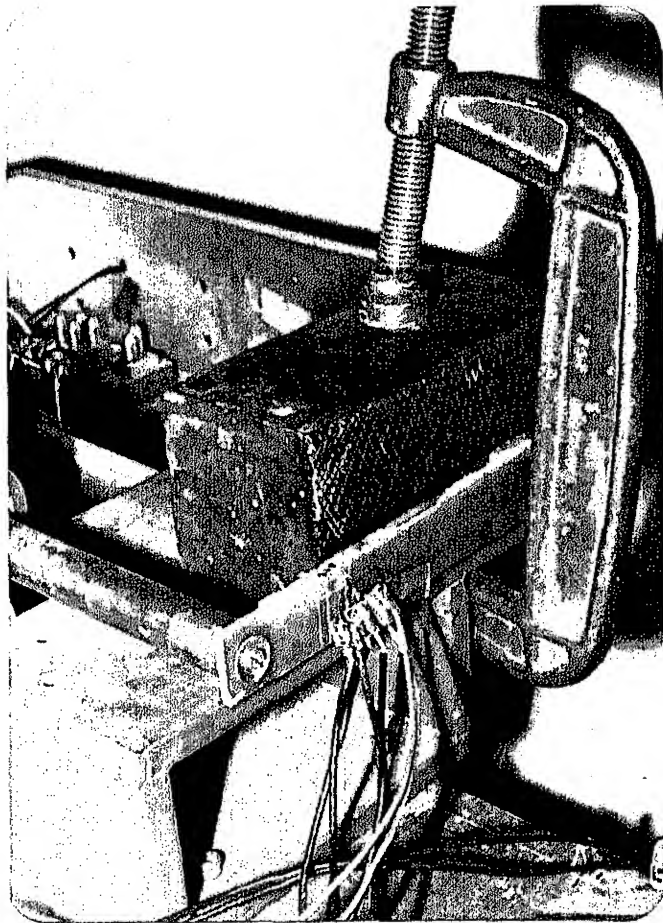


Fig.3.3 Photograph of the blown up view of experimental setup

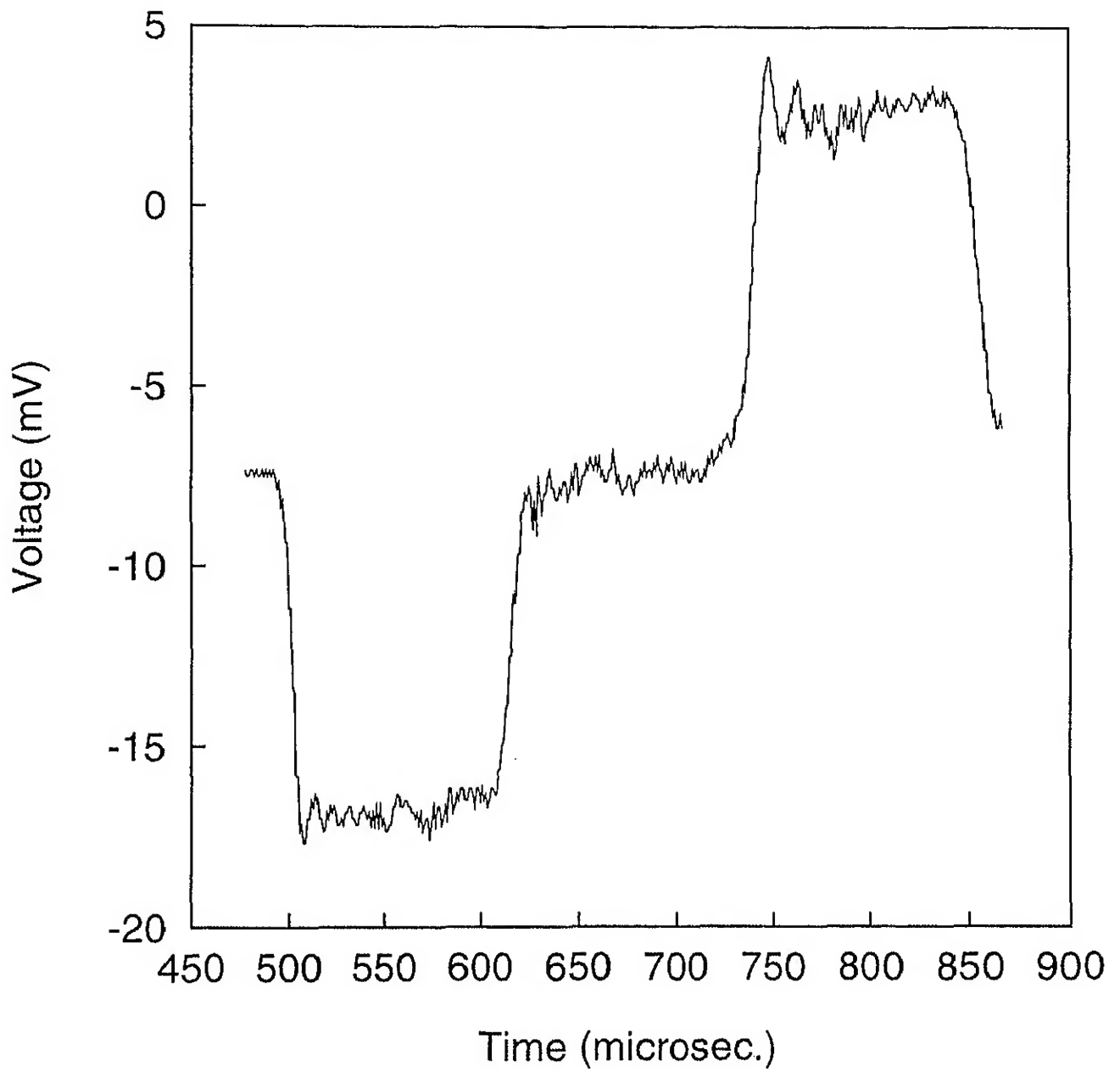


Fig.3.4 A typical record of stress pulses in the load bar

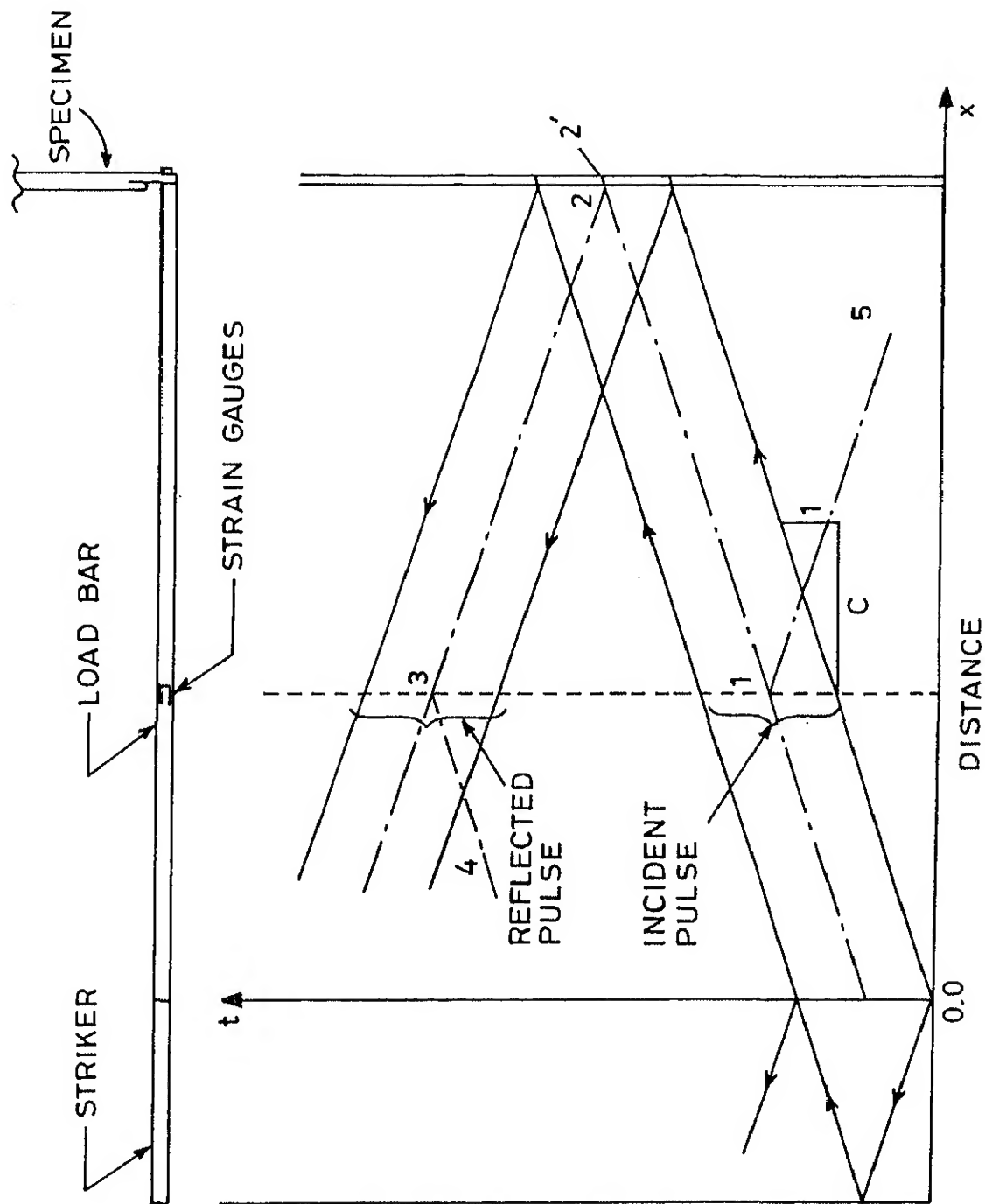


Fig. 3.5 Time-distance ($t-x$) diagram.

R_1, R_3 : ACTIVE GAUGES

R_2, R_4 : DUMMY GAUGES

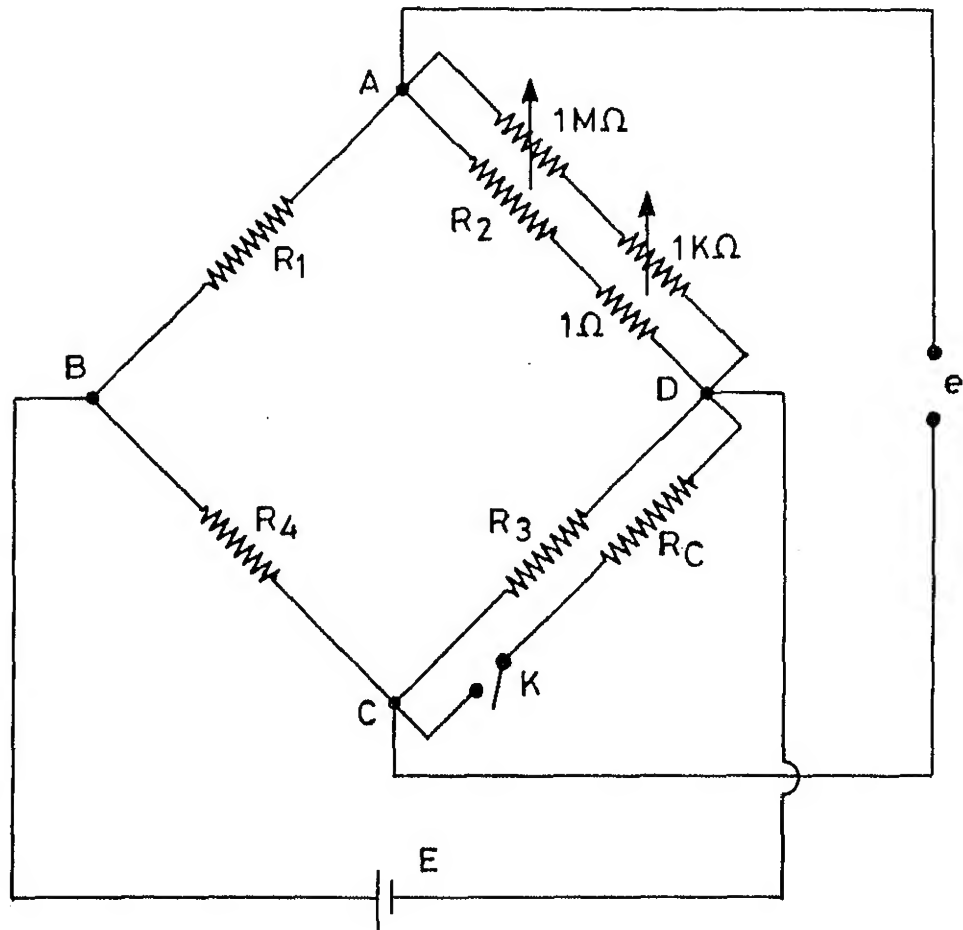


Fig. 3.6 Bridge circuit.

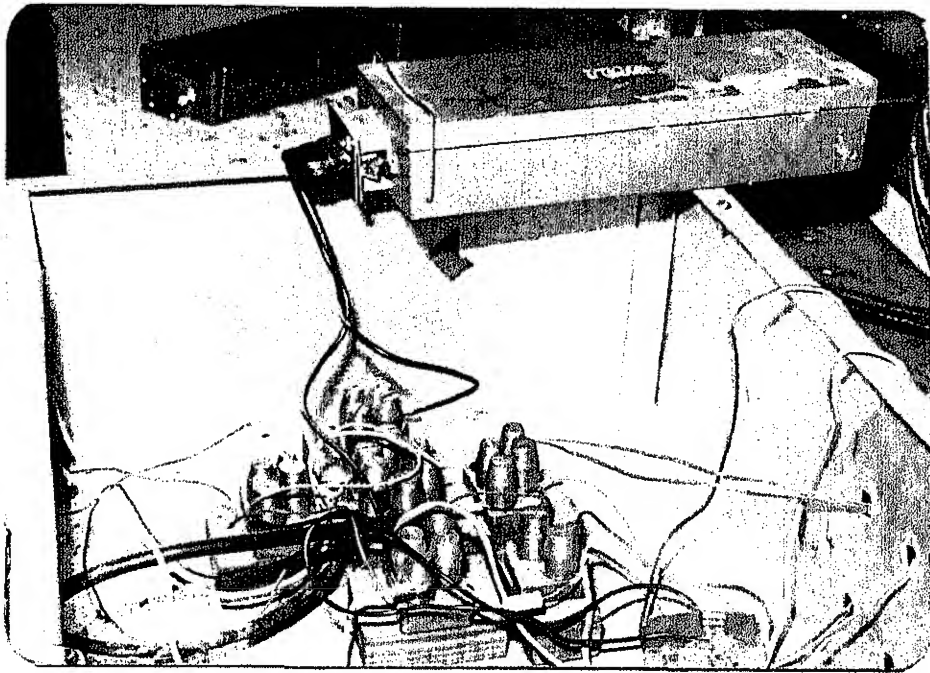


Fig.3.7 Photograph of the bridge circuit

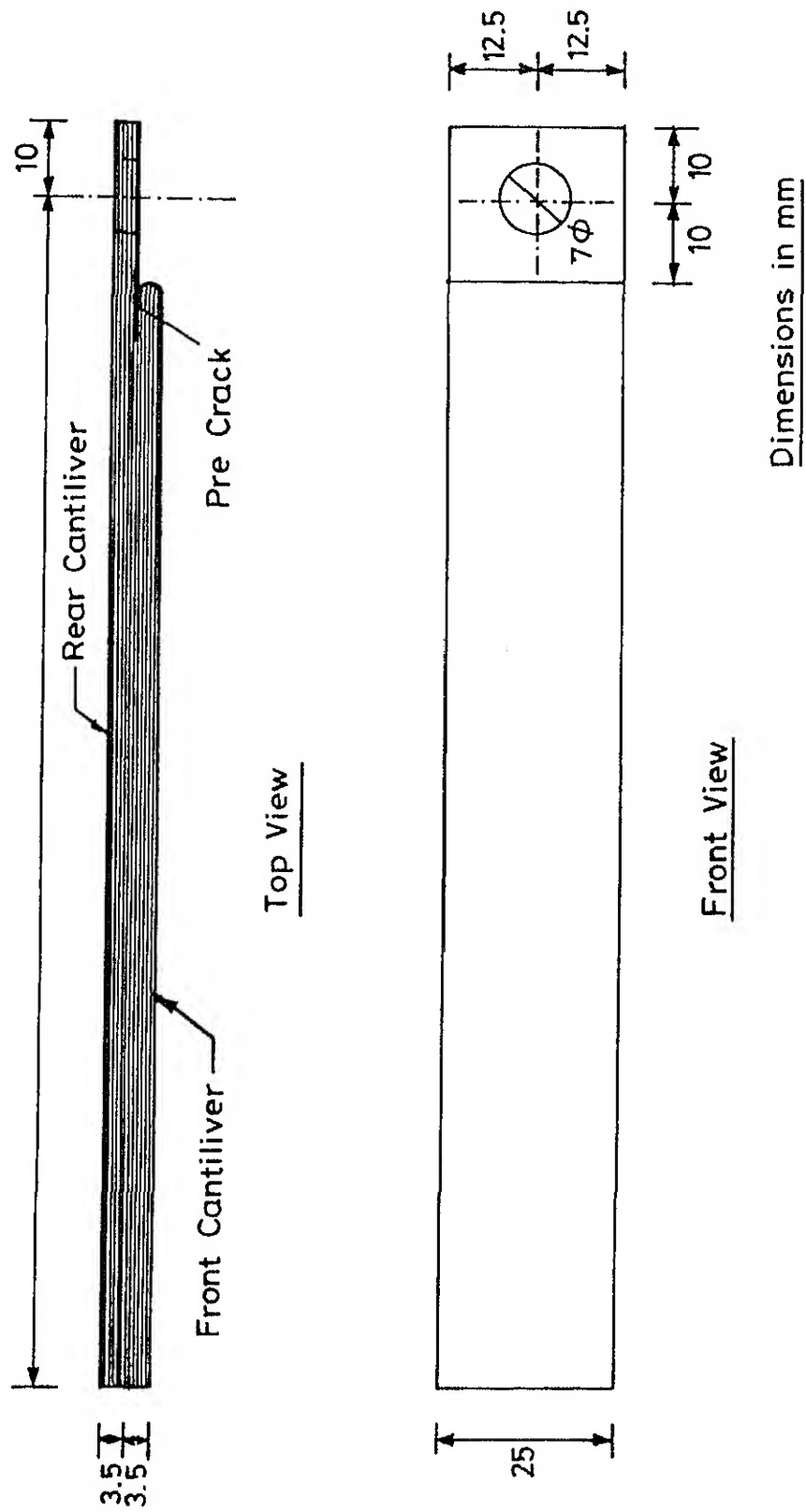


Fig. 3.8 DCB specimen.

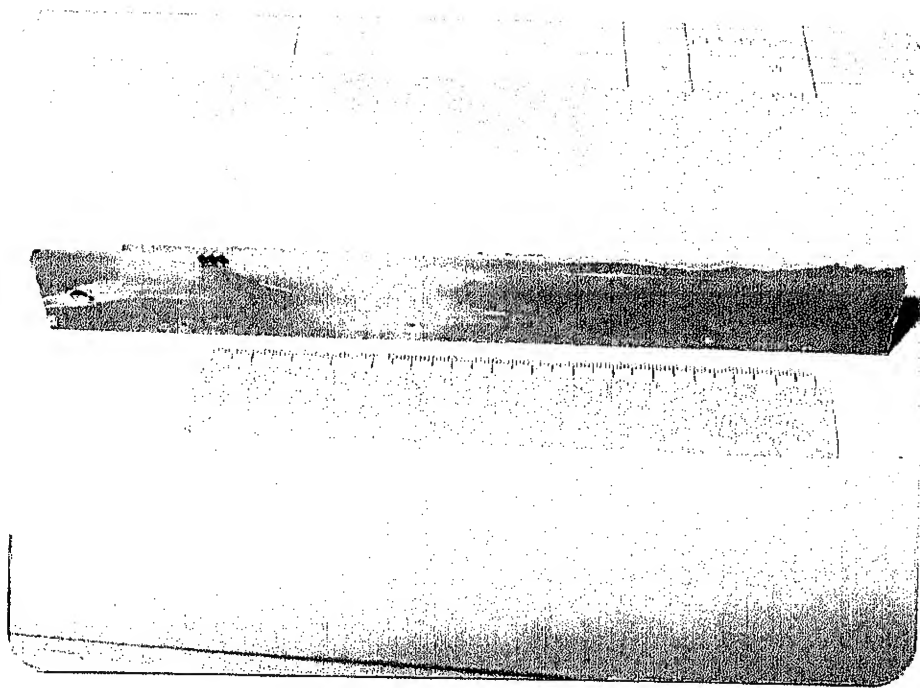


Fig.3.9 Photograph of the DCB specimen

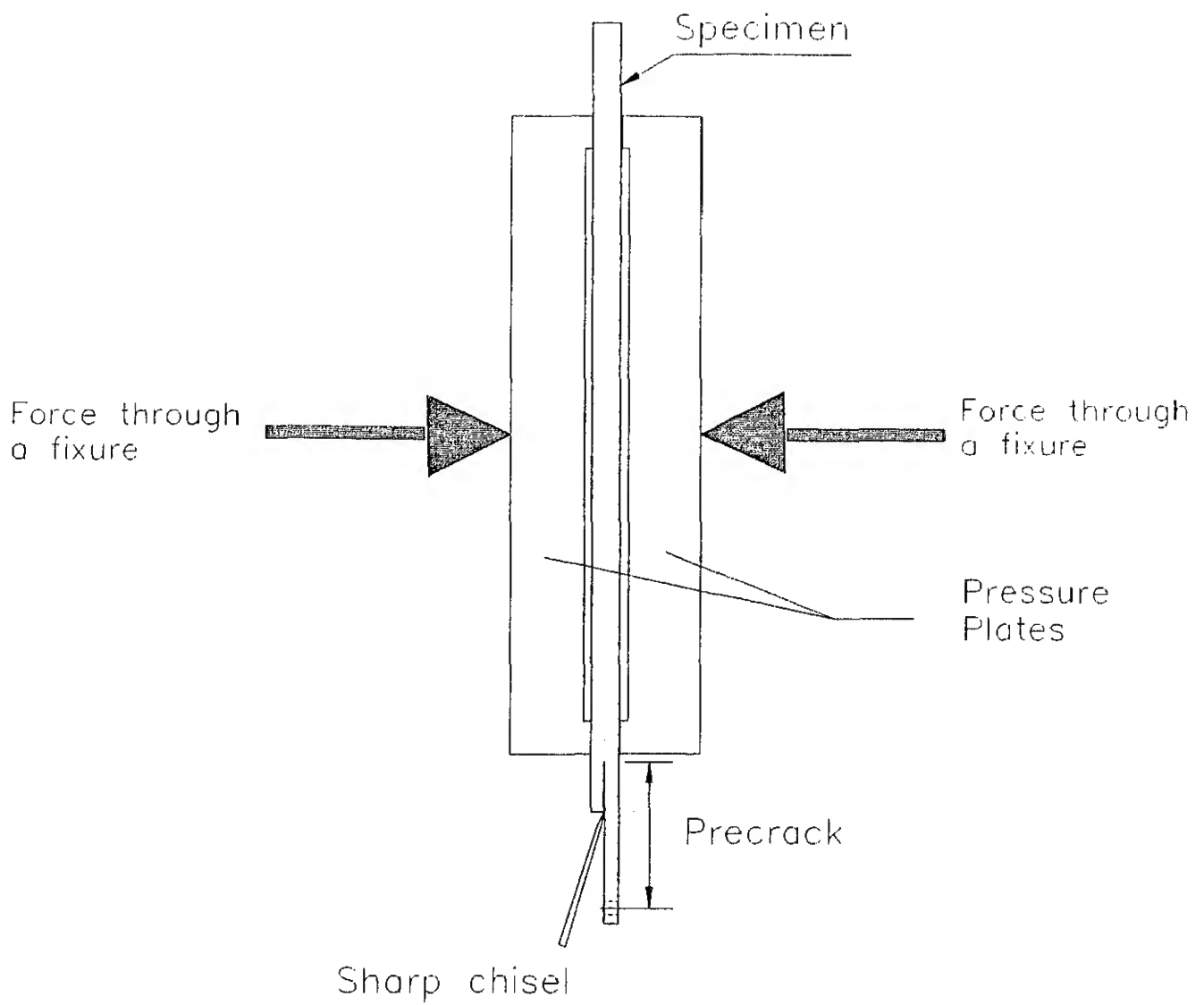


Fig.3.10 Crack sharpening fixture

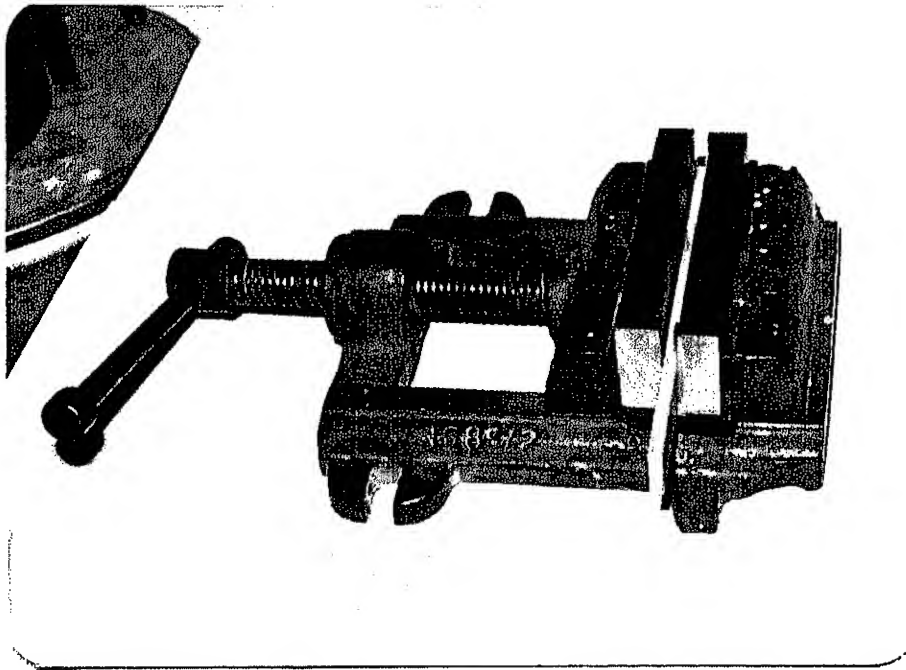
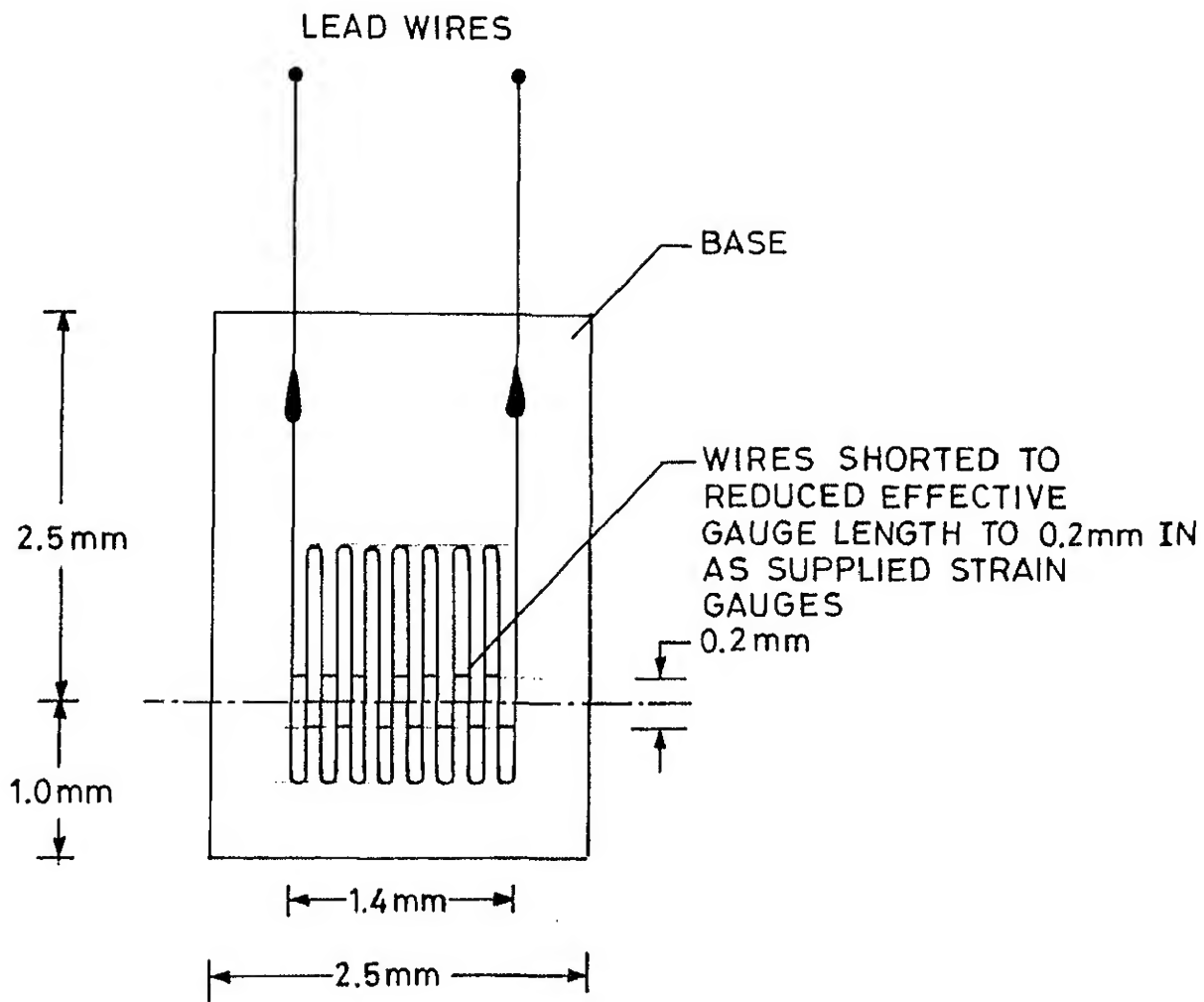


Fig.3.11 Photograph of the crack sharpening fixture



MAGNIFICATION x 20

Fig. 3.12 Schematic diagram of strain gauge of 0.2mm gauge length supplied by Tokyosokki Kenkyujo Co., Ltd., Japan.

CHAPTER-4

RESULTS AND DISCUSSION

4.1 INTRODUCTION

This chapter deals with the experimental results needed to evaluate the dynamic interlaminar initiation and propagation toughness of DCB specimen through experimental-cum-numerical technique. The input required for the evaluation of J-integral from the finite element programme are (i) The deflection of cantilever end with time (ii) The crack initiation time (iii) The crack propagation history. In the impact setup, as discussed in chapter 3, the load bar imparts impact energy (Fig.2.1) to end of rear cantilever of the DCB specimen and the strain gauges mounted on the side face of rear cantilever monitors the crack velocity. The deflection of the cantilever end with respect to time is obtained analyzing the incident and reflected pulses in the load bar as discussed in Sec.3.3.3.

The location of strain gauges ahead of the crack tip is premeasured accurately and the time at which the peak appears on strain gauge record, can be obtained from the oscilloscope trace. A relation is thus obtained between the crack location and the time. The crack initiation time is obtained by extrapolating the fitted curve to initial crack length. The slope of this curve gives crack velocity.

4.2 RESULTS OF INTERLAMINAR INITIATION TOUGHNESS

A total of 5 experiments are conducted to determine the interlaminar initiation toughness and propagation toughness. Out of which Expts.1-3 were conducted with a precrack in the range of 43.5-46.5mm and Expts.4-5 were with a precrack in the range

of 30-34mm. The details of crack length and strain gauge locations for different specimens are given in Table 4.1.

Table 4.1 Length of precrack in the DCB specimen and strain gauge locations for Expt. 1 to 5.

Expt. No.	Crack Length (mm)	First* Strain Gauge Location (mm)	Second** Strain Gauge Location (mm)	Third*** Strain Gauge Location (mm)
1	46.5	3.0	3.1	2.71
2	43.5	3.0	3.6	4.00
3	44.0	5.0	2.9	2.40
4	30.0	2.05	2.41	2.36
5	34.0	2.6	2.32	2.49

* distance measured from the crack tip

** distance measured from the first strain gauge

*** distance measured from the second strain gauge

Experimental No. 1

The oscilloscope trace for Expt. 1 is shown in Fig 4.1. Channel 1 gives the record of incident and reflected pulses in the load bar. Channels 2, 3, and 4 give the records of the strain gauges mounted on the side face of the cantilever ahead of the crack tip of the specimen. The duration of the square incident pulse is nearly $130 \mu s$. The velocity of the load bar end vs. time plots (Fig. 4.2(a)) were obtained from the incident and reflected pulses as described in Sec. 3.3.3. When the velocity of load bar end vs. time plot is integrated with respect to time, it gives the displacement of the load bar end face with time. This displacement is equivalent to the deflection of cantilever end as shown in Fig. 4.2(b), because the load-bar-end is screwed to the cantilever end. The loading of the cantilever starts at the time corresponding to midpoint of the head of the incident pulse and head of the reflected pulse. This is denoted as 'REFERENCE' in the Fig. 4.1.

The first strain gauge on the specimen is mounted 3.0 mm ahead of the crack tip and to determine the initiation time, the response of all the three strain gauges are considered. A magnified view of the three strain gauges readings is shown in the Fig. 4.3. The crack length as a function of time is plotted in the Fig. 4.4(a). A second degree polynomial is fitted through three data points and extrapolated to the initial length of the crack, it provides the initiation time as 52.8 μ s. The variation of crack velocity with respect to time (Fig. 4.4(b)) is obtained by differentiating crack length vs. time curve. The crack velocity decreases from a higher value of 850 m/s at the initial crack tip to 105 m/s at the third strain gauge location.

The finite element code (Chapter 2) was executed using the displacement boundary conditions given by Fig. 4.2(b). The variation of J-integral with respect to time was obtained as shown in Fig. 4.5. The initiation toughness was obtained corresponding to the initiation time as shown in the figure. The initiation toughness for Expt. 1 is 230 J/m².

Experiment Nos. 2-3

The details of initiation time and initiation toughness (J_{ini}) is given in Table 4.2 for Expt. 1 to 5.

Table 4.2 Crack lengths, time at different gauges, initiation time and initiation toughness for Expt. 1 to 5.

Exp No.	Crack Length (mm)	1st SG from C-tip (mm)	Time* of strain gauge peak (μ s)			Init. Time# (μ s)	J_{init} (J/m ²)
			SG1	SG2	SG3		
1	46.5	3.0	55.8	58.86	69.60	52.80	230
2	43.5	3.0	55.6	59.66	65.03	52.20	145
3	44.0	5.0	46.5	50.0	54.0	43.00	102
4	30.0	2.05	39.5	42.25	47.17	37.10	123
5	34.0	2.66	44.2	46.90	51.90	39.00	91

SG1 - First Strain Gauge on the Specimen

SG2 - Second Strain Gauge

SG3 - Third Strain Gauge

C-tip - Crack Tip

Init. Time - Initiation time

* measured with respect to starting of loading of cantilever

by extrapolation

J_{init} = Initiation toughness

Similar to Expt. 1, the oscilloscope records and processed data of boundary conditions at the cantilever end and crack velocity variation are shown for Expt. 2 in Figs. 4.6 to 4.9. From the initiation time obtained through Fig. 4.8(a), the J_{init} toughness is determined in Fig. 4.9 as 145 J/m².

Figures 4.10 to 4.13 provide the details of experimental records and processed data for Expt. 3. The initiation toughness obtained for this experiment (J_{init}) is 102 J/m².

Experiment No. 4-5

These experiments were conducted with low impact velocity and with smaller precrack length compared to Expt. Nos.1-3.

Similar to earlier experiments, Figs.4.14-4.11 and Figs.4.18-4.21 provides the details of experimental records and processed data for Expt.4 and Expt.5 respectively. The value of J-integral for Expt.4 was found to be 123 J/m^2 , and for Expt.5 was found to be 91 J/m^2 .

4.3 RESULTS OF INTERLAMINAR PROPAGATION TOUGHNESS

For determining the interlaminar propagation toughness (J_{prop}) the input to the finite element code consists of the variation of crack length with time, apart from the cantilever end deflections with time. While executing the FE code, the crack propagation algorithm is called after the initiation time for the crack propagation analysis. As presented earlier for the initiation toughness of different experiments, here also results of Expt.1 is discussed in detail and then the results for other experiments are highlighted whenever necessary.

Experiment 1

As discussed by Verma[1996], once the FE code is executed upto the time of crack initiation, the crack propagation module is called. The advancement of crack in each iteration is to be known so that an appropriate factor can be applied to the holding back force for modelling the crack propagation. The advancement of crack in each iteration is calculated, as discussed in Sec. 2.4 of chapter 2, by the second degree polynomial fitted through the three data points of peak response of the strain gauges. Using the boundary conditions and the crack propagation data, the dynamic FE analysis determine the stress/strain field in the specimen in successive time steps. Then the variation of J-integral with time is obtained as shown in Fig. 4.22. In the beginning the crack remain stationary upto the initiation time and J-integral increases. A stage is reached at the initiation time when the crack tip starts growing under the known dynamic displacement boundary conditions. The computer code provides the J-integral for the measured crack velocity. Fig. 4.23 shows the magnified view of the J-integral of the crack moving at high speed.

The sharp drop in J-integral occurs because, as the crack starts moving, a large amount of energy is consumed to accelerate the crack. Once the crack is accelerated to a high speeds J-integral drops down to a low value, because with decreasing crack velocity the energy required to move the crack is less. The value of the J-integral for the propagating crack, for this case, is varying between 15-50 J/m². The oscillatory behaviour of J-integral, as explained by Verma[1996], is due to several reasons. First the free surfaces of DCB specimen are very close to the crack tip. In fact, propagation time for some stress waves to emanate from the crack tip and return to the tip are as small as 1-2 μ s. The superpositions of the these waves and their effect on \hat{J} -integral will provide ripples. Second in the finite element modelling, the crack tip is moved from one point to other point in discrete steps by linearly decreasing holding back force. Thus, the FE code may not be simulating the crack propagation behaviour very accurately. Stress/strain field near the tip may be oscillating resulting into oscillatory behaviour of J_{prop} . Release of node forces have been improved over the models of other investigators by employing three node points rather than two. It is recommended that in future node release mechanism may be further improved to rule out the effect of simulation, if any.

Experiment Nos 2-5

The variation of J-integral with time of Expt. 2 for stationary crack and propagating crack is shown in Fig. 4.24 and the magnified view of propagation phase for the same experiment is shown in Fig. 4.25. In this case, it can be observed that the J-integral drops sharply initially once the crack start propagating similar to the Expt. 1. The value of the J-integral for propagating crack of this experiment is 1-30 J/m².

Variation of the J-integral with time for Expt.3 is shown in Figs. 4.26 and 4.27. In this case J-integral drops to a low value very sharply compared with other cases. The crack velocity in this case (Fig.4.12) is very high compared with other experiments. The faster the crack speed, the more is the radiated kinetic energy and bigger the drop of J-integral value. The negative value of J_{prop} is not understood. At very high crack speed, crack propagation simulation may not be working well.

The history of J-integral for Expts. 4 and 5 are shown in Figs. 4.28 to 4.31. Their behaviour is similar to that of Expts. 1 and 2.

The average crack velocities between first and second gauge and second and third strain gauge and the initiation toughness are given in Table 4.3 for all the five experiments.

Table 4.3 Crack velocity, initiation toughness and propagation toughness for Expt.1 to 5.

Expt. No.	Length of pre-crack (mm)	Average Crack Velocity (m/s)		J_{init} (J/m ²)
		\dot{a}_1^*	$\dot{a}_2^\#$	
1.	46.5	622	361	230
2.	43.5	898	743	145
3.	44.0	1016	751	102
4.	30.0	730	572	118
5.	34.0	734	543	91

* Average crack velocity between first and second strain gauge

Average crack velocity between second and third strain gauge

J_{prop} Propagation toughness

4.4 COMPARISON OF DYNAMIC INTERLAMINAR TOUGHNESS WITH QUASISTATIC INTERLAMINAR TOUGHNESS

Inorder to compare the J-integral under dynamic loading with quasistatic interlaminar toughness, three experiments were conducted to determine the quasistatic interlaminar toughness. The table 4.4 gives the values of quasistatic interlaminar toughness (G_{ic}).

Table 4.4 Quasistatic interlaminar toughness for Expt. Q1 to Q3.

Expt. No.	Quasistatic Interlaminar Toughness (G_{Ic}), J/m ²
Q1	423
Q2	344
Q3	478

It is observed from the table 4.4, that the quasistatic interlaminar toughness, which is varying between 344-478 J/m², is significantly higher than that of the dynamic fracture toughness, which is varying between 91-230 J/m², obtained for different experiments. It is important to characterize the interlaminar fracture toughness under dynamic crack propagation in composite laminates so as to maximize its performance level.

4.5 CLOSURE

The aim of this chapter was to find out the initiation toughness and propagation toughness of interlaminar cracks in glass fibre reinforced epoxy laminates. The experimental measurements, consists of cantilever end deflection with respect to time, crack propagation history and crack initiation time, are used as input to the FE code to simulate the dynamic fracture behaviour of the FRP laminate. The initiation toughness was found to vary between 91-230 J/m² and the propagation toughness was found to vary between 1-50 J/m². Inorder to compare the toughness under dynamic conditions with that under static conditions, the value of quasistatic interlaminar toughness was found to vary between 344-478 J/m².

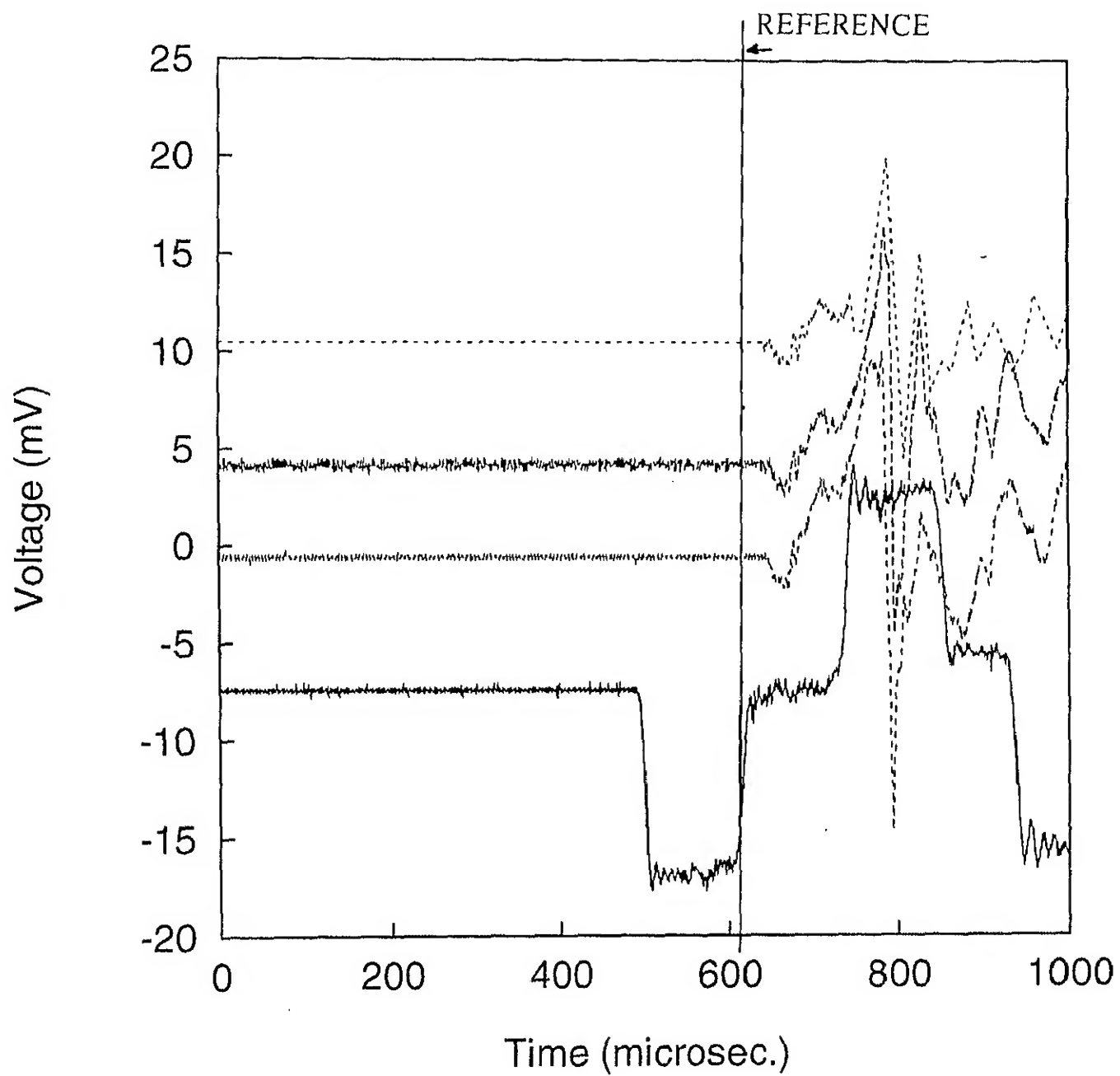


Fig.4.1 Oscilloscope traces of Expt.-1

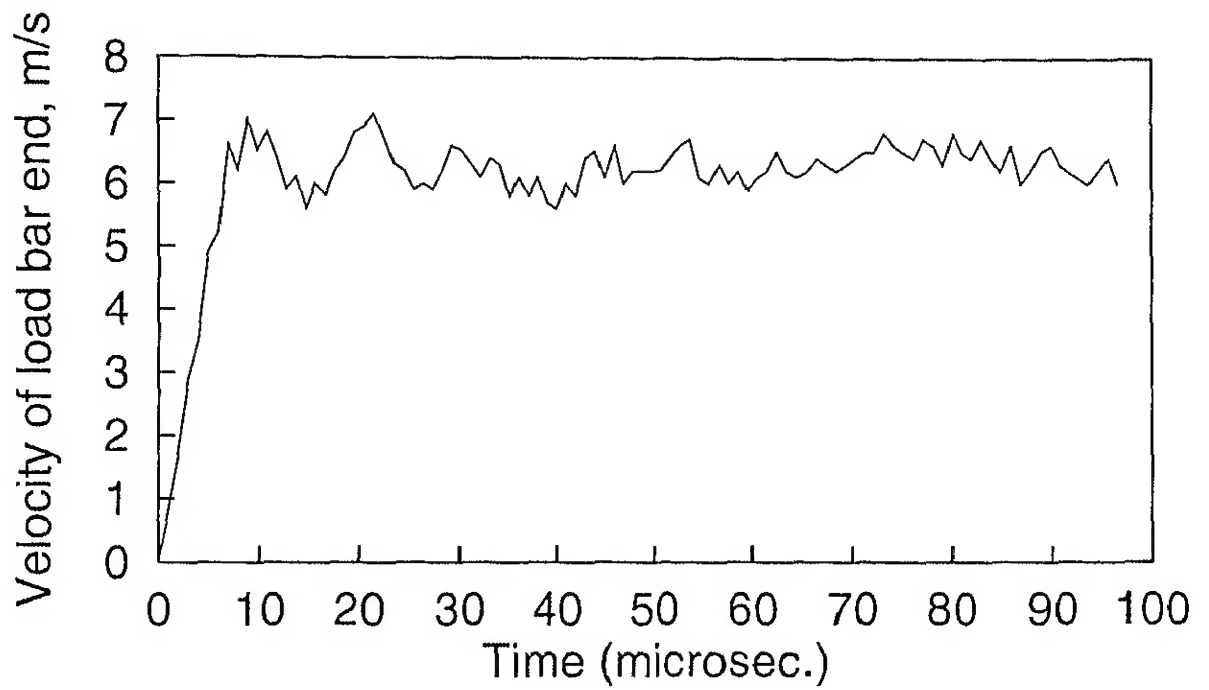


Fig.4.2(a) Velocity input at the cantilever end of the specimen obtained through incident and reflected pulses of the load bar for Expt.-1

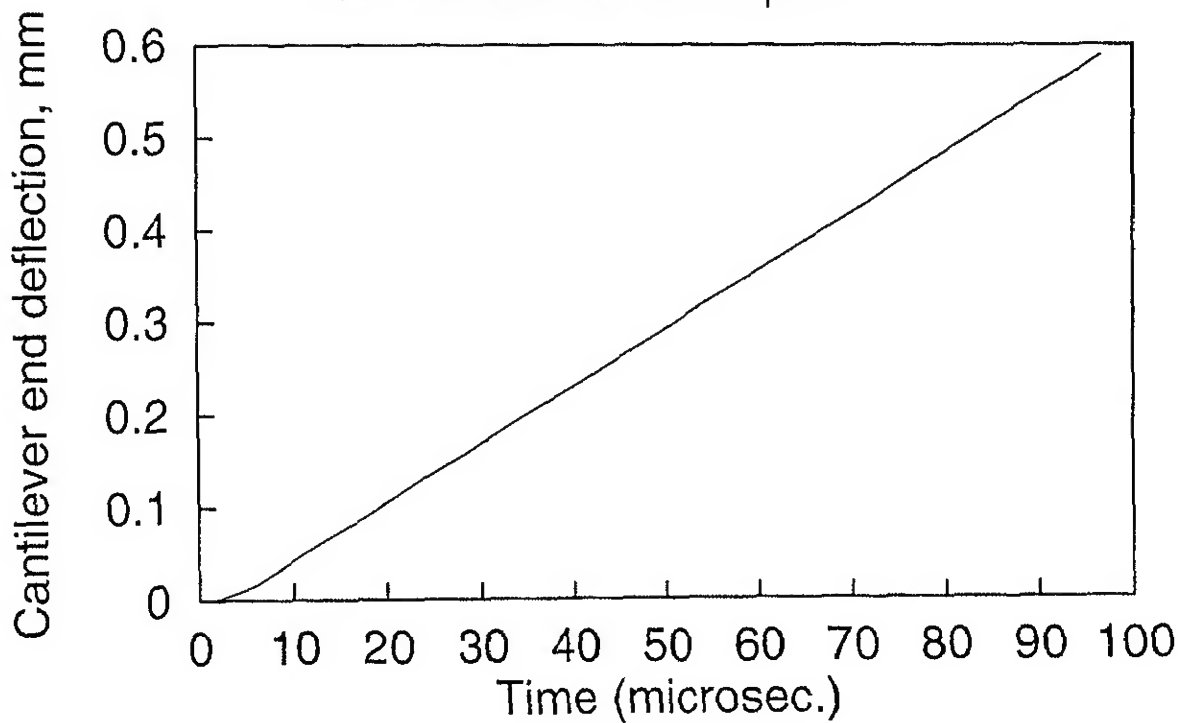


Fig.4.2(b) Cantilever end deflection vs time obtained by integrating the velocity input curve

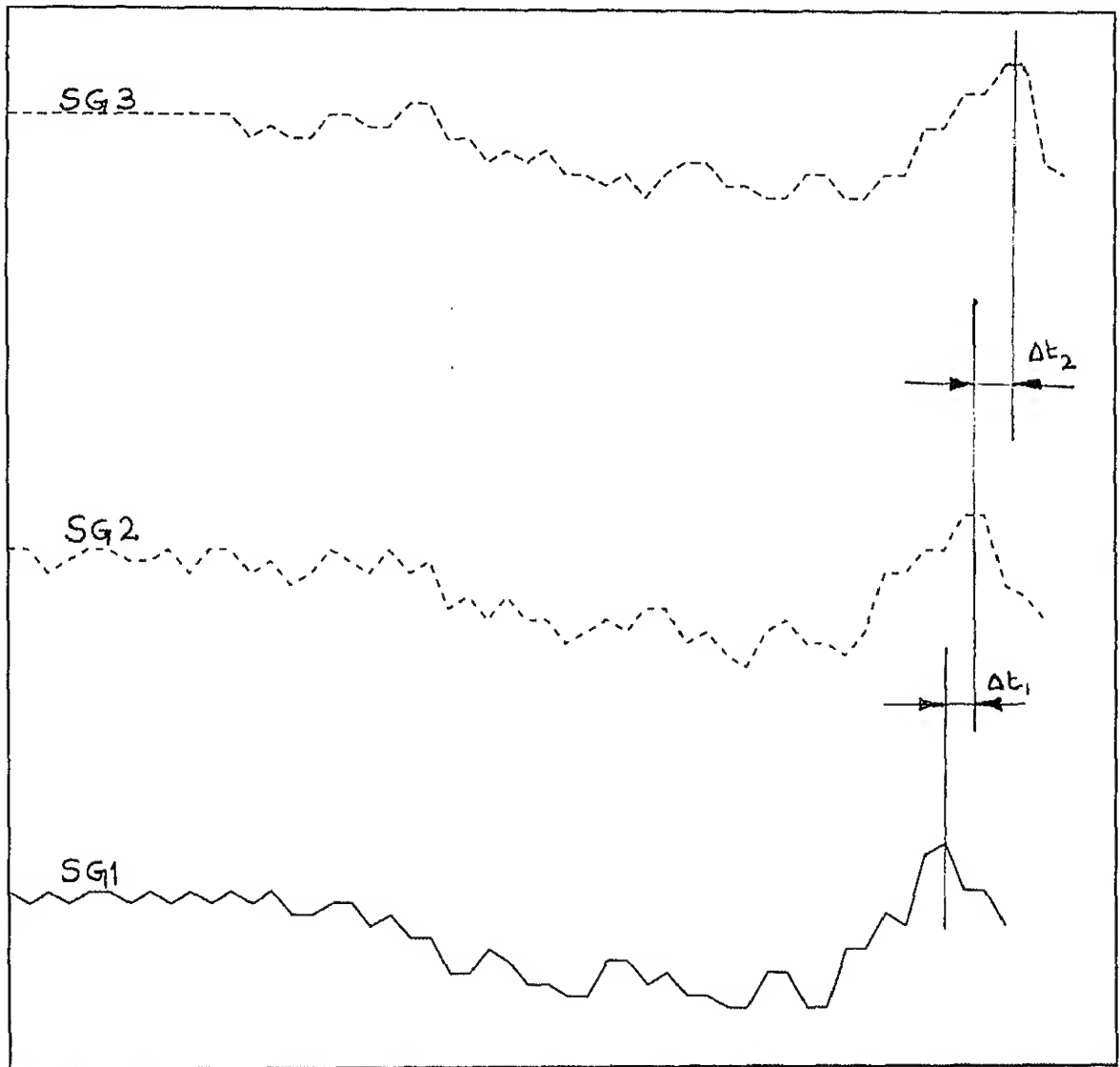


Fig.4.3 Blown up view of the recorded peak responses of strain gauges bonded to the specimen

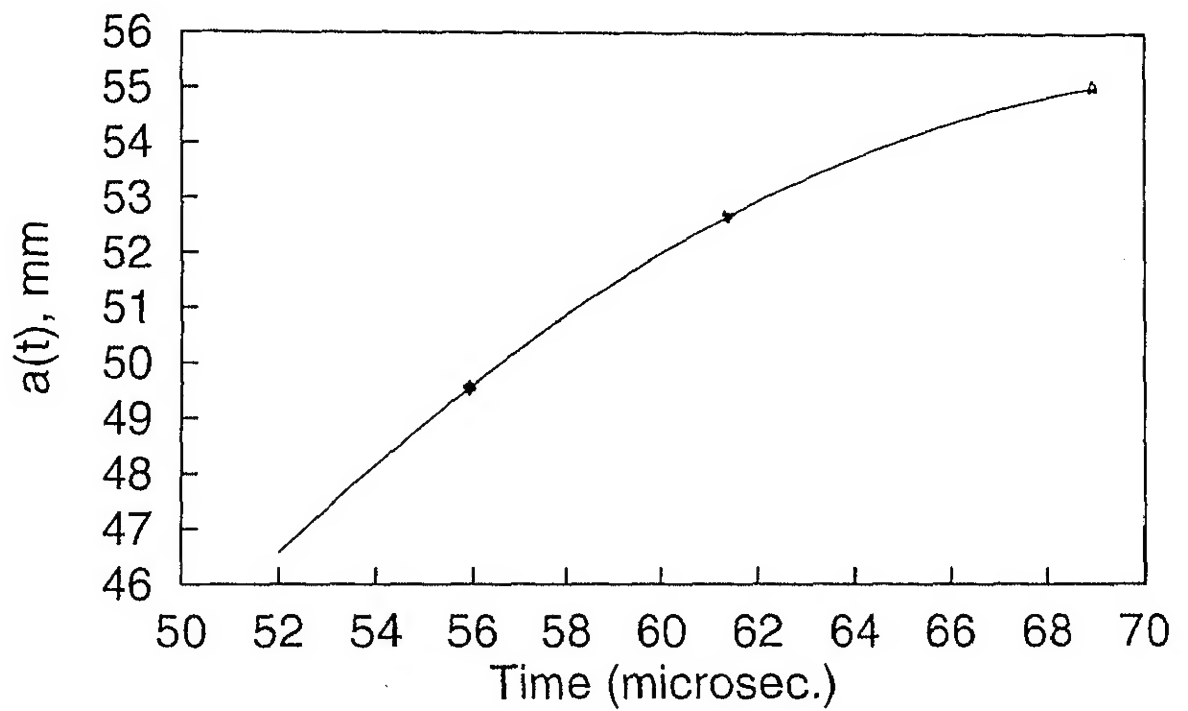


Fig.4.4(a) Variation of crack length with time of Expt.-1 showr with interpolation upto the length of precrack

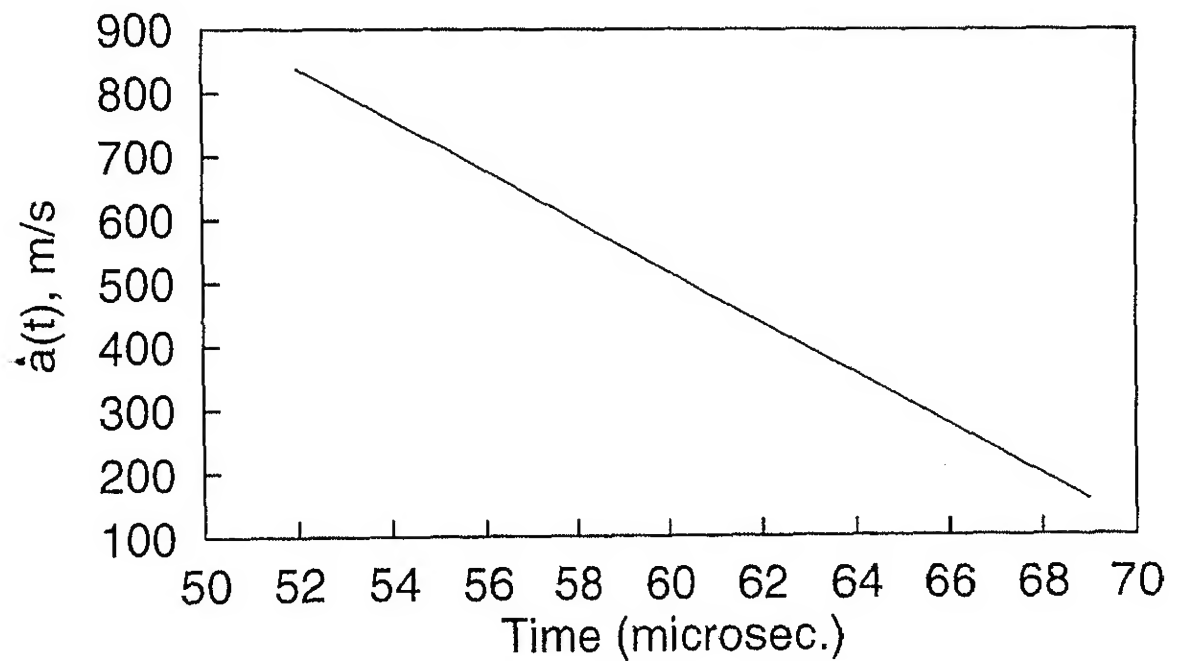


Fig.4.4(b) Variation of crack propagation speed with time obtained by differentiating the crack length vs time curve

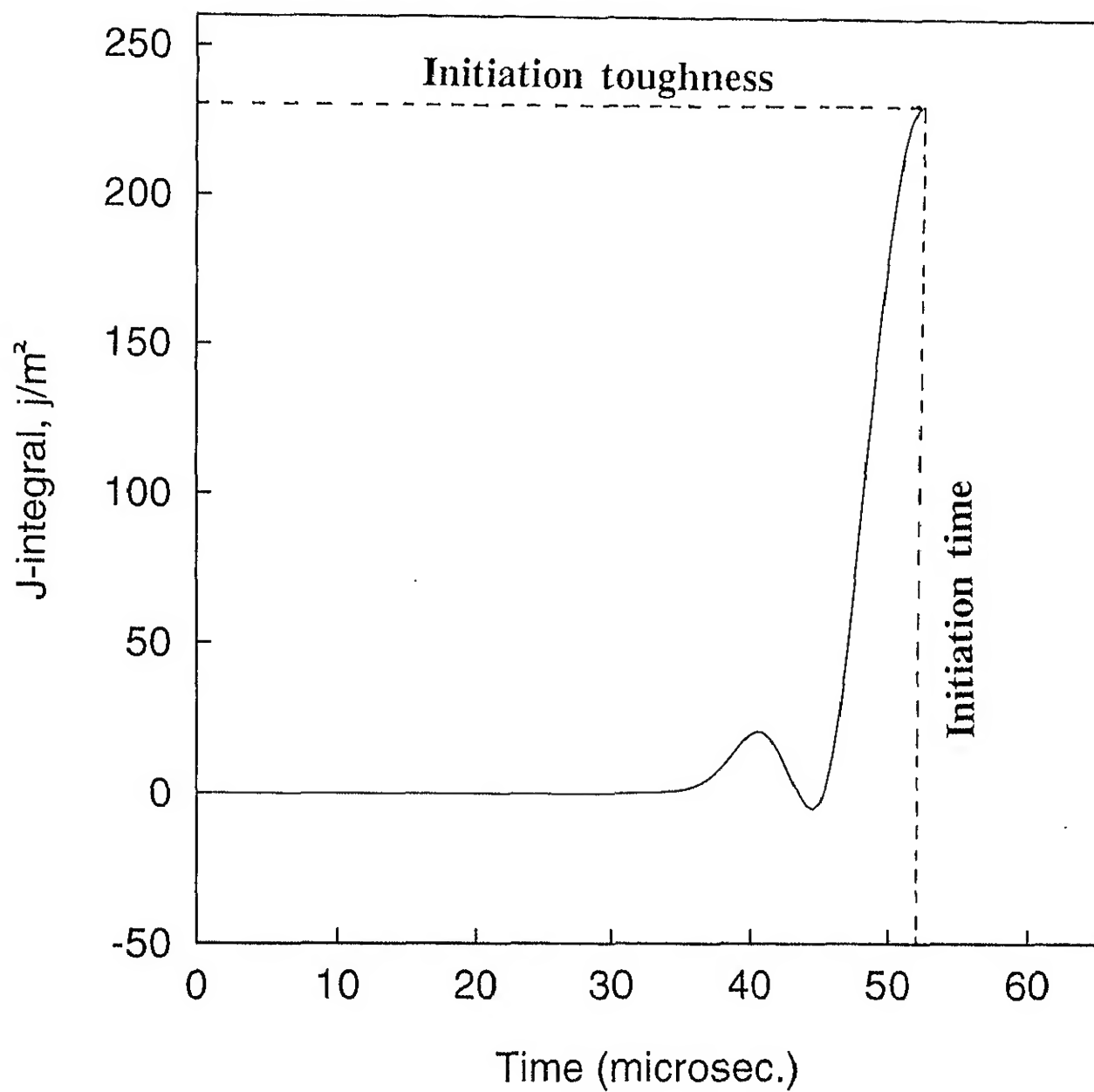


Fig.4.5 Initiation Toughness of Expt.-1

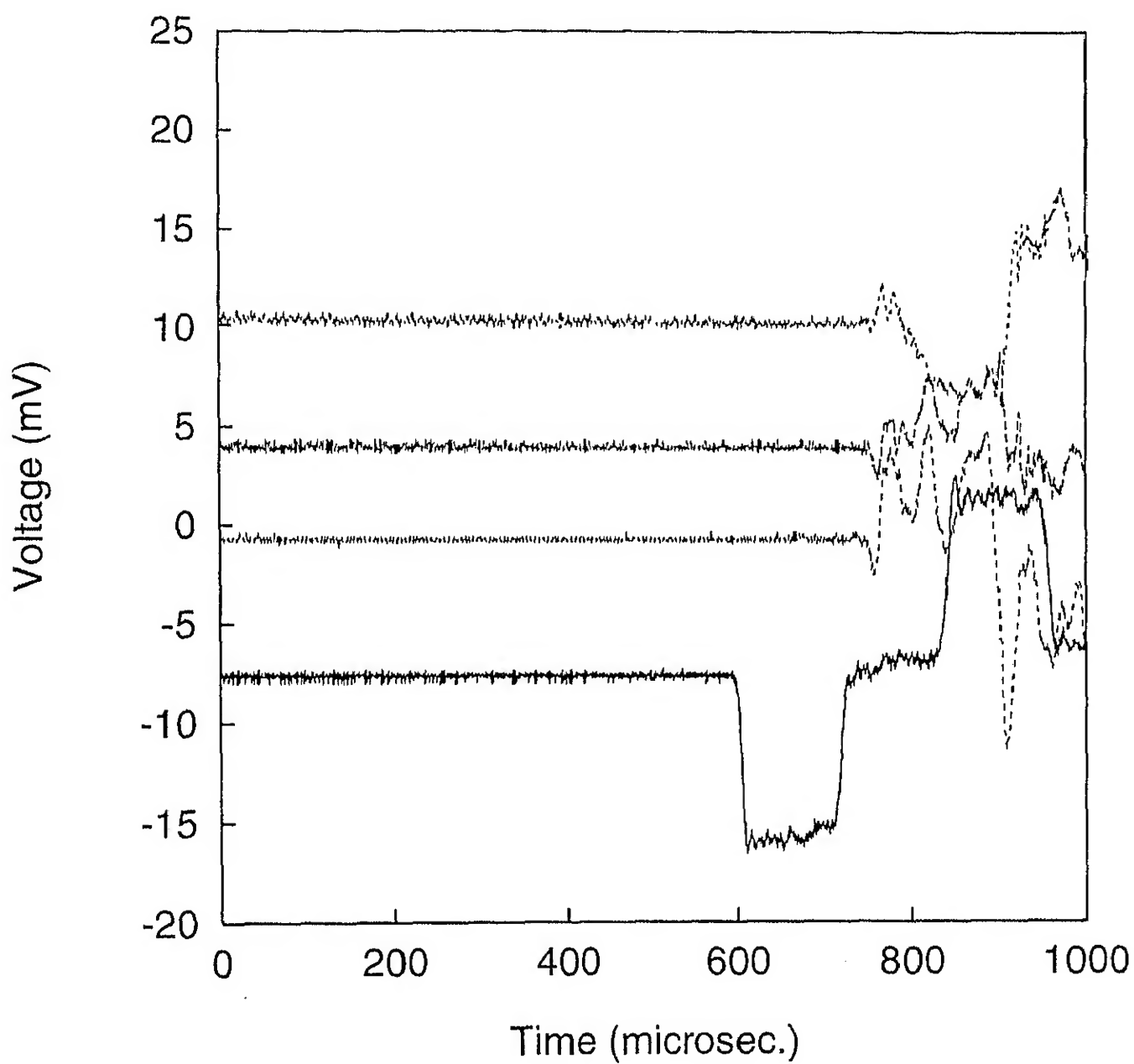


Fig.4.6 Oscilloscope traces of Expt.-2

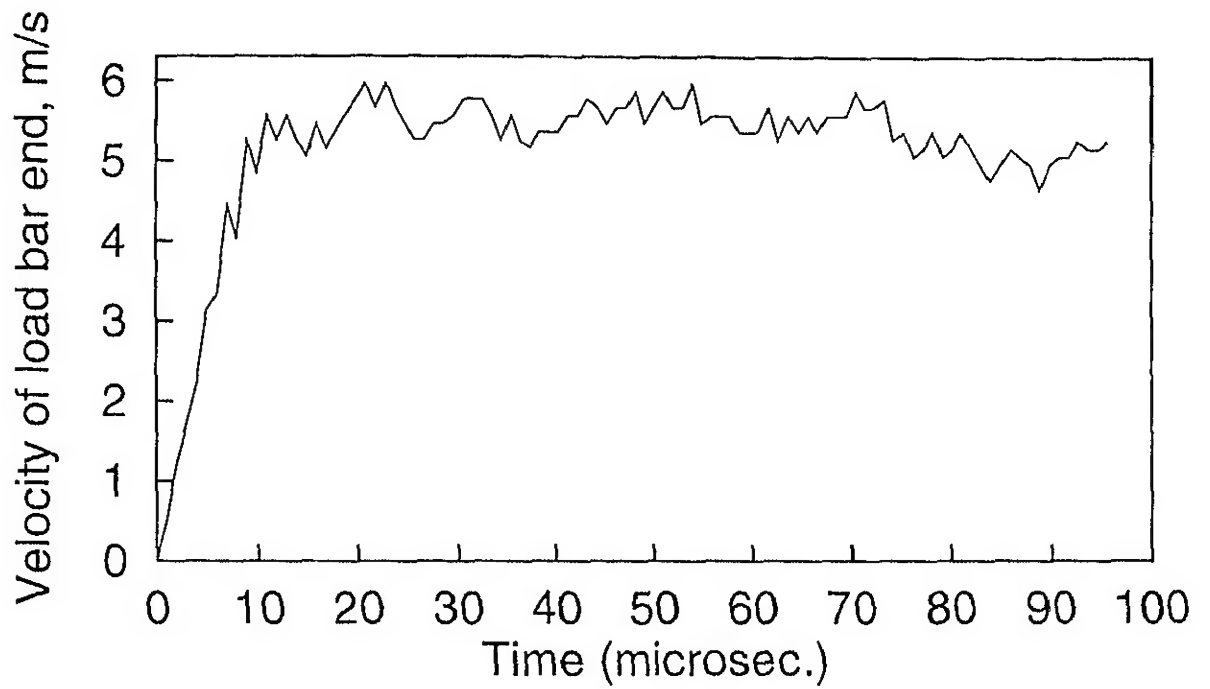


Fig.4.7(a) Velocity input at the cantilever end of the specimen obtained through incident and reflected pulses of the load bar for Expt.-2

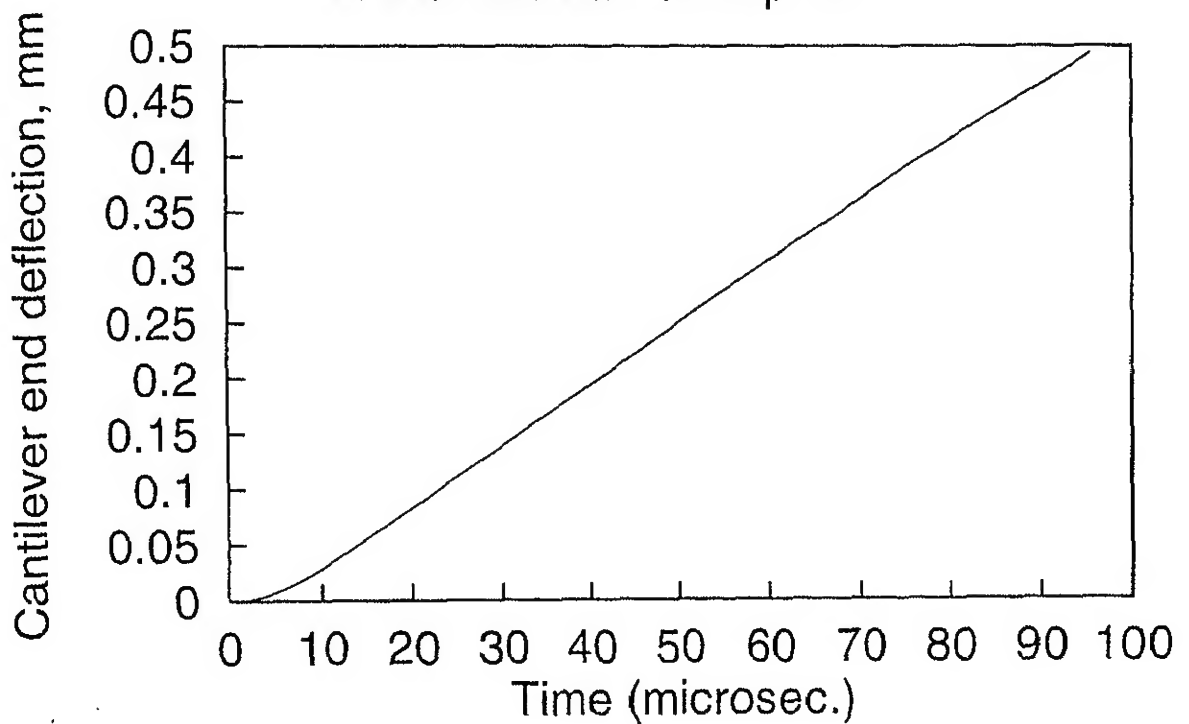


Fig.4.7(b) Cantilever end deflection vs time obtained by integrating the velocity input curve

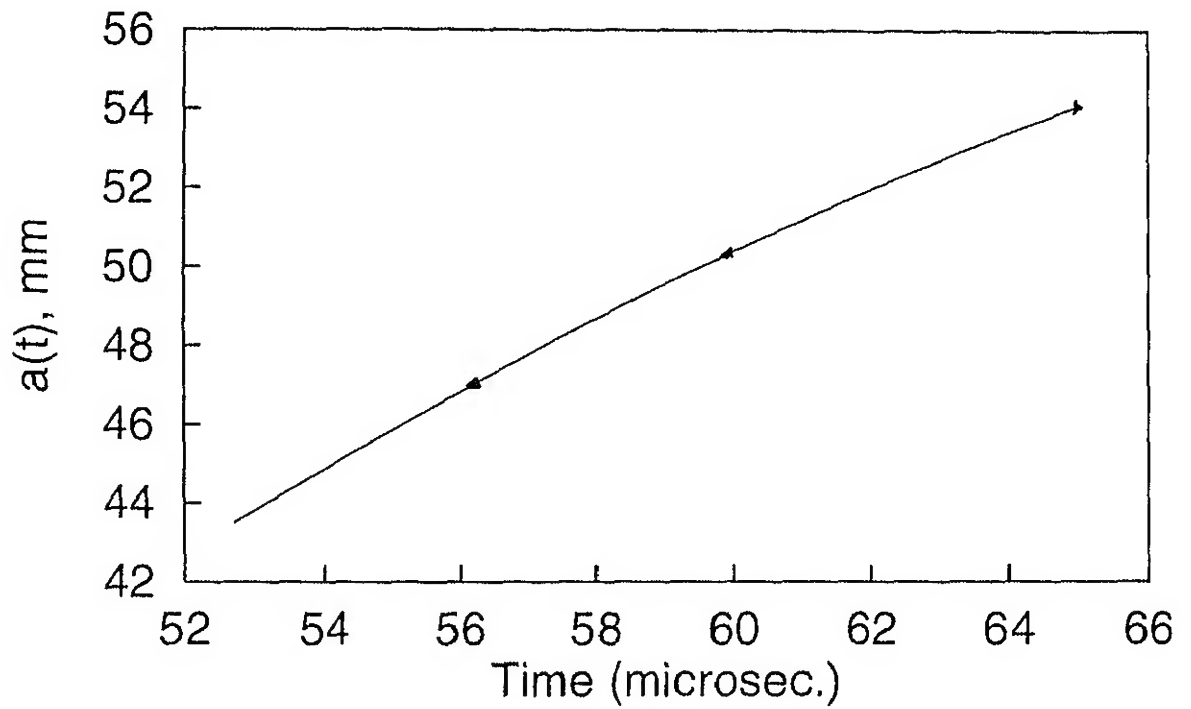


Fig.4.8(a) Variation of crack length with time of Expt.-2 shown with interpolation upto the length of precrack

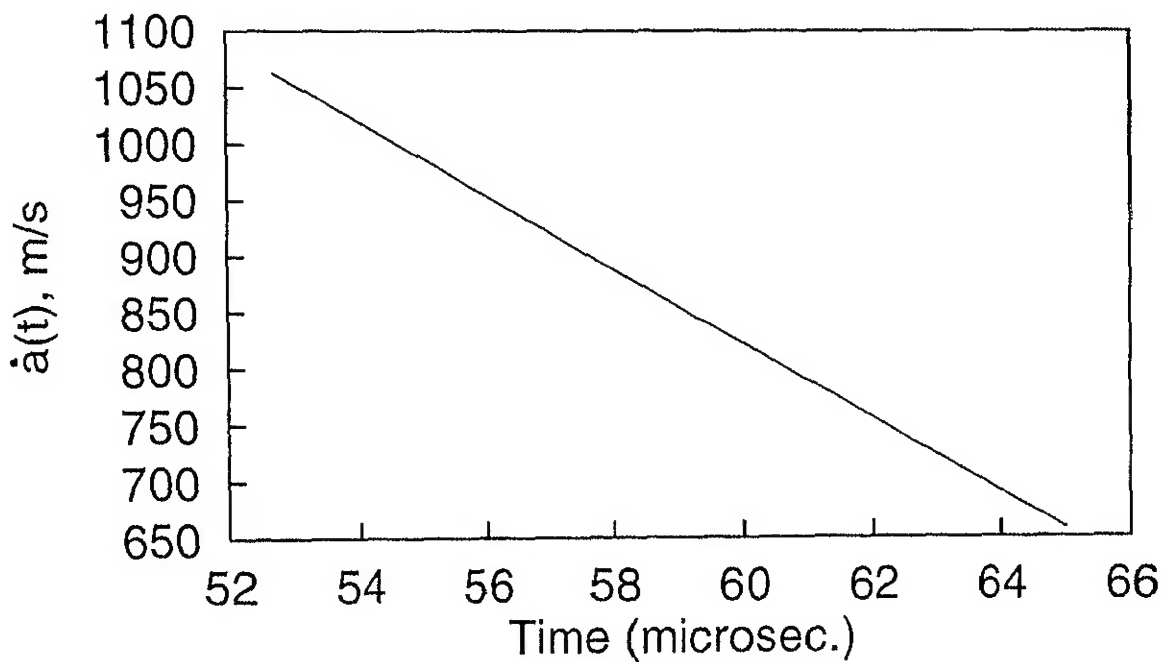


Fig.4.8(b) Variation of crack propagation speed with time obtained by differentiating the crack length vs time curve

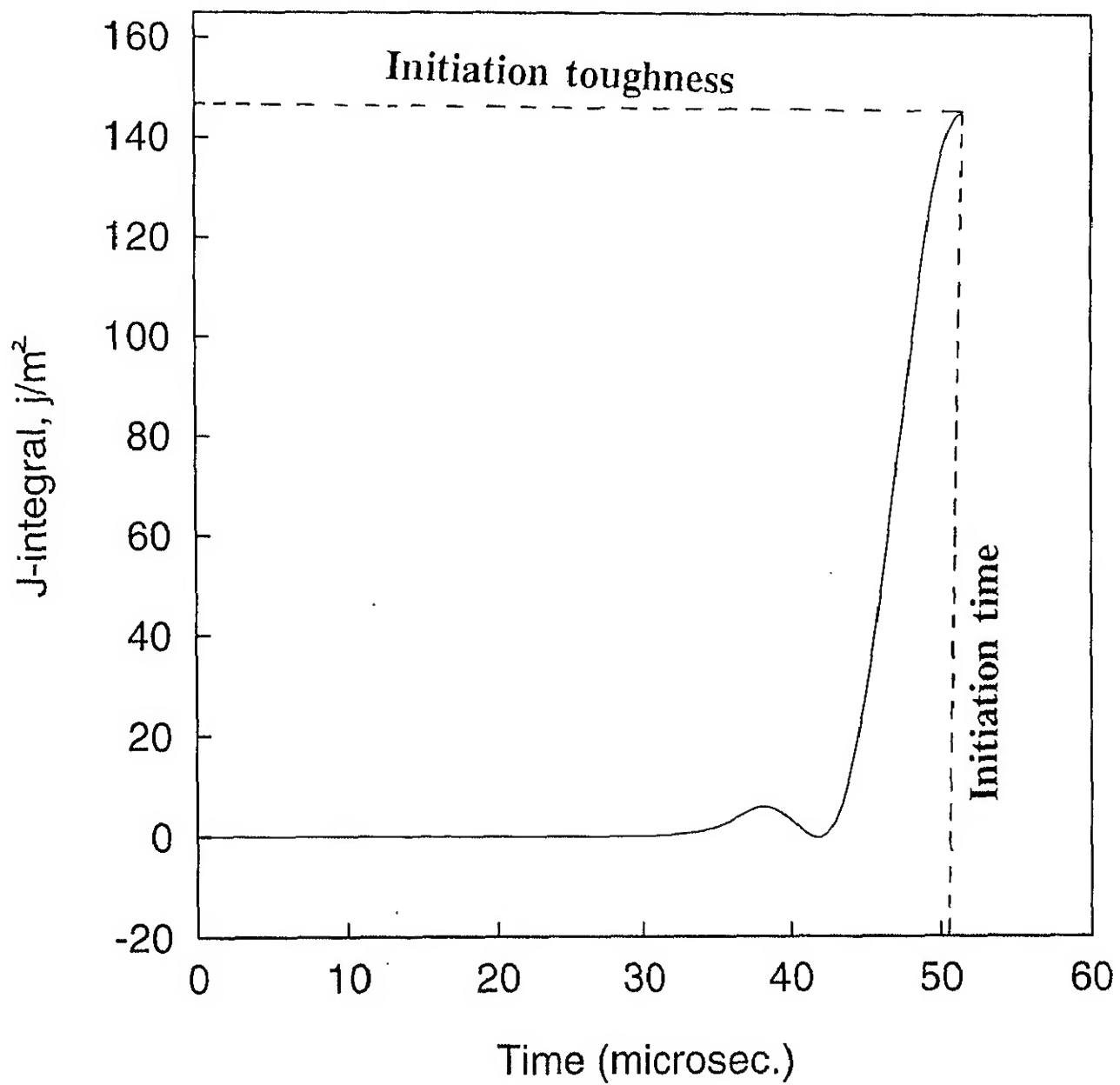


Fig.4.9 Initiation Toughness of Expt.-2

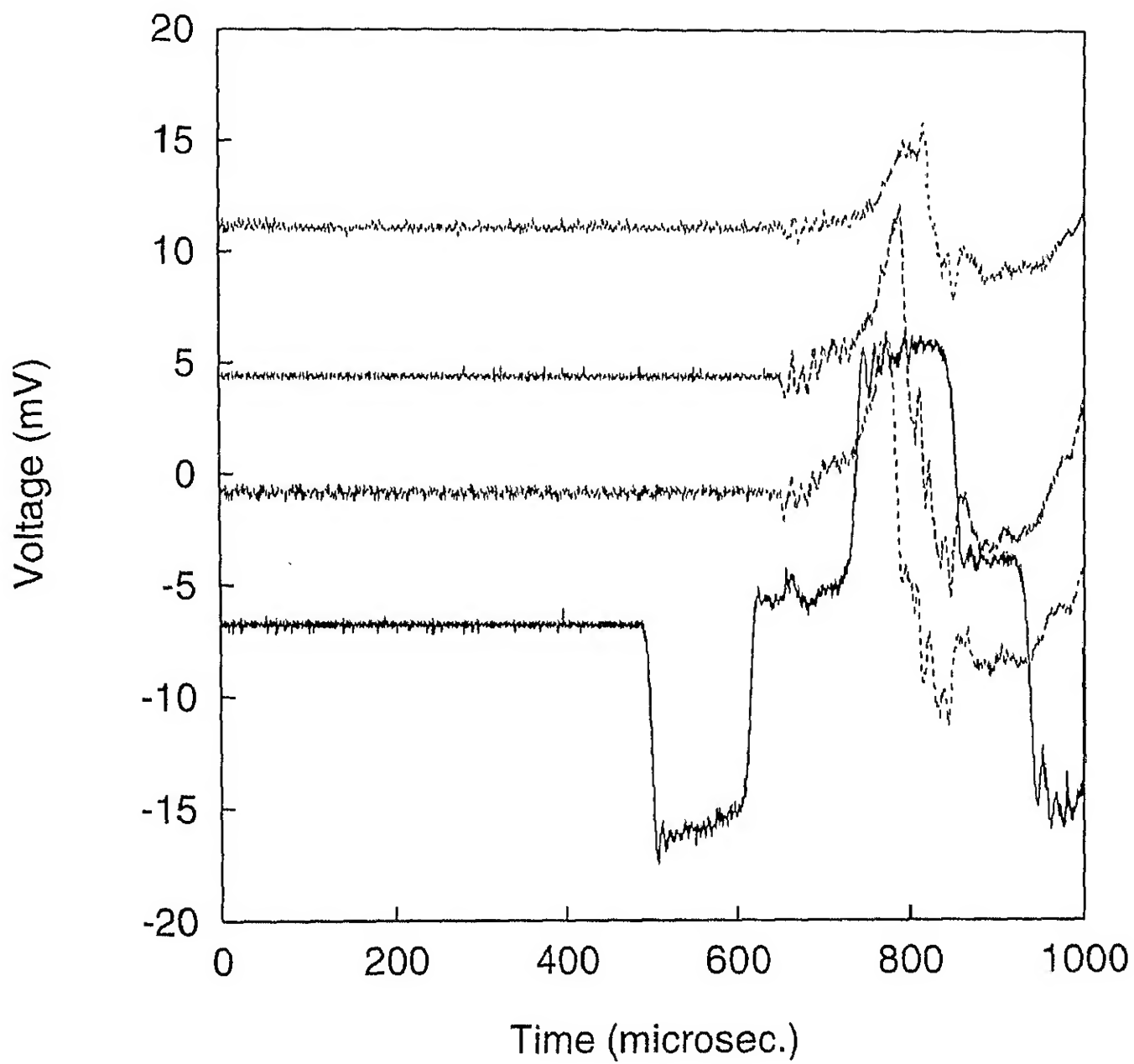


Fig.4.10 Oscilloscope traces of Expt.-3

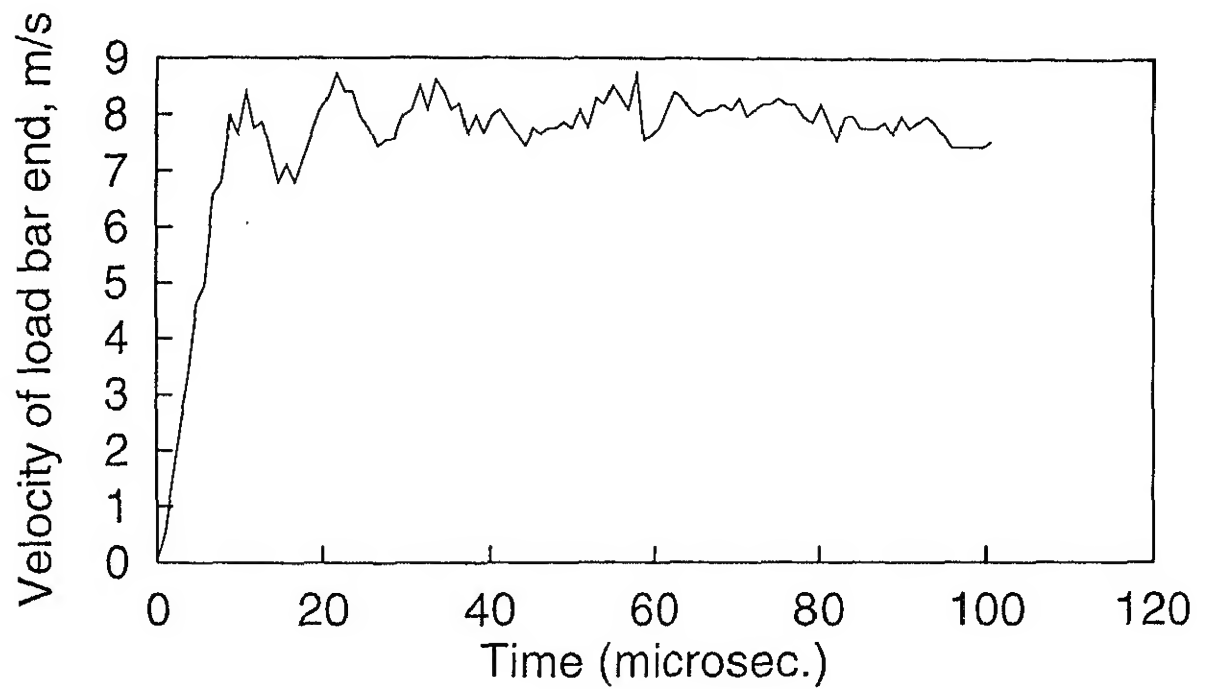


Fig.4.11(a) Velocity input at the cantilever end of the specimen obtained through incident and reflected pulses of the load bar for Expt.-3

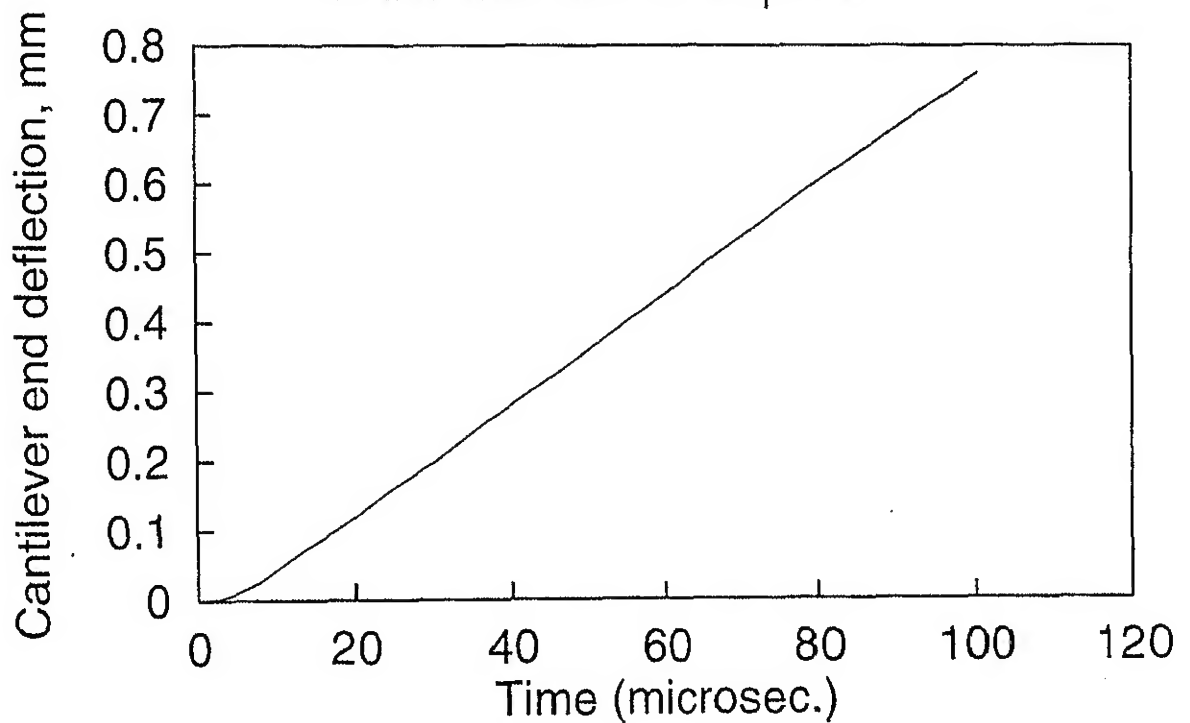


Fig.4.11(b) Cantilever end deflection vs time obtained by integrating the velocity input curve

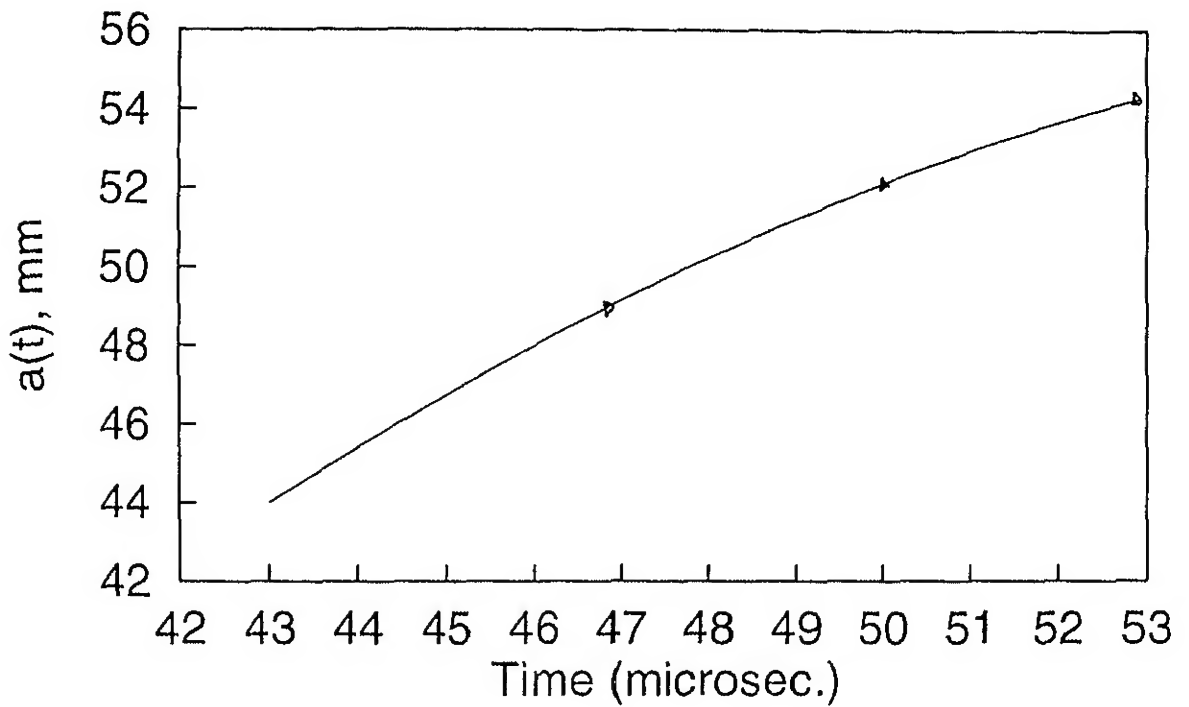


Fig.4.12(a) Variation of crack length with time of Expt.-3 shown with interpolation upto the length of precrack

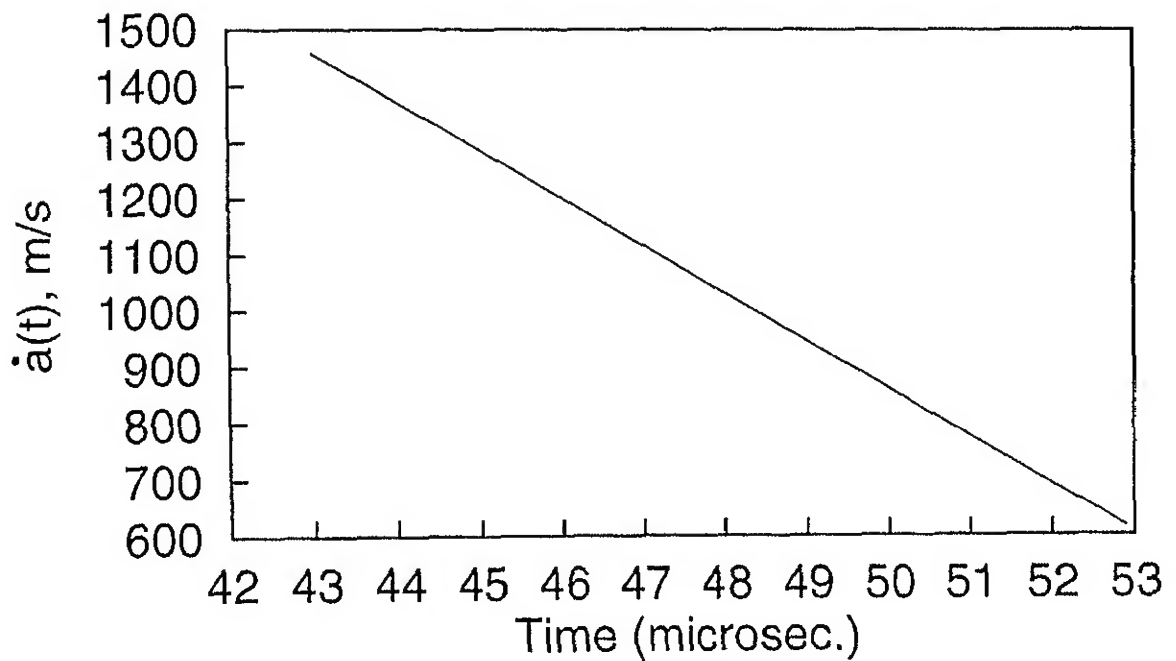


Fig.4.12(b) Variation of crack propagation speed with time obtained by differentiating the crack length vs time curve

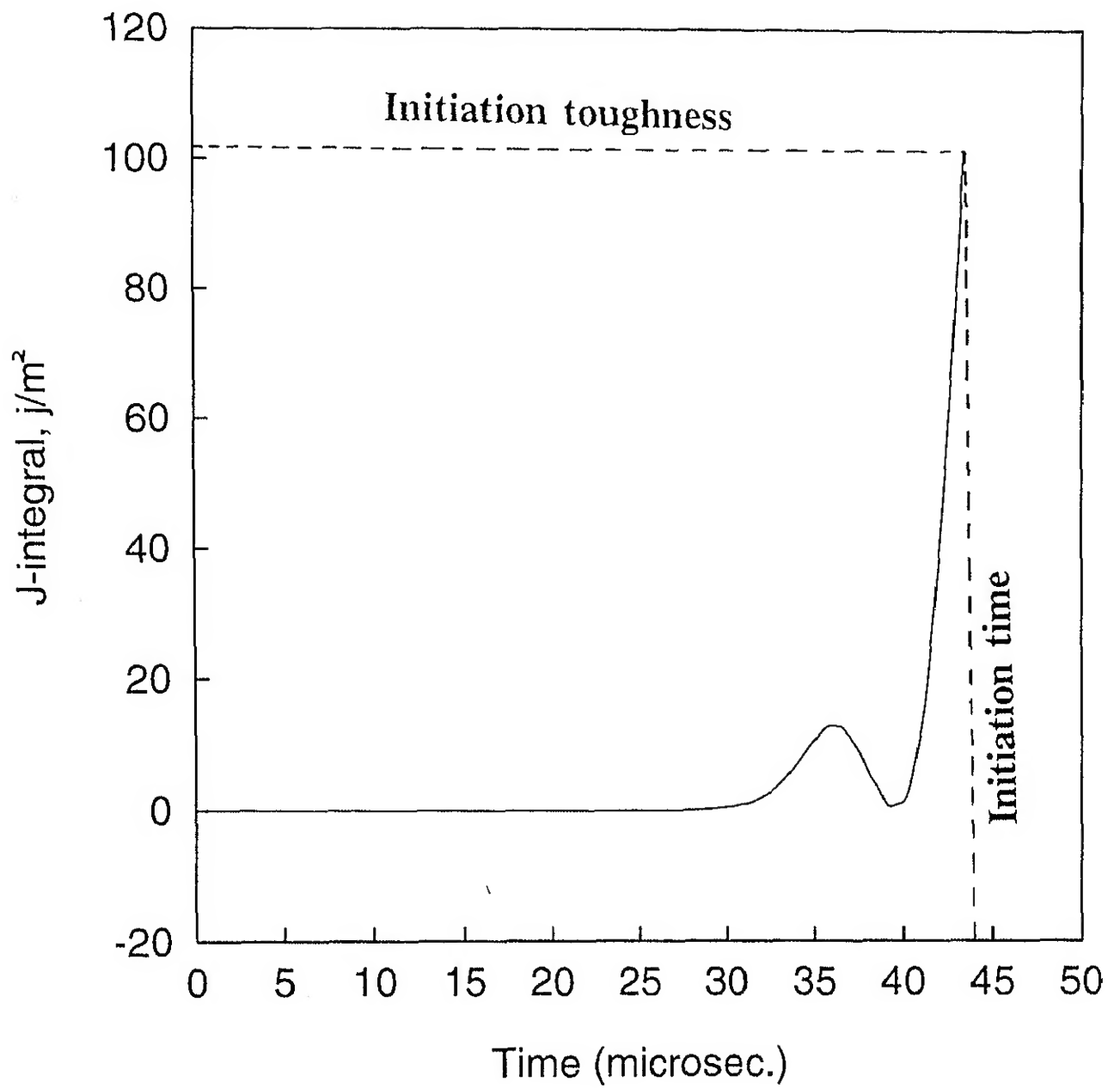


Fig.4.13 Initiation Toughness of Expt.-3

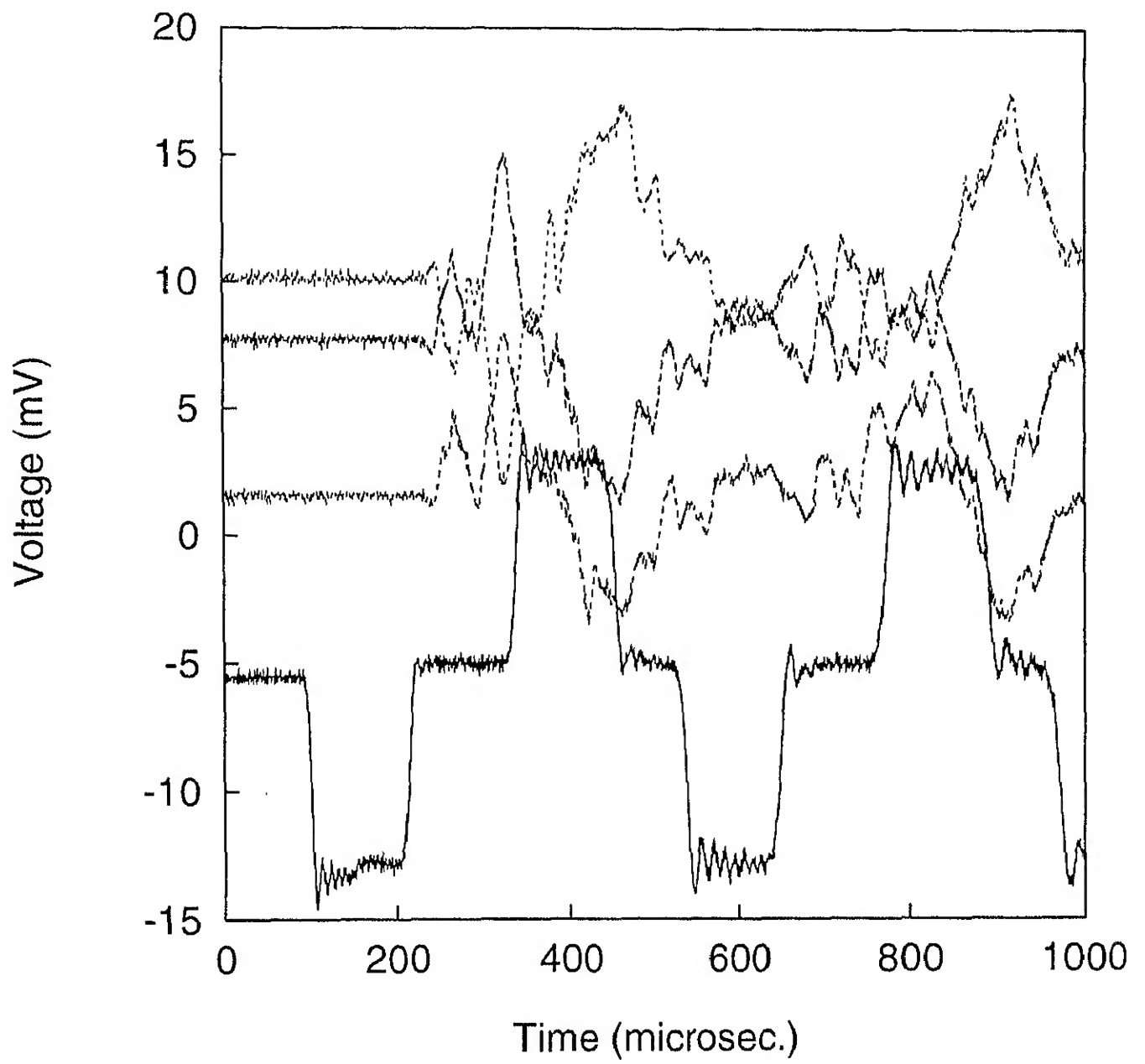


Fig.4.14 Oscilloscope traces of Expt.-4

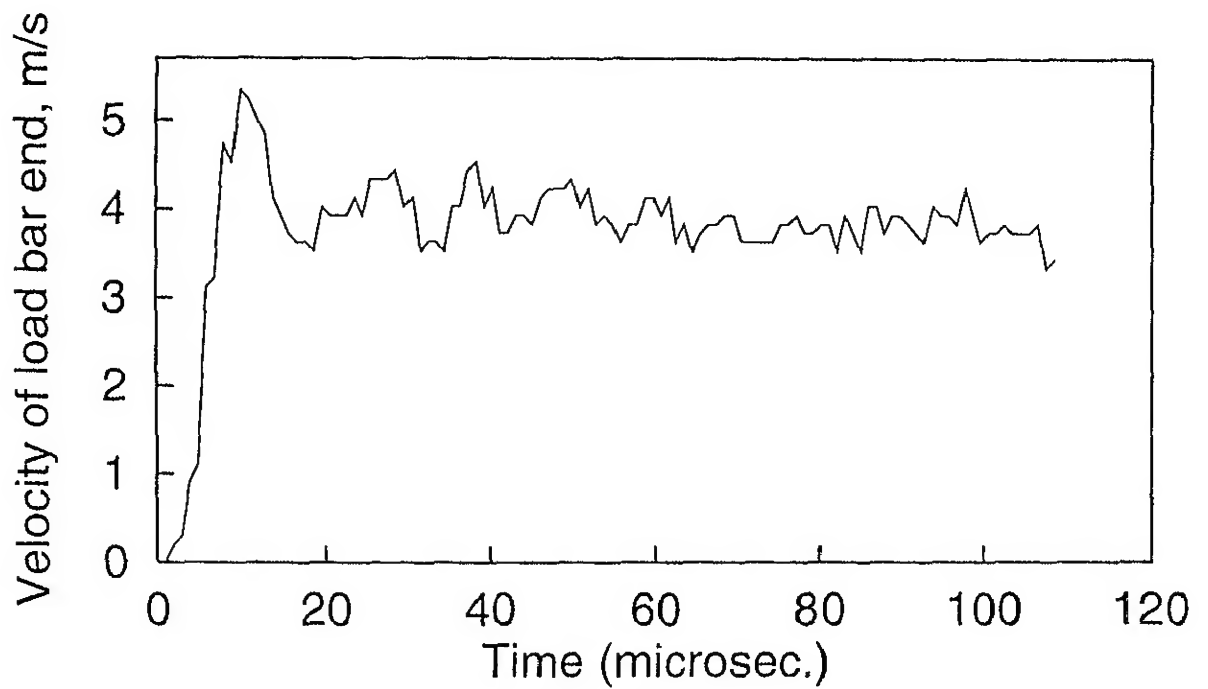


Fig.4.15(a) Velocity input at the cantilever end of the specimen obtained through incident and reflected pulses of the load bar for Expt.-4

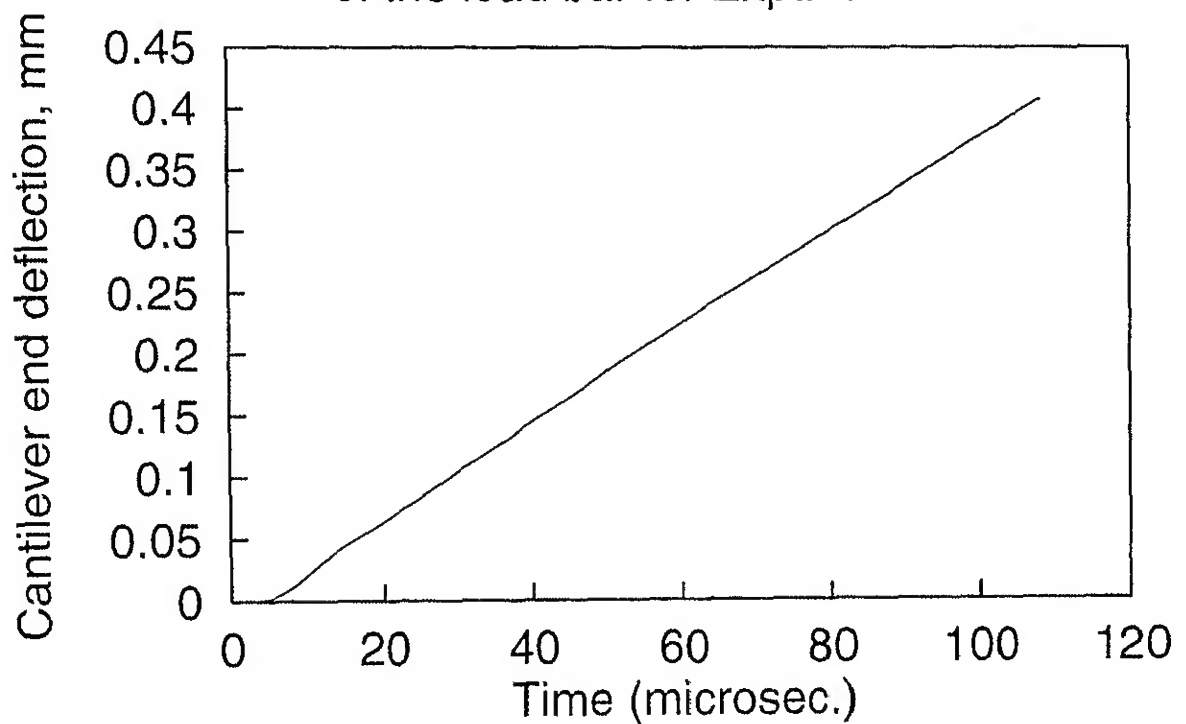


Fig.4.15(b) Cantilever end deflection vs time obtained by integrating the velocity input curve

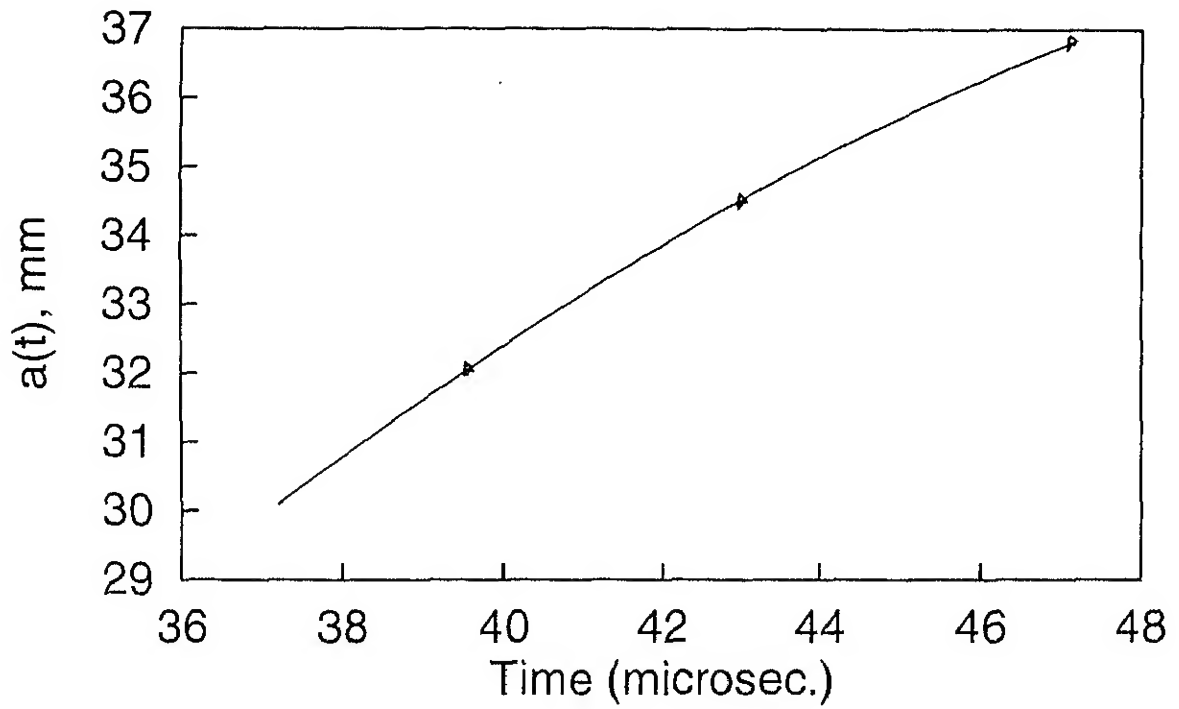


Fig.4.16(a) Variation of crack length with time of Expt.-4 shown with interpolation upto the length of precrack

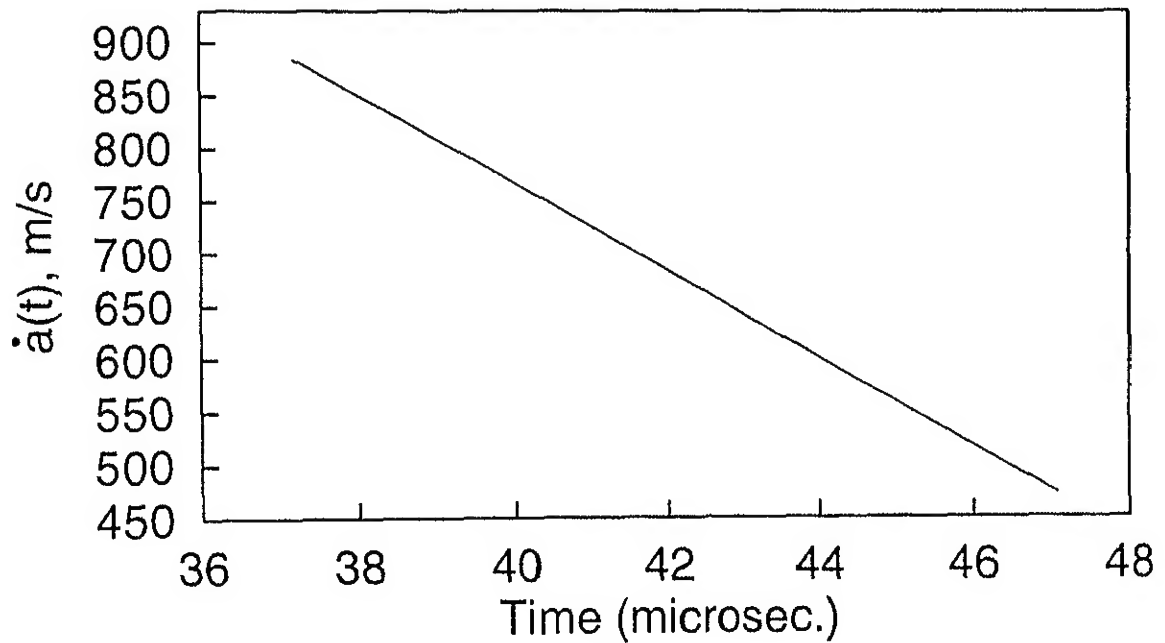


Fig.4.16(b) Variation of crack propagation speed with time obtained by differentiating the crack length vs time curve

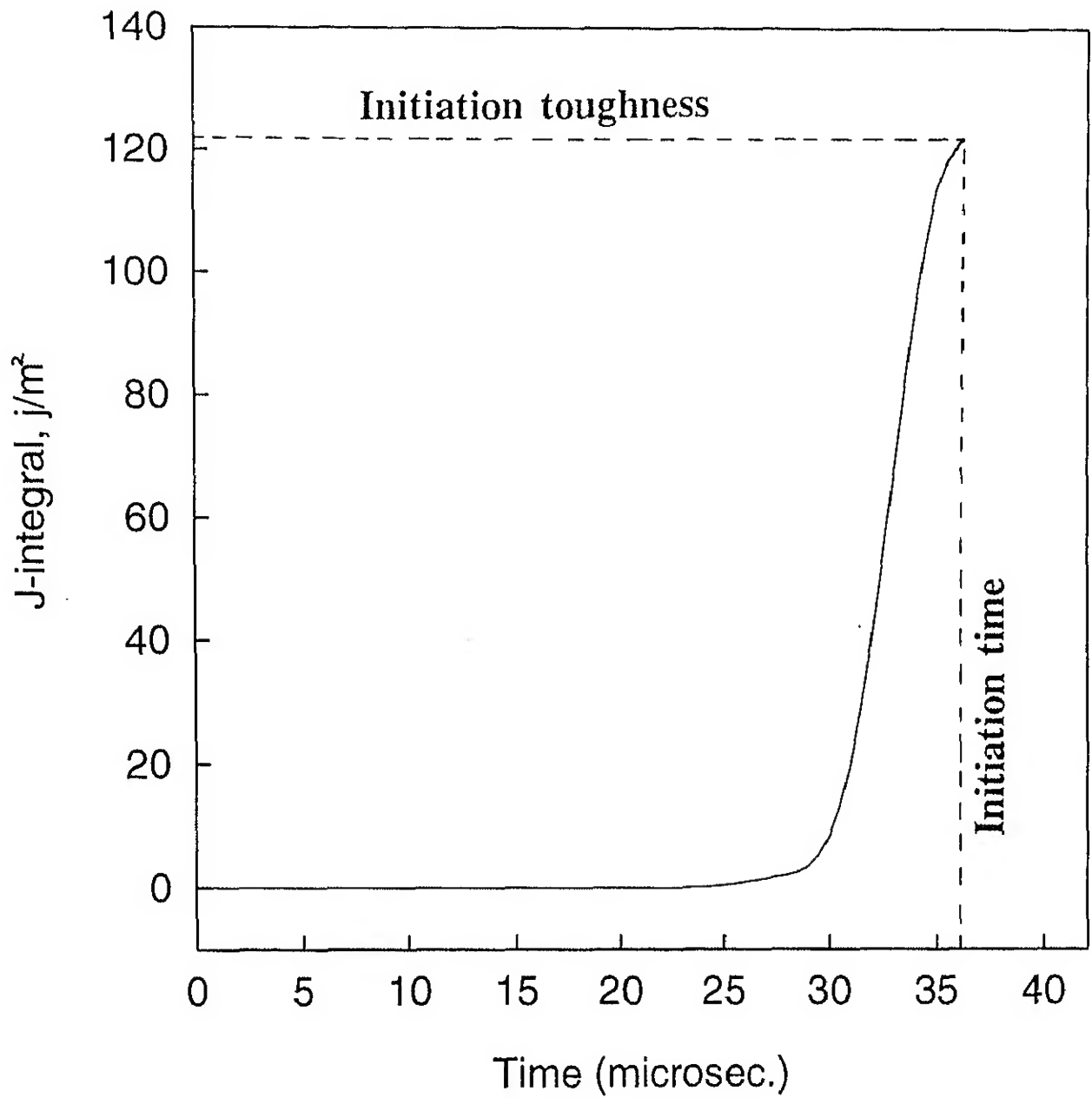


Fig.4.17 Initiation Toughness of Expt.-4

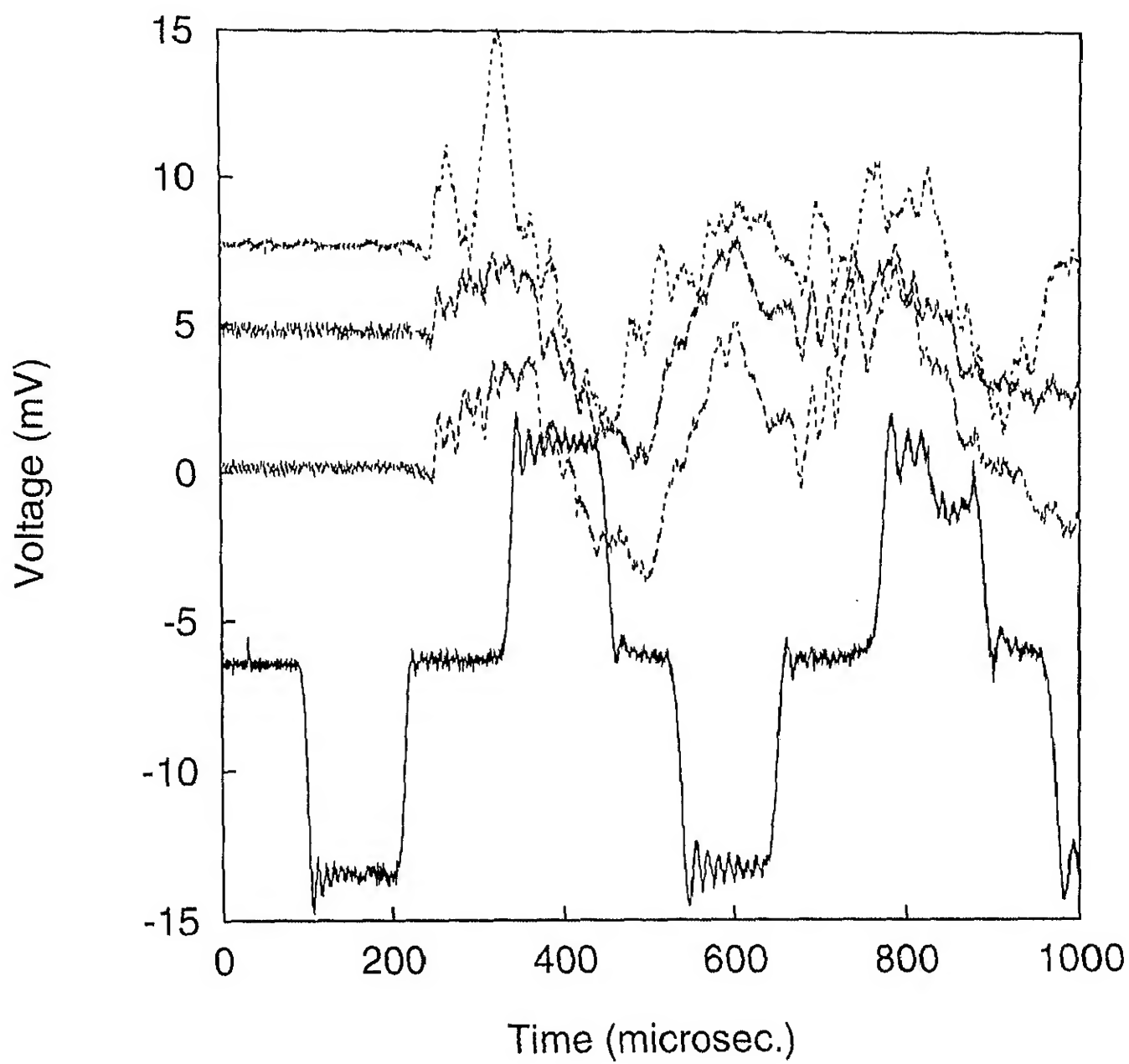


Fig.4.18 Oscilloscope traces of Expt.-5

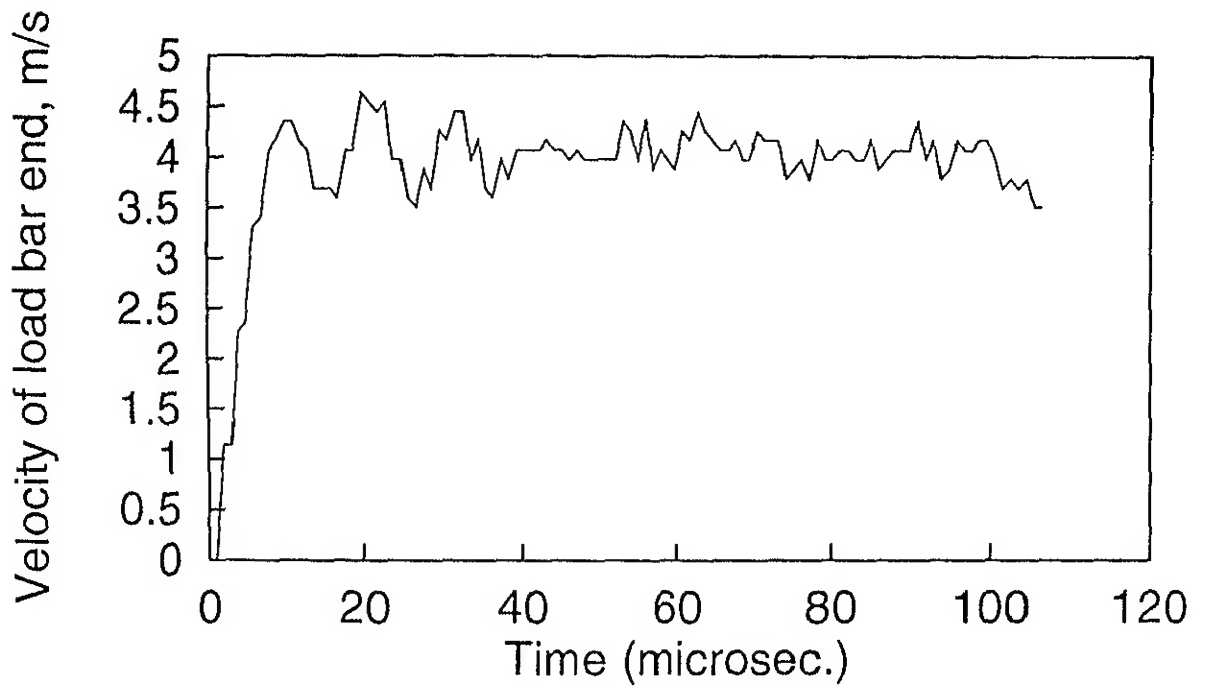


Fig.4.19(a) Velocity input at the cantilever end of the specimen obtained through incident and reflected pulses of the load bar for Expt.-5

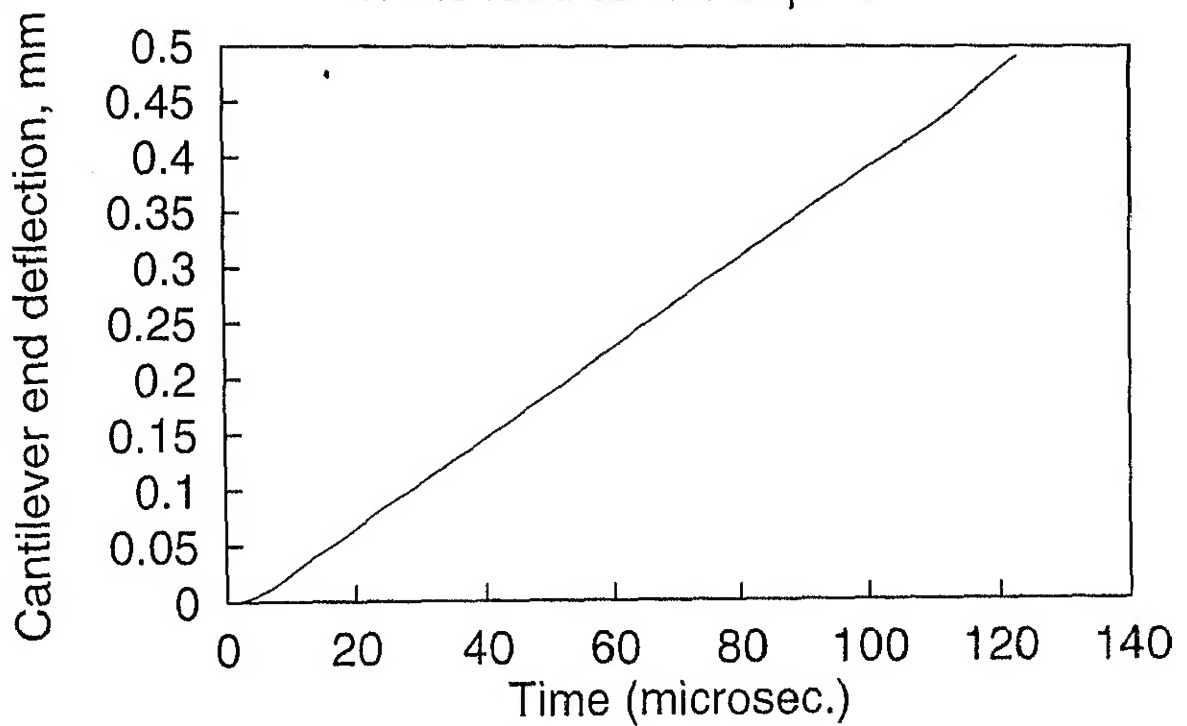


Fig.4.19(b) Cantilever end deflection vs time obtained by integrating the velocity input curve

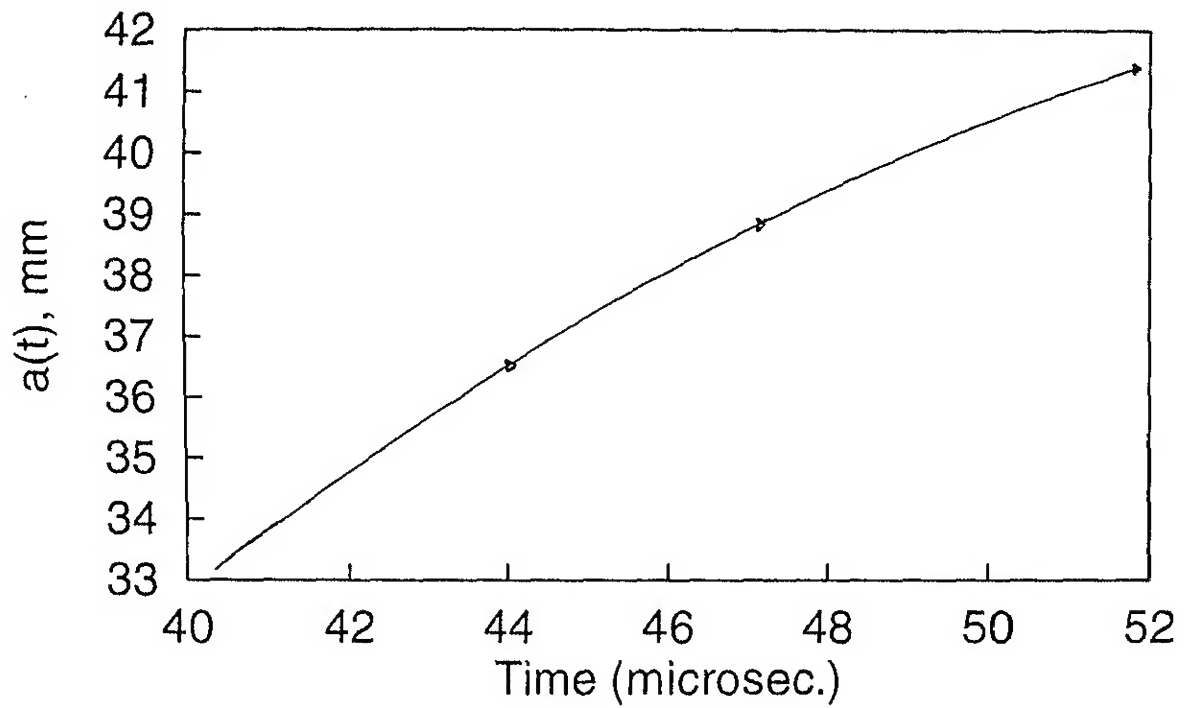


Fig.4.20(a) Variation of crack length with time of Expt.-5 shown with interpolation upto the length of precrack

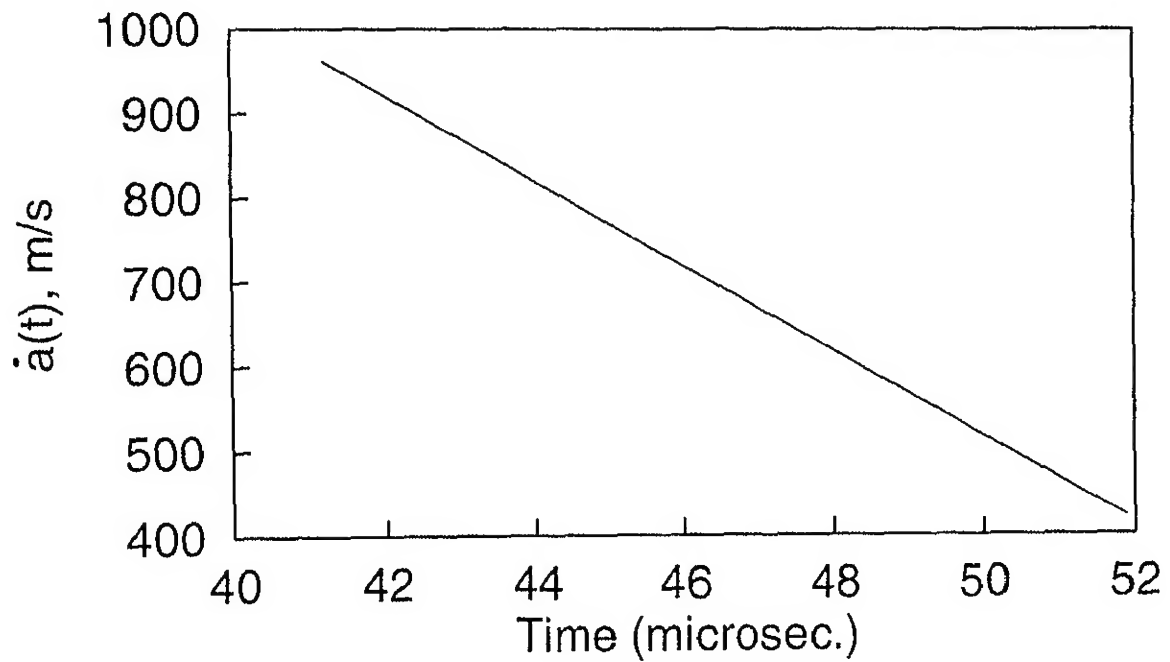


Fig.4.20(b) Variation of crack propagation speed with time obtained by differentiating the crack length vs time curve

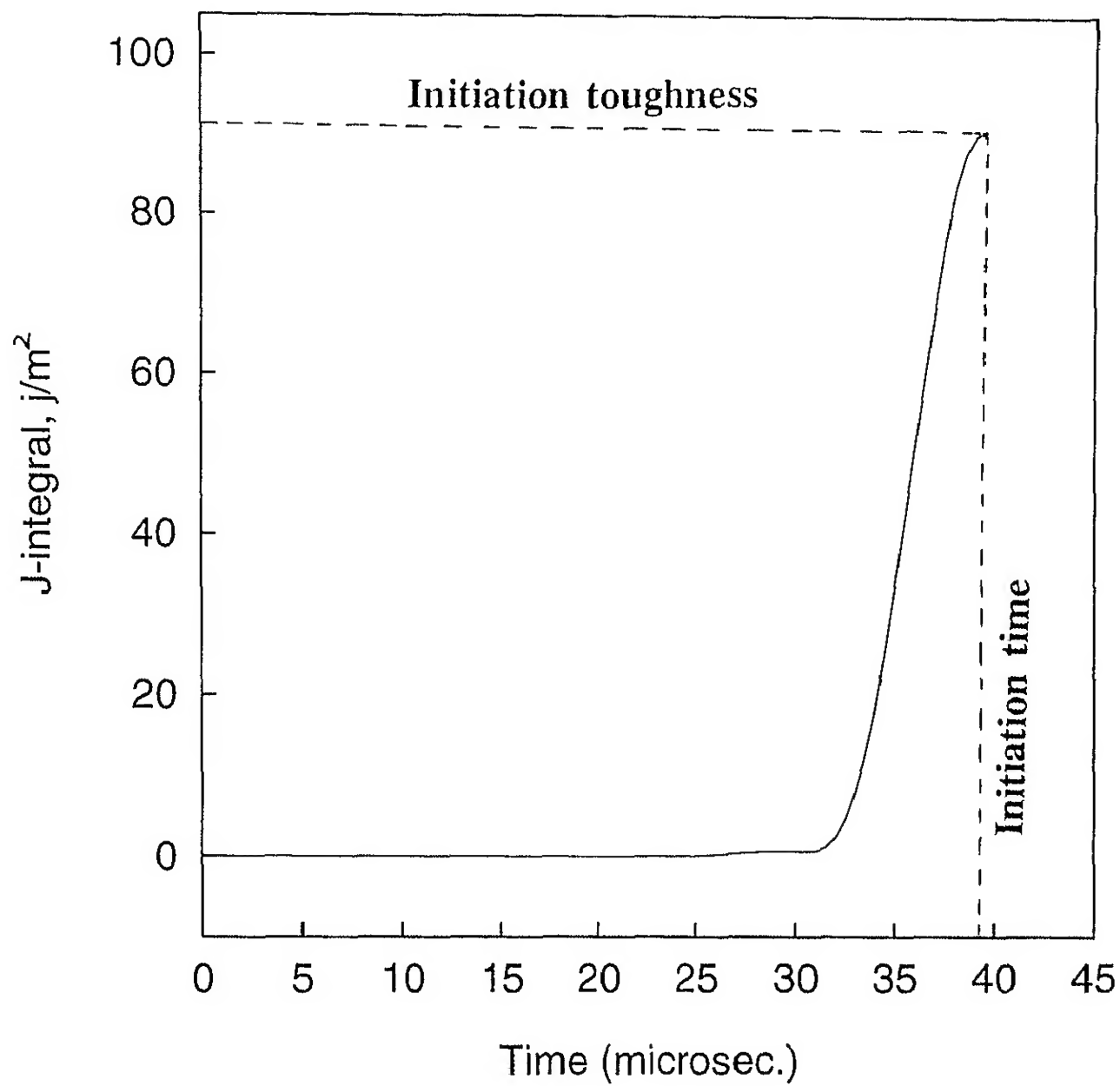


Fig.4.21 Initiation Toughness of Expt.-5

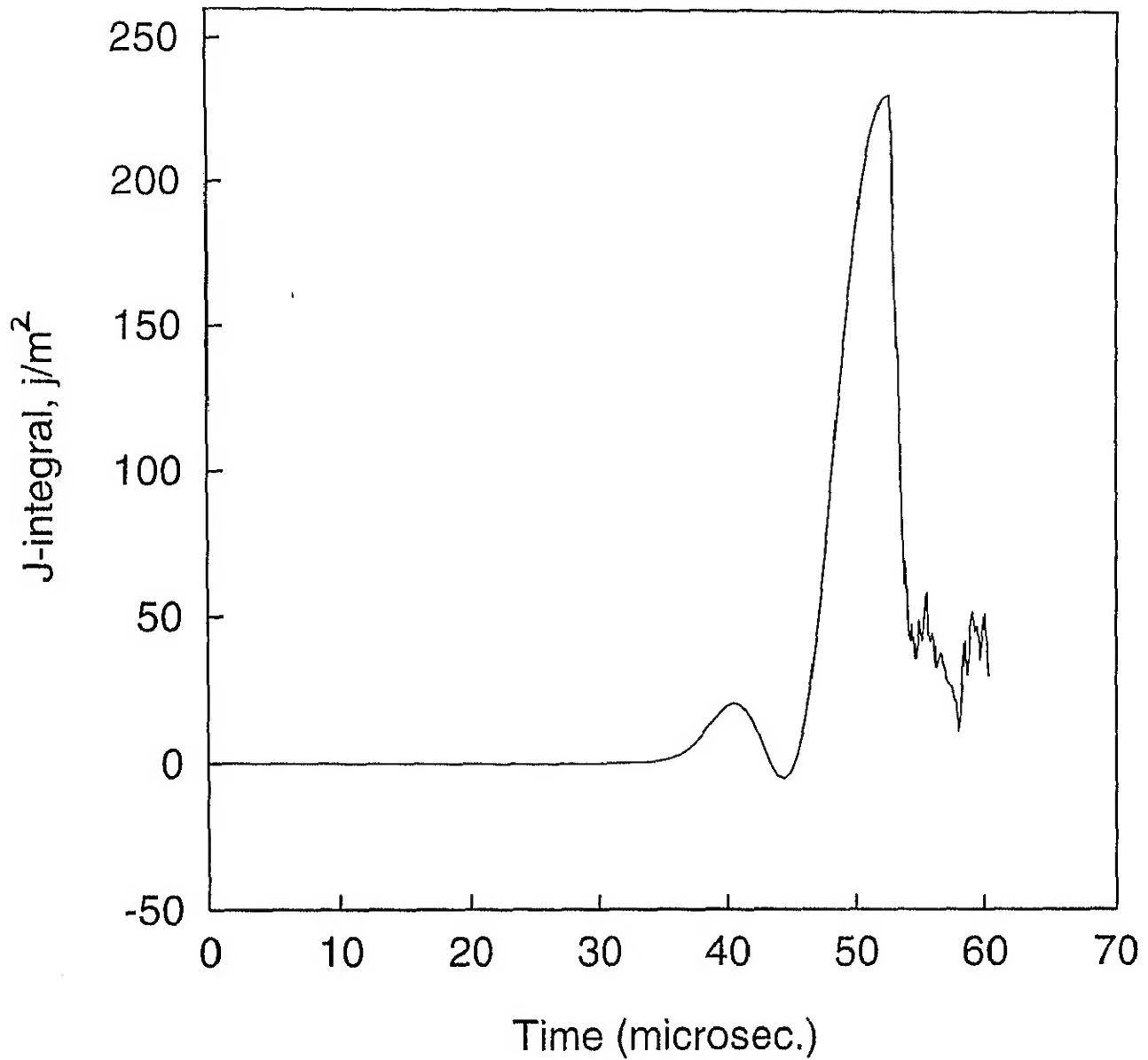


Fig.4.22 Variation of J-integral with time for stationary crack and propagating crack of Expt.-1

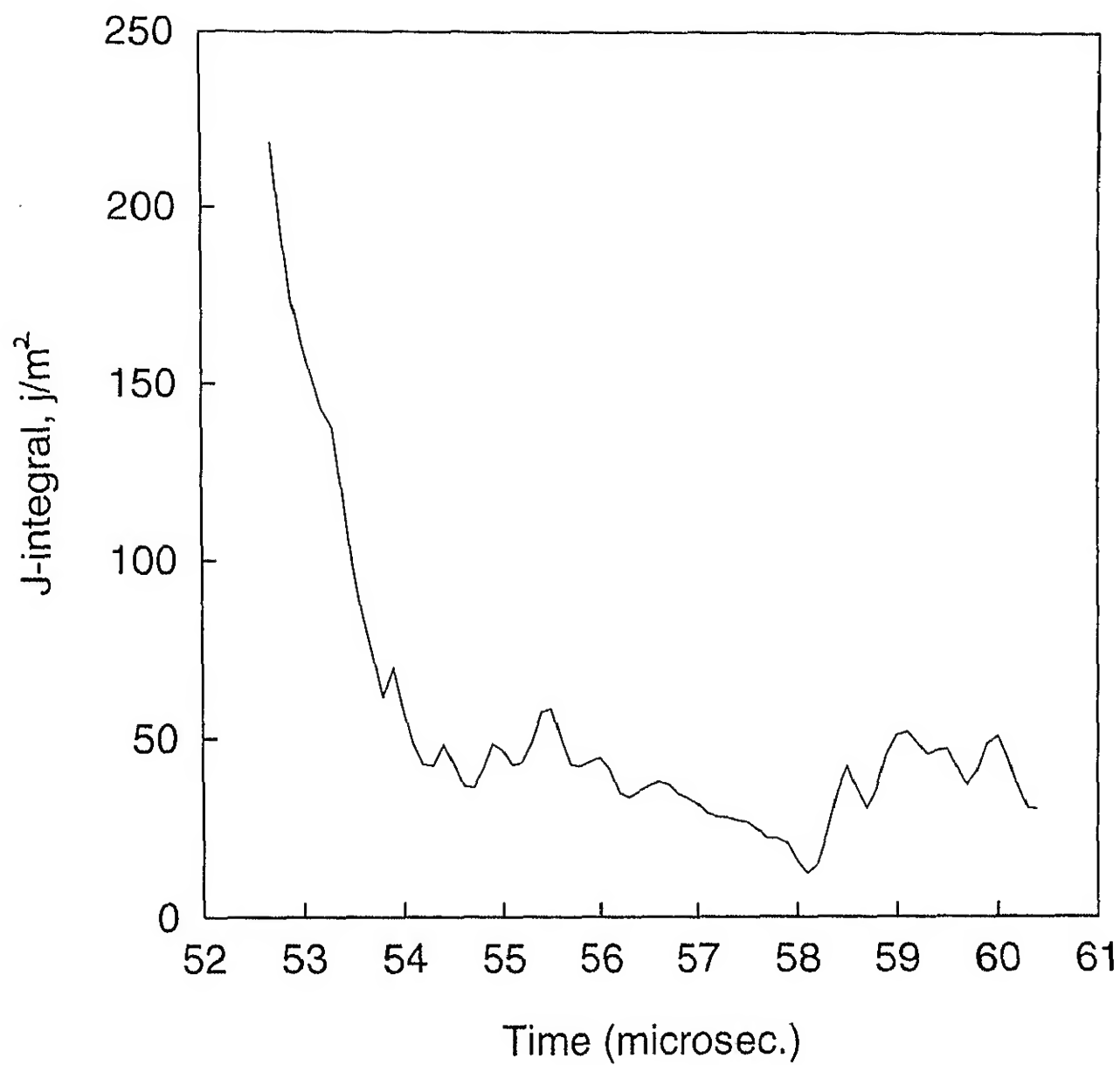


Fig.4.23 Variation of J-integral after the crack start propagating for Expt.-1

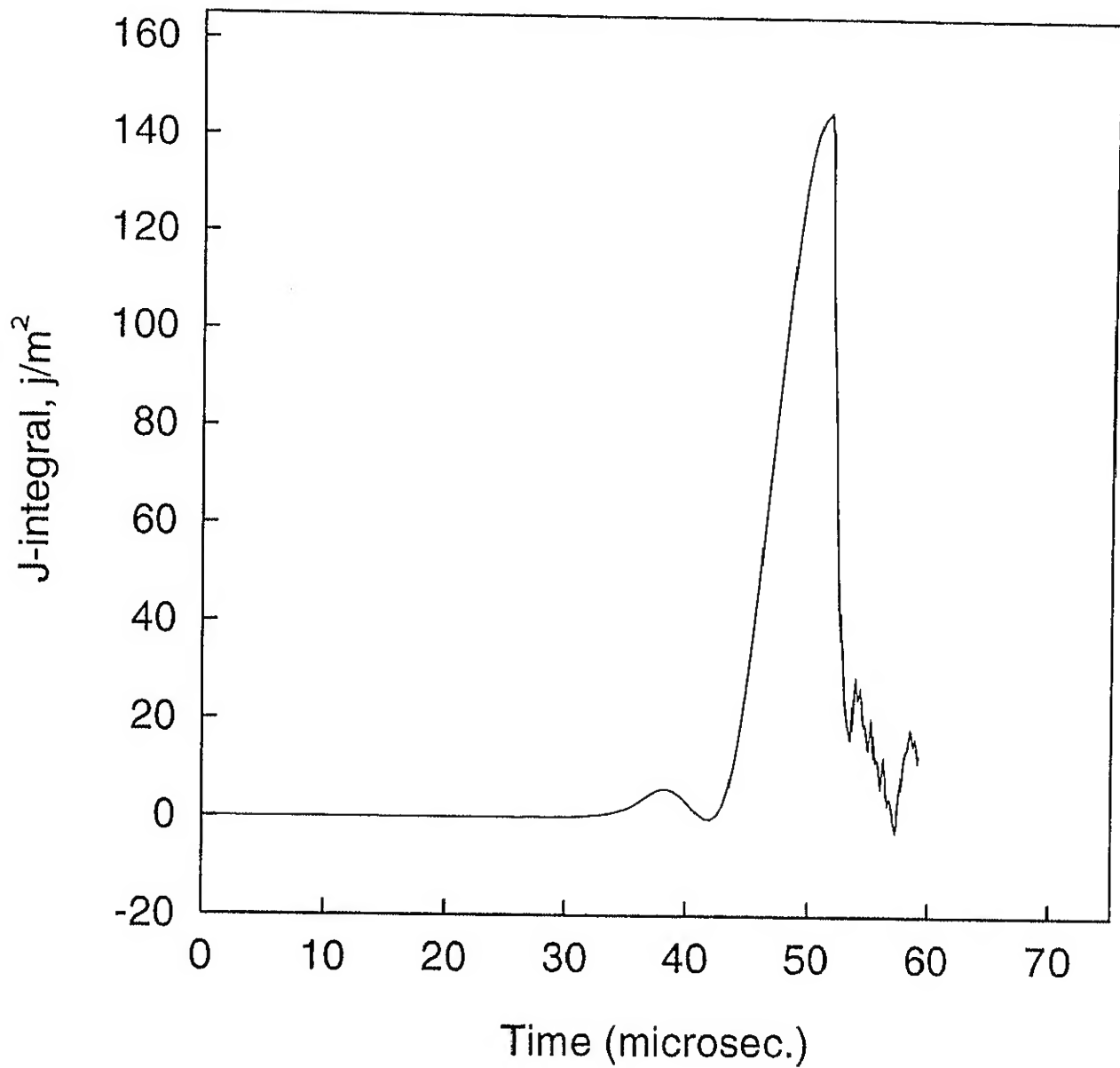


Fig.4.24 Variation of J-integral with time for stationary crack and propagating crack of Expt.-2

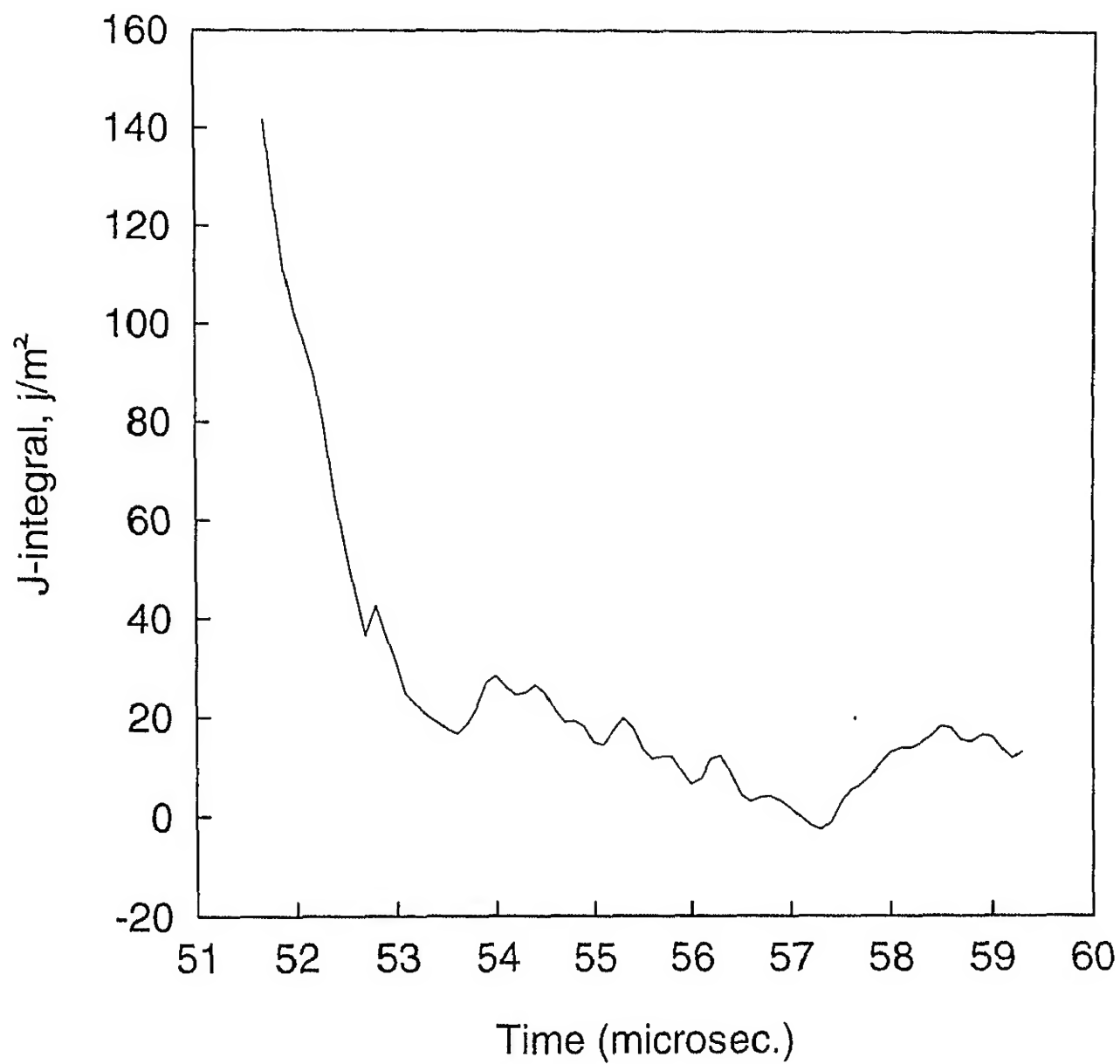


Fig.4.25 Variation of J-integral after the crack start propagating for Expt.-2

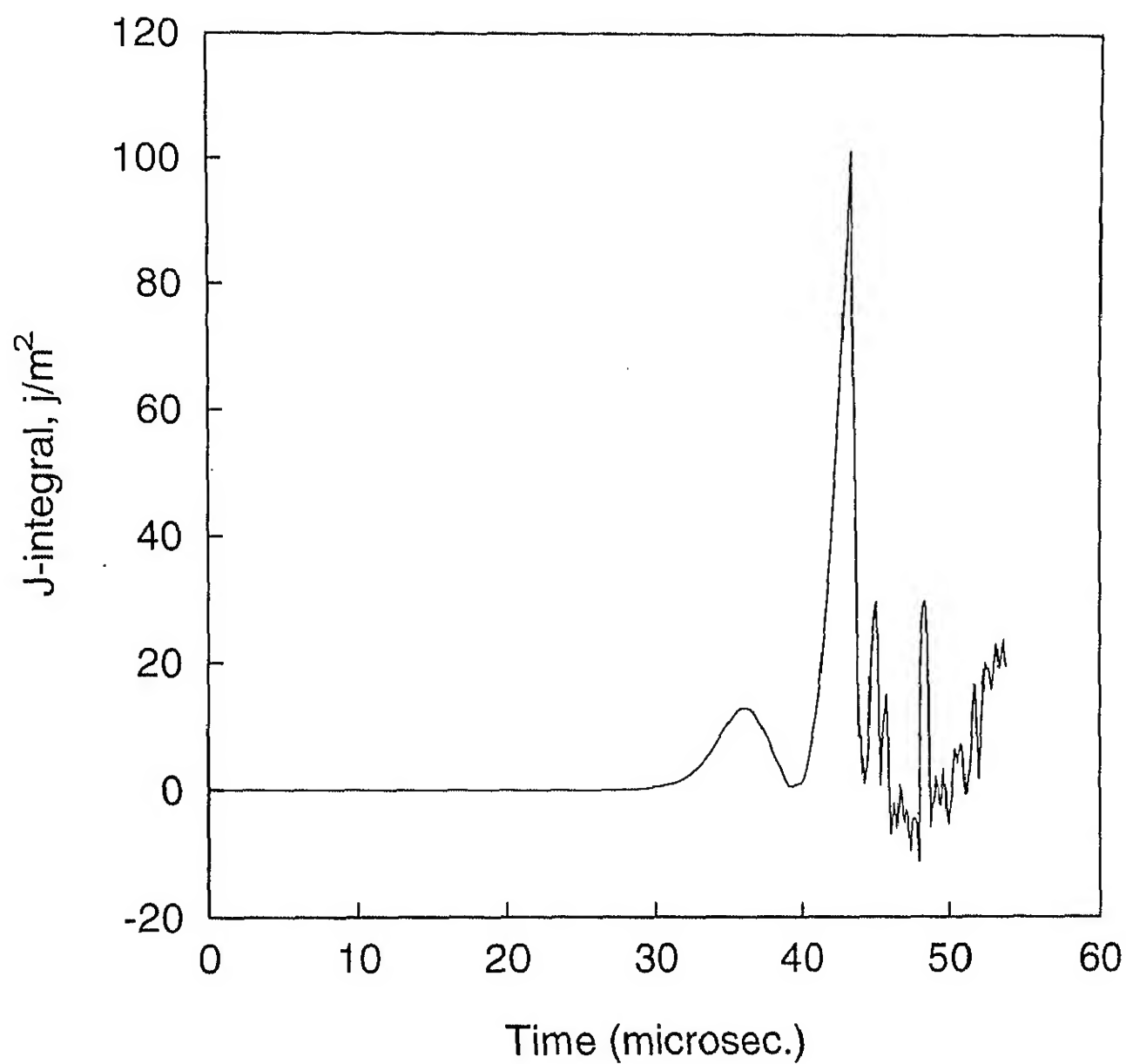


Fig.4.26 Variation of J-integral with time for stationary crack and propagating crack of Expt.-3

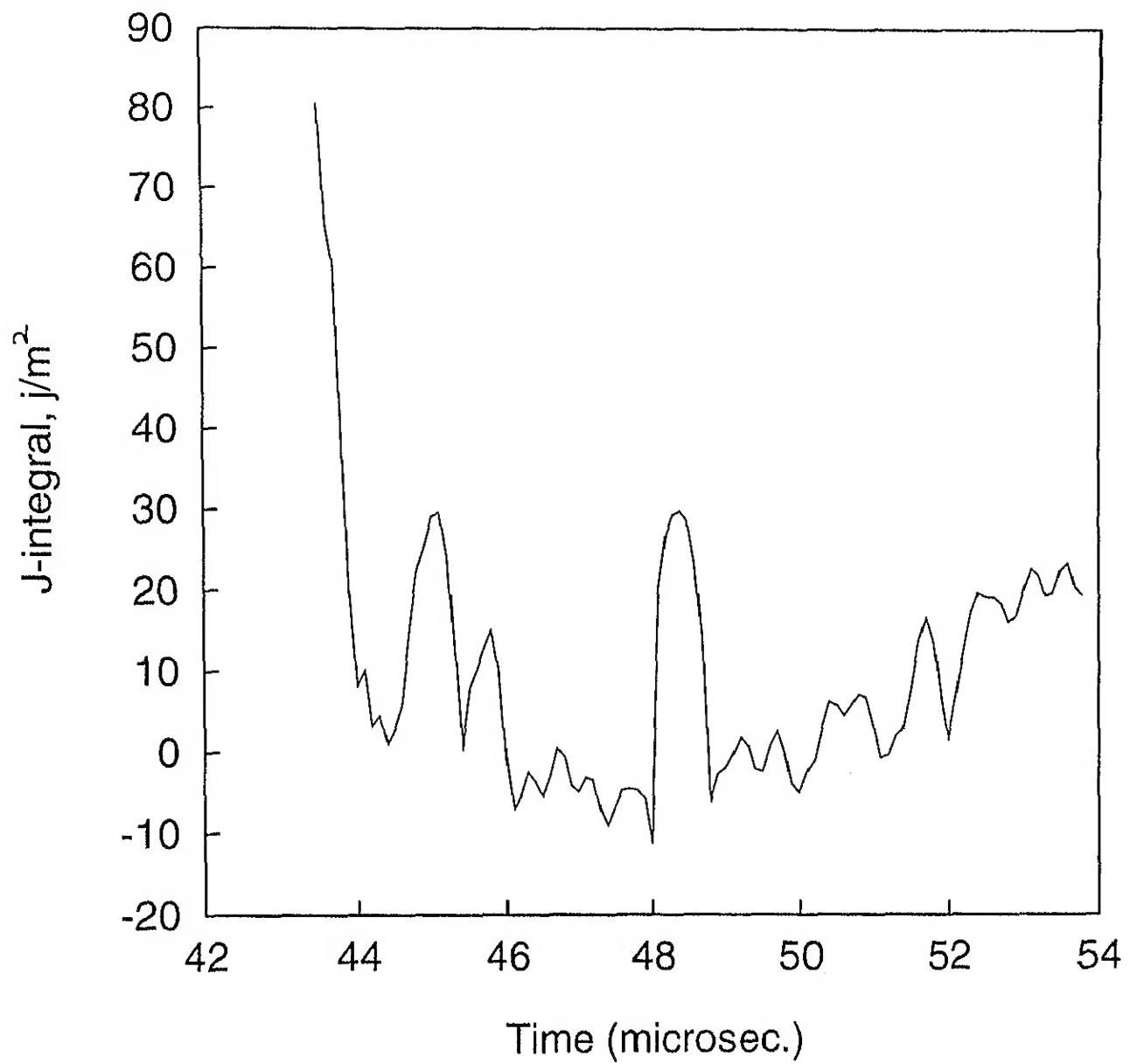


Fig.4.27 Variation of J-integral after the crack start propagating for Expt.-3

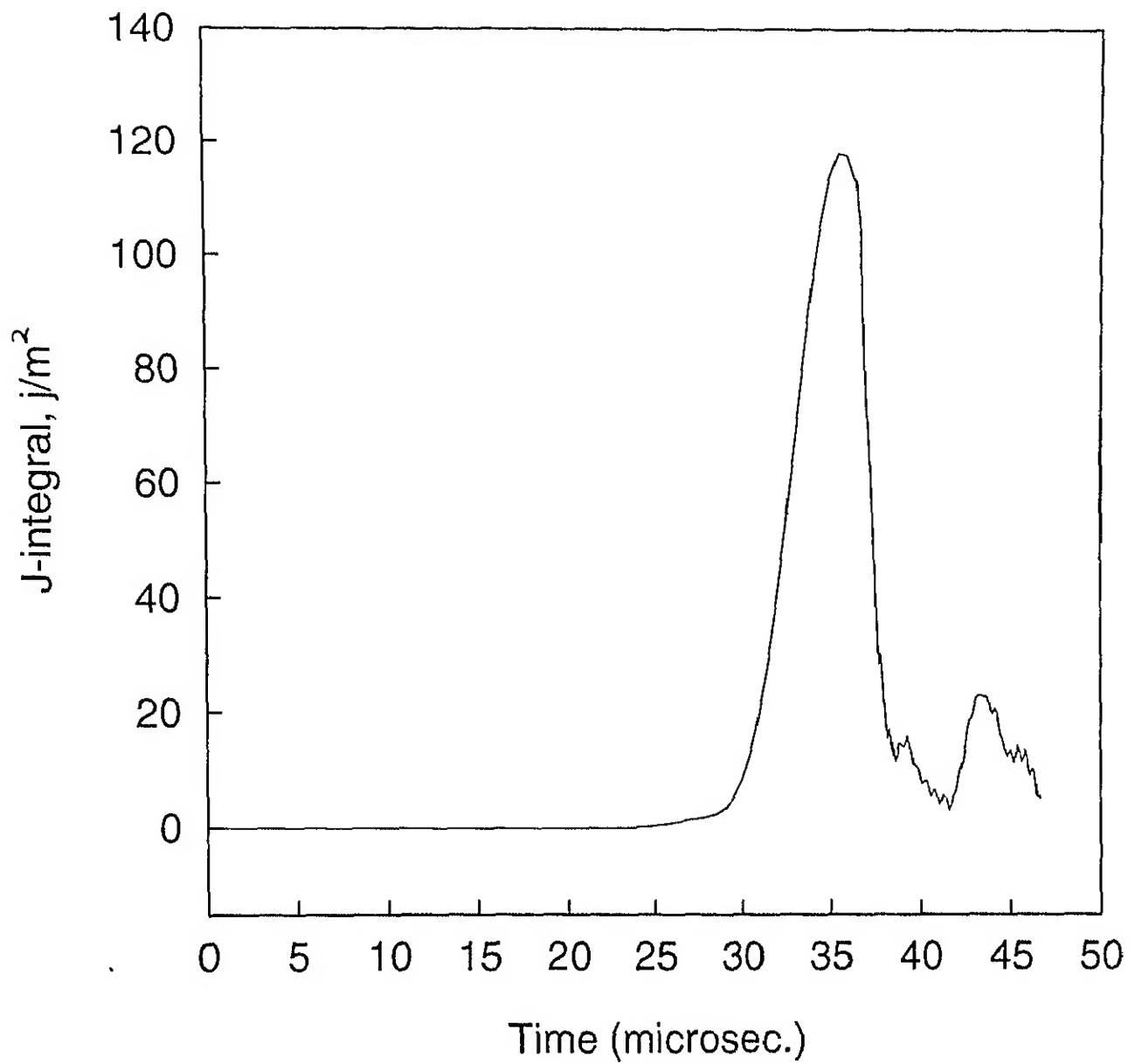


Fig.4.28 Variation of J-integral with time for stationary crack and propagating crack of Expt.-4

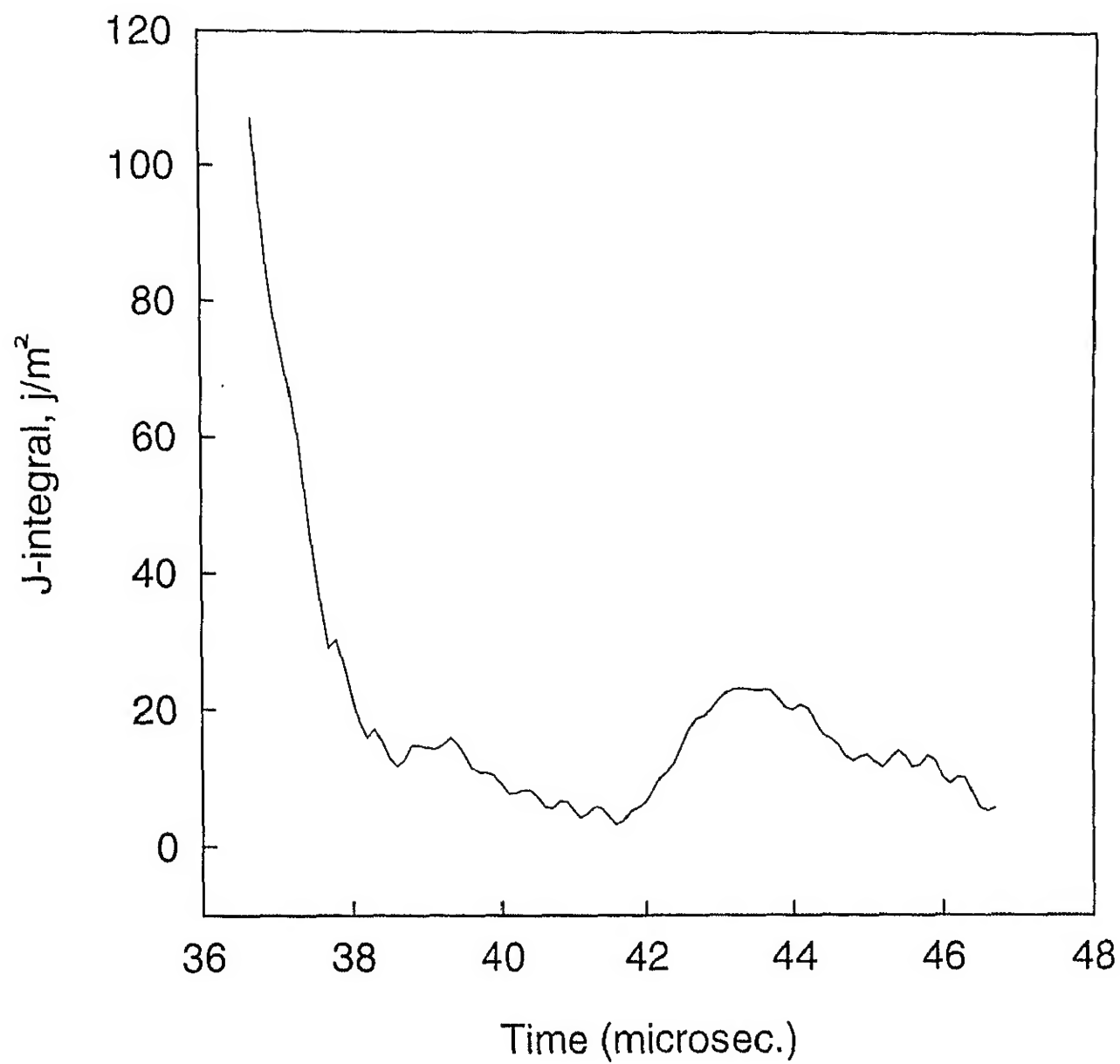


Fig.4.29 Variation of J-integral after the crack start propagating for Expt.-4

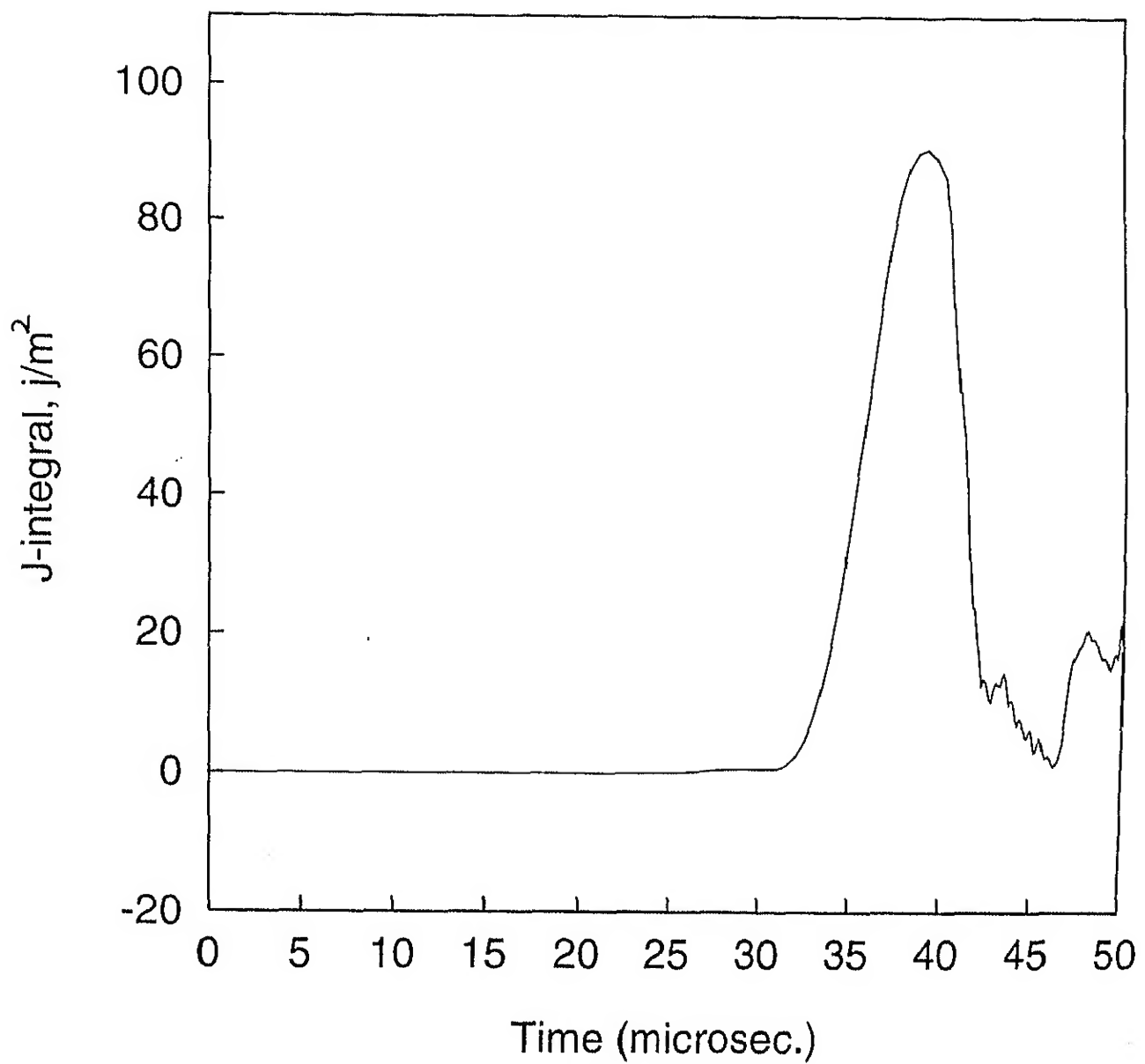


Fig.4.30 Variation of J-integral with time for stationary crack and propagating crack of Expt.-5

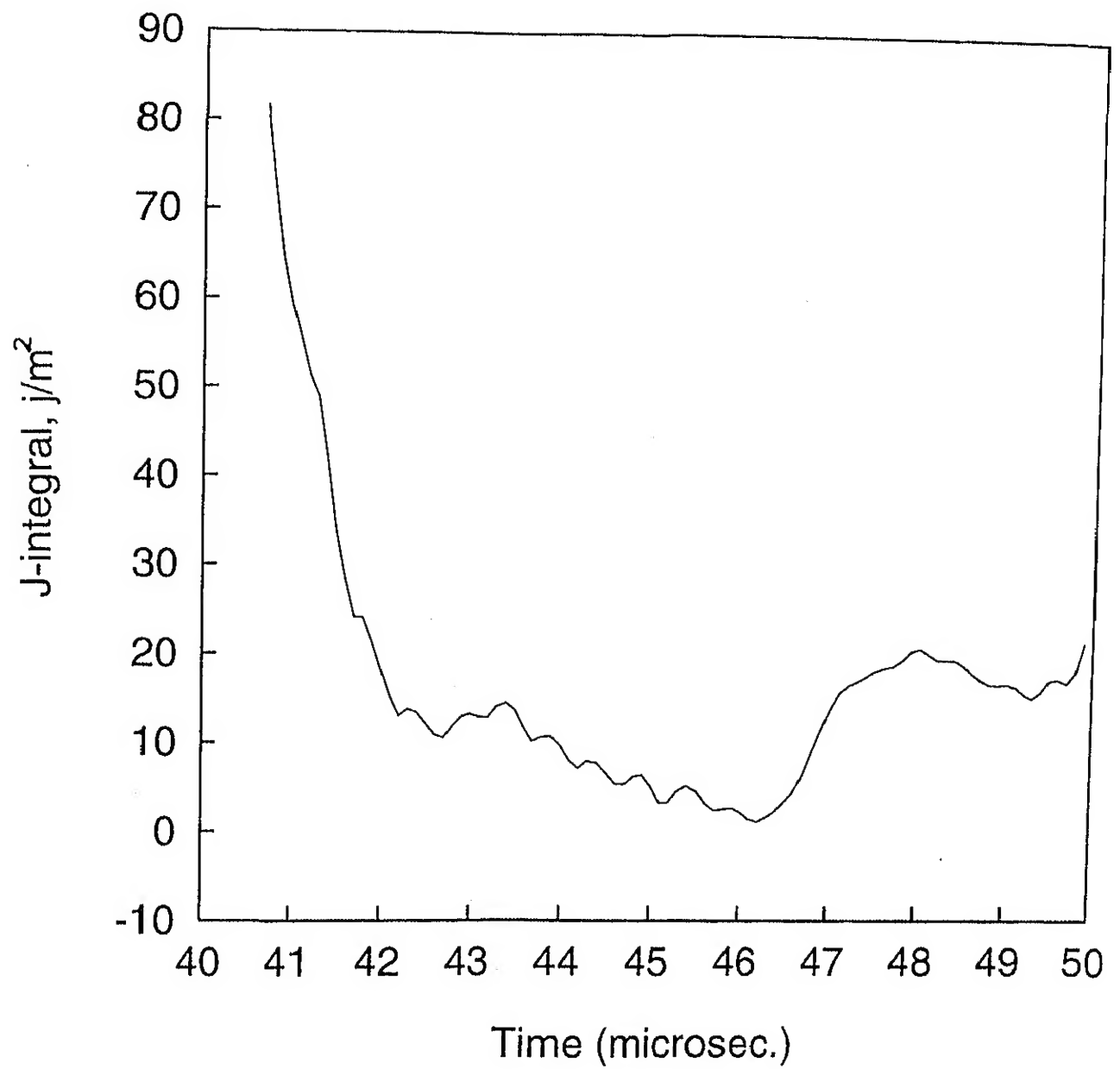


Fig.4.31 Variation of J-integral after the crack start propagating for Expt.-5

CHAPTER-5

CONCLUSIONS AND SUGGESTIONS FOR FUTURE WORK

5.1 CONCLUSIONS

A technique, which was developed by Verma[1996] on a steel specimen, has been applied to determine the initiation and propagation toughness of interlaminar cracks in unidirectional glass fibre reinforced epoxy laminates. This technique employs a combined experimental and numerical work. The aim of the present work has been to experimentally determine the cantilever-end-deflection with respect to time, crack velocity, crack initiation time. These experimental data is used as input to finite element code.

The experimental technique consists of one of the cantilevers of DCB specimen was glued to a rigid block and the other cantilever was bonded through a load bar. The load bar is impacted by a striker accelerated in an air gun. The displacement of the load bar end was calculated using one dimensional wave propagation analysis. The crack velocity was measured by monitoring the strain responses of the three strain gauges bonded on one side face of the DCB specimen ahead of the crack tip.

After feeding the experimental data, the initiation toughness (J_{init}) for different experiments from the FE code was found to vary between 91 and 230 J/m² which is significantly smaller than the quasistatic interlaminar toughness ($G_{ic} = 415$ J/m²). The propagation toughness (J_{prop}) was found to vary between 1 and 50 J/m₂ depending on the crack velocity which was varying between 100-1400 m/s.

5.2 SUGGESTIONS FOR FURTHER WORK

- (1) More experiments should be conducted by varying initial crack length and displacement boundary conditions at the cantilever's end.
- (2) The work may be extended to angle ply laminate. This would require further modification of the computer code.

REFERENCES

Agarwal B.D. and Broutman L.J., 1980, Analysis and Performance of Fiber Composites, John Wiley & Sons.

Broek D., 1984, Elementary Engineering Fracture Mechanics, Martinus Nijhoff Publishers, The Hague.

Kesavan Potty P.K., 1992, Experimental and FEM Investigation of SIF in DCB specimen, M.Tech. Thesis, Mech. Dept., IIT, Kanpur.

Kishore N.N., Kumar Prashant and Verma S.K., 1993, Numerical Methods in Dynamic Fracture, Journal of Aeronautical Society of India, Vol.45, No.4, pp. 323-333.

Kolednik O., 1991, On the Physical Meaning of the J- Δa Curves, Engineering Fracture Mechanics, Vol.38, No.6, pp. 403-412.

Nishioka Toshihisa, Murakami Tatsuyuki, Uchiyama Hidetoshi, Shakakura Keigo and Kittaka Hiroyuki, 1991, Specimen Size Effects on Dynamic Crack Propagation and Arrest in DCB specimens, Engineering Fracture Mechanics, Vol.39, No.4, pp. 757-767.

Ravichandran G. and Clifton R.J., 1989, Dynamic Fracture Under Plane Wave Loading, International Journal of Fracture, Vol.40, pp. 157-201.

Rosakis A.J., Duffy J. and Freund L.B., 1984, The determination of Dynamic Fracture Toughness of AISI 4340 steel by the shadow spot method, Journal of Mechanical Physics and Solids, No.4, pp. 443-640.

Sun C.T. and Grady J.E., 1988, Dynamic Delamination Fracture Toughness of a Graphite/Epoxy Laminate Under Impact, Composite Science and Technology, Vol.31,

pp. 55-72.

Takahashi K. and Arakawa K., June 1987, Dependence of Crack Acceleration on the Dynamic Stress Intensity Factors in Polymers, *Experimental Mechanics*, pp. 195-200.

Verma S.K., 1996, Determination of Static and Dynamic Interlaminar Fracture Toughness - A Combined Experimental And Finite Element Method, Ph.D. Thesis, Mech. Dept., IIT, Kanpur.

APPENDIX - A

For an orthotropic composite lamina the principal material directions are designated by the longitudinal direction L and the transverse direction T (considering two-dimensional case shown in the Fig.A1 below). The usual engineering constants are elastic moduli in the longitudinal and transverse direction, E_L and E_T respectively, the shearing modulus associated with the principal material directions, G_{LT} , the major Poisson ratio ν_{LT} and the minor Poisson ratio, ν_{TL} .

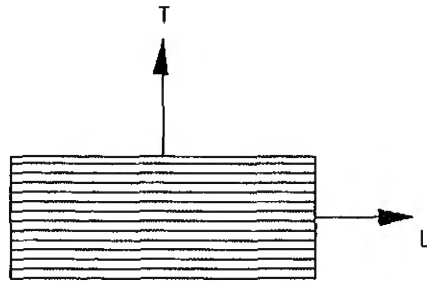


Fig. A1 Principal material directions of an orthotropic lamina

The stiffness matrix for composite laminate used in FE code is given by

$$[D] = \begin{bmatrix} Q_{11} & Q_{12} & 0 \\ Q_{21} & Q_{22} & 0 \\ 0 & 0 & Q_{33} \end{bmatrix}$$

Where Q_{ij} are the stiffness coefficients for the laminate. The relation between the engineering constants and the material stiffness coefficients is given by

$$Q_{11} = \frac{E_L}{1 - \nu_{LT}\nu_{TL}}$$

$$Q_{12} = \frac{\nu_{LT}E_T}{1 - \nu_{LT}\nu_{TL}} = \frac{\nu_{TL}E_L}{1 - \nu_{LT}\nu_{TL}}$$

$$Q_{66} = G_{LT}$$

$$\frac{\nu_{LT}}{E_L} = \frac{\nu_{TL}}{E_T}$$

E_L and E_T were found by conducting a tensile test along the fibre direction and across the fibre direction respectively. For finding out the G_{LT} , E_{45} is found for the specimen in which fibres are oriented at 45° to the longitudinal axis. Then G_{LT} is obtained by substituting E_L , E_T and E_{45} in the following formula [Agarwal and Broutman (1980)].

$$\frac{1}{E_{45}} = \frac{1}{E_L} + \frac{1}{E_T} + \frac{1}{4} \left\{ \frac{1}{G_{LT}} - \frac{2\nu_{LT}}{E_L} \right\}$$

where ν_{LT} is taken equal to 0.25.

The elastic modulus obtained from the tensile tests for various configurations are given in the tables below

Table A1. Values of elastic modulus in longitudinal direction

Expt. No	E_L , GPa
1	37.64
2	39.33
3	43.37

Table A2. Values of elastic modulus in transverse direction

Expt.No	E_L , GPa
1	6.67
2	7.90
3	6.01

Table A3. Values of modulus of rigidity

Expt. No.	E_{45}	G_{LT} , GPa
1	8.65	3.33
2	7.74	2.82
3	8.96	3.46

